Sponsor TBD Report No.

PROJECT C: MICROSTRUCTURE ENGINEERING IN HOT STRIP MILLS
Part 1 of 2: Integrated Mathematical Model

FINAL REPORT

May 1, 1993 - April 30,1998

By

J.K. Brimacombe
I.V. Samarasekera
E.B. Hawbolt
T.R. Meadowcroft
M. Militzer
W.J. Poole
D.Q. Jin

September 1998

13205

Worked performed under Cooperative Agreement No. DE-FC07-93ID3205
Prepared for
American Iron and Steel Institute
Advanced Process Control Program

Report Documentation Page Information

Title and Subtitle:
Project C: Microstructure Engineering in Hot Strip Mills
Part 1 of 2: Integrated Mathematical Model

Authors:
J.K. Brimacombe, I.V. Samarasekera, E.B. Hawbolt, T.R. Meadowcroft, M. Militzer, W.J. Poole and D. Q. Jin

Performing Organization Names, Address:

The University of British Columbia (LTBC)
The Centre for Metallurgical Process Engineering
Advanced Materials and Process Engineering Laboratory
Room 11 1 - 2355 East Mall
Vancouver, B.C. V6T IZ4
Canada

Abstract:

The current work was aimed at developing an integrated model which includes mathematical models of roughing mill, finishing mill, deformation in the roll-bite, runout out table cooling, down coiler and Steckel mill. These models can be used to predict the thermal history, deformation, roll forces, rnicrostructural evolution and mechanical properties of steel strip in- a hot-strip mill. The model has been extended to a Steckel Mill which has been developed @y incorporating the reversing roughing mill model and the coil box model. Also, a down coiler model has been developed and incorporated into the runout table model. A finite-difference scheme was employed in the roughing model, finishing mill model, runout table cooling model and down coiler model. A finite-element model was utilized to provide a complete description of the temperature, inhomogeneous strain and strain rate through the thickness in the roll-bite. The models for microstructural evolution have been incorporated and coupled with the thermal deformation simulation for A36, DQSK, HSLA-V, HSLA-NB, HSLA-Nb/Ti5O, HSLA-Nb/Ti8O, IF-Ti/Nb-rich and IF-Ti/Nb-lean steel grades. The predicted thermal history, deformation, roll forces, microstructural evolution and mechanical properties of the steel strip have been compared, with experimental and industrial mill measurements. The model developed proves to be accurate enough to give good predictions for the thermal, deformation and microstructure evolution during hot rolling of steel strip.

The latest version of HSMM 4.0, shown in Figure 1.1, contains roughing mill, finishing mill, runout table cooling and down coiling models for a Tandem hot strip mill; reversing roughing mill, reversing finishing mill and coil box / coil furnace models for a semi-continuous hot strip mill and a Steckel mill; and a deformation model for the simulation of deformation at each rolling stand. The eight grades which were studied are A36, DQSK, HSLA-NB, HSLA-V, two IF steels, HSLA-Nb/Ti5O and HSLA-Nb/Ti8O grades. Clearly, the effort required to develop models that can predict the thermomechanical and microstructural evolution for any mill with minimal tuning is formidable. The structure of the hot strip mill model is presented in Figure 1.2 and shows the submodels mentioned earlier and the relationship among them.

A TRIBUTE

On December 16th 1997, J. Keith Brimacombe, O.C., one of the finest metallurgical engineers on the world stage in this century passed away. Dr. Brimacombe pioneered the application of mathematical models, laboratory and industrial measurements, to shed light on complex metallurgical processes spanning both the steel and non-ferrous industries. For his ground-breaking research he has earned the reputation of being one of the most innovative intellectual giants in his field for which he received global recognition. He dedicated his career to developing the intellectual potential of young people and believed passionately in the importance of the human resource to the well being of a nation. Through his work he exemplified how universities should work with industry - by providing leadership in areas that are intellectually challenging and of long term benefit to the economy.

It was Dr. Brimacombe's scientific leadership and vision, which resulted in this project - Microstructure Engineering in Hot-Strip Mills, which he so ably led until his death last year. Beginning in the early eighties, working with Professor E. Bruce Hawbolt under the auspices of the Stelco/NSERC Chair, he developed the concept of microstructural engineering, calling it a marriage of mechanical engineering and physical metallurgy. He demonstrated the power of this approach for optimizing the solid state processing of steel through the development of the Stelmor model. The concept was subsequently extended to hot rolling of steel. Dr.Brimacombe's rare capacity to envision important directions for research and development placed him at the forefront of iron and steel research in the world. Dr. Brimacombe was not only a visionary but also a missionary. He believed passionately in translating research results into practical terms, which would benefit workers on the shop floor and lead to the creation of wealth. To fulfill this mission he travelled the world to every continent to share his knowledge with people - from company presidents to shop floor workers. He had a great love of life and thrived on human interaction. All of us who were privileged to have worked with him were inspired, challenged and transformed by having known him.

Professor Brimacombe's human qualities were deeply admired by those who knew him well. His strength of character, high principles, purity of will, deep concern for co-workers, warmth, humility and generosity of spirit were very special. Keith Brimacombe's sense of humour and love of life enriched every encounter one had with him. His ideals will live on through his many outstanding contributions and through the men and women he mentored in his life time. Larry Kavanagh, Vice-President of the American Iron and Steel Institute, had these words to say at the time of Dr. Brimacombe's passing, - " *Keith fulfilled the greatest calling of all - teaching. His thoughts and ideas had the power to change our industry - to challenge us and push us forward. He sharpened our minds and our principles, but most of all he was our friend and we'll miss him*". And indeed we do. He will remain deeply cherished in our collective memory.

FOREWORD

This project on Microstructure Engineering in Hot-Strip Mills, conducted over 5 years could not have been completed without the hard work and commitment of numerous students, staff and technicians. Dr. D.Q. Jin's extraordinary dedication to the development of the model and Dr. Militzer's intellectual leadership in the formulation of models to characterize microstructural evolution were critical to the successful completion of the project and we are most grateful to them. The efforts of B. Chau, X. Chen, who were responsible for the test work on the Gleeble and Torsion machines were also critical to the project and we are appreciative of their contribution. We would like to recognize the strong technical contributions of Dr.'s W.P. Sun, T. Cheng, Mr. S. Lechuk and Dr. Z. Wang, in the area of physical metallurgy and model development respectively. The technical support provided by R. McLeod and C. Ng in machining samples, R. Cardeno and P. Wenman in sample preparation is gratefully acknowledged. The following graduate students provided important intellectual input during the course of the project- A. Giumelli, R. Pandi, V.H. Avila, C.F. Huang, C. Muojekwu. The efforts of C.O. Hlady, C. Mui and G. Jope in the development of the interface of the hot- strip model are gratefully acknowledged. This task which was critical to the "user-friendliness" of the model was subsequently undertaken by Kent Alstad at Eclipse in Vancouver and Kent Ball in Pittsburgh and without them we could not have produced the robust version finally delivered to all the companies. We would like to thank Mary Jansepar from the Centre for her secretarial support in preparing reports, arranging meetings and helping with the numerous tasks associated with the project. We would also like to recognize the efforts of Carole Duerden and her assistance with administration of the project at UBC. The University of British Columbia deserves credit for their support of this project, especially Angus Livingstone at the University Industry Liaison Office whose assistance during the early stages of negotiation and throughout the course of the project were invaluable.

This project exemplified the importance of university industry interaction, which the late Keith Brimacombe was a strong proponent of, and we are most grateful for the enthusiasm and support of all the participating companies. We would particularly like to acknowledge the efforts of Paul Repas of U.S. Steel, Brian Nelson of Dofasco, Keith Barnes, Brian Joel and Dave Overby of Stelco, Oscar Lanzi of Inland Steel, and Steve Feldbauer of Geneva Steel for the invaluable input they have provided over the course of the five-year project. We are also grateful to all the companies for providing operating data and for their feedback following the workshops.

We are most appreciative of the financial support that we have received from the American Iron and Steel Institute and the Department of Energy over the five years. We have valued the assistance and support of Larry Kavanagh, and Joe Vehec in their capacity as successive Directors of the Advanced Control Program. The staff at the American Iron and Steel Institute, especially Lori, are warmly thanked for their efforts in arranging meetings and workshops.

TABLE OF CONTENTS

LIST OF FIGURES

LIST OF TABLES

EXECUTIVE SUMMARY

The current work was aimed at developing an integrated model which includes mathematical models of roughing mill, finishing mill, deformation in the roll-bite, runout out table cooling, down coiler and Steckel mill. These models can be used to predict the thermal history, deformation, roll forces, microstructural evolution and mechanical properties of steel strip in a hot-strip mill. The model has been extended to a Steckel Mill which has been developed by incorporating the reversing roughing mill model and the coil box model. Also, a down coiler model has been developed and incorporated into the runout table model. A finite-difference scheme was employed in the roughing model, finishing mill model, runout table cooling model and down coiler model. A finite-element model was utilized to provide a complete description of the temperature, inhomogeneous strain and strain rate through the thickness in the roll-bite. The models for microstructural evolution have been incorporated and coupled with the thermal deformation simulation for A36, DQSK, HSLA-V, HSLA-Nb, HSLA-Nb/Ti50, HSLA-Nb/Ti80, IF-Ti/Nb-rich and IF-Ti/Nb-lean steel grades. The predicted thermal history, deformation, roll forces, microstructural evolution and mechanical properties of the steel strip have been compared with experimental and industrial mill measurements. The model developed proves to be accurate enough to give good predictions for the thermal, deformation and microstructure evolution during hot rolling of steel strip.

The latest version of HSMM 4.0, shown in Figure 1.1, contains roughing mill, finishing mill, runout table cooling and down colling models for a Tandem hot strip mill; reversing roughing mill, reversing finishing mill and coil box / coil furnace models for a semi-continuous hot strip mill and a Steckel mill; and a deformation model for the simulation of deformation at each rolling stand. The eight grades which were studied are A36, DQSK, HSLA-Nb, HSLA-V, two IF steels, HSLA-Nb/Ti50 and HSLA-Nb/Ti80 grades. Clearly, the effort required to develop models that can predict the thermomechanical and microstructural evolution for any mill with minimal tuning is formidable. The structure of the hot strip mill model is presented in Figure 1.2 and shows the submodels mentioned earlier and the relationship among them.

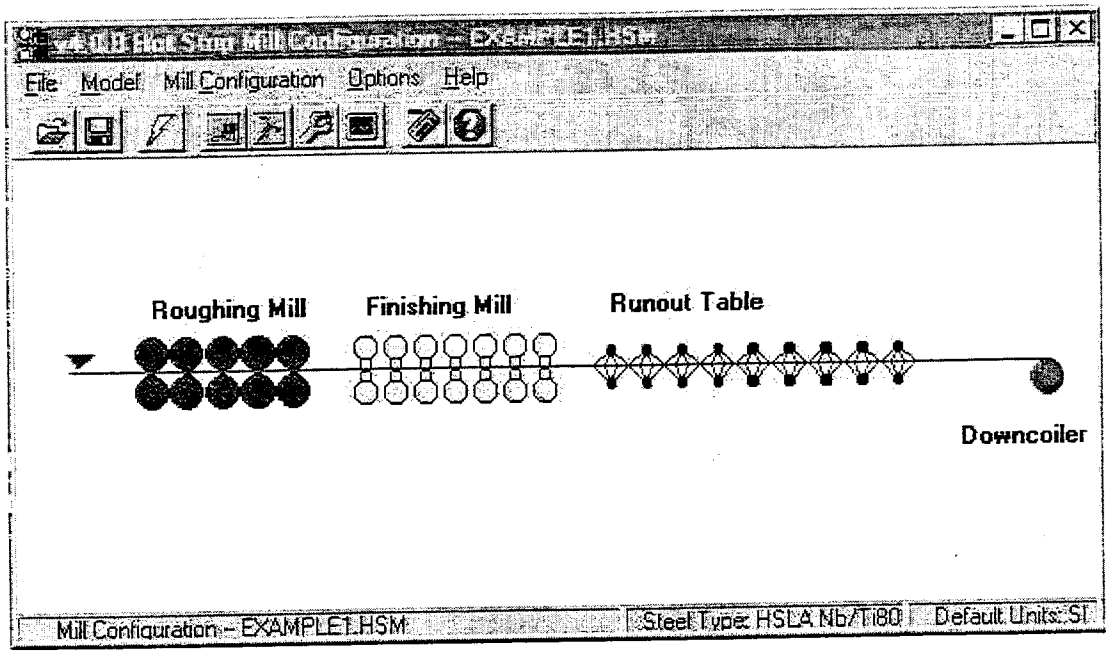

Figure 1.1. User interface of Hot Strip Mill Model

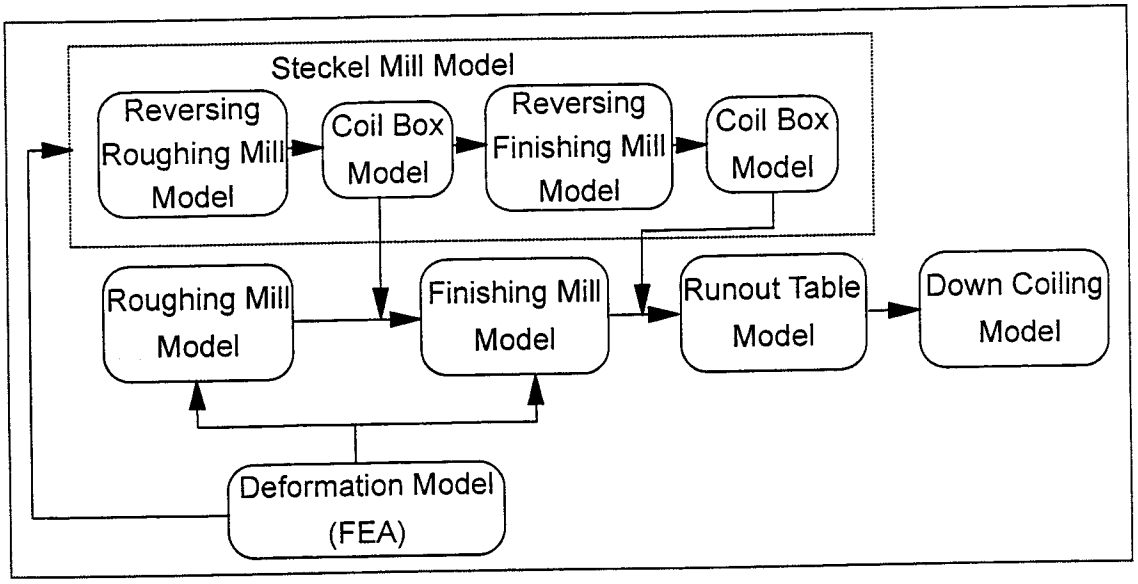

Figure 1.2. The structure of Hot Strip Mill Model

1.0. COMPUTER MODELING

1.1. Verification of Existing Temperature-Microstructure Model

Roughing Mill Temperature Model

In the roughing temperature range (1300°C to 1050°C), the slab is reduced in thickness from approximately 250mm to a 25~35mm transfer bar and the microstructure is refined by breakdown of the austenite grain size from 1000 μm to 200 μm during deformation and by static and dynamic recrystallization between passes. Oxide scale growth will have a significant influence on the strip temperature. In the temperature range (1100°C to 800°C) in which strip is processed in the finishing passes of a hot strip mill, austenite grain size is further refined to 10 -50 μm. A mathematical model developed by Chen et al. for Stelco has been modified to predict the thermal and microstructural evolution during rolling on a reversing or tandem roughing mill. In this model the effects of scale on the surface of the strip have been ignored because it is assumed to be in the 1-10μm range. The model assumes uniform strain and strain rate through the thickness and the deformation heat is also distributed uniformly in the strip.

A roughing or a finishing mill configuration includes descalers, rolling stands, backwash sprays and interstand sprays. The interrelationship between temperature, deformation and micro-structure development suggests that an overall model requires a high level of sophistication and coupling. A finite-difference scheme has been applied to the thermal calculation in these models.

The governing heat conduction equation for the strip is expressed as follows:

$$\frac{\partial}{\partial x}\left(k\frac{\partial T}{\partial x}\right)+\frac{\partial}{\partial y}\left(k\frac{\partial T}{\partial x}\right)-\rho C_p u\frac{\partial T}{\partial x}-v\frac{\partial T}{\partial y}+Q_p=0 \qquad (1.1)$$

where Q_p is the heat generation due to the deformation in the roll bite. For the free surfaces at each side of the roll bite, the boundary conditions were specified as

$$-k\frac{\partial T}{\partial y}=h_r\left(T-T_o\right) \qquad (1.2)$$

where h_r is the combined heat transfer coefficient for radiation and natural convection and obeys the Stefan-Boltzmann law.

The heat transfer coefficient between workroll and strip was determined from experimental measurements by Chen et. al. on a laboratory and pilot rolling mill and is expressed as a function of mean pressure.

$$H_{rs}=\left(696.5p-34396\right) \qquad (1.3)$$

where p is the mean pressure in MPa, and H_{rs} is the heat transfer coefficient between work roll and strip in W/m^2 °C. The heat transfer coefficients for the convection and water cooling which were used for descalers, interstand sprays and backwash spray were described by Devadas et al. In the roll bite the thermal model of the strip is coupled to a detailed heat-transfer model of the rolls. The governing equation for rolls was expressed as

$$\frac{1}{r}\frac{\partial}{\partial r}\left(rk_r\frac{\partial T_r}{\partial r}\right) = \rho_r C_{pr}\frac{\partial T}{\partial t} \tag{1.4}$$

The heat transfer coefficient for the work roll cooling varied with the roll cooling modes as described by Devadas et al.

In roughing, reversing roughing and finishing mills, oxide scale growth plays an important role in temperature prediction due to the long transfer time and is described by Chen et. al. The parabolic rate law was applied to describe the growth rate

$$\frac{dx}{dt} = \frac{k_p}{x} \tag{1.5}$$

where x is the oxide scale thickness and k_p is the parabolic rate constant and according to Paidassi's study, total growth rate can be expressed by

$$k_p = 3.05\exp\left(\frac{40500}{RT}\right)\left(cm^2 s^{-1}\right) \tag{1.6}$$

The traditional Sim's equation has been employed to calculate the roll forces as follows:

$$F = \frac{2}{\sqrt{3}}\sigma Q_p\sqrt{R'\Delta h} \tag{1.7}$$

Here, deformed work roll radius is

$$R' = R(1.0 + \frac{16}{\pi E'}\frac{F}{\Delta h}) \tag{1.8}$$

Parameters in Sim's equation are calculated as follows:

$$Q_p = \frac{\pi}{2f(h)}\tan^{-1} f(h) - \frac{\pi}{4} - \left(\frac{\sqrt{R'/h_2}}{f(h)}\right)\times\left[\ln\left(\frac{2R'(1-\cos\phi)+h_2}{h_2}\right) + \frac{1}{2}\ln(1-r)\right]$$

$$\phi = \tan\left[\frac{\pi\ln(1-r)}{8\sqrt{R'/h_2}} + 0.5\tan^{-1} f(h)\right]/\sqrt{R'/h_2} \tag{1.9}$$

where r is reduction and $\Delta h = h_1 - h_2$, $f(h) = \sqrt{r/(1-r)}$.

The equations for recrystallization kinetics, austenite grain size and grain growth have been developed by other researchers and details of the measurements conducted to obtain the equations are referred to in each case. It was found that large grain austenite (d>240μm) behaves differently from austenite with smaller grain sizes and recrystallization kinetics and the boundary between static and metadynamic recrystallization is altered.

A finite-difference scheme has been applied to compute the thermal history of the strip and the work roll during rough rolling. The model assumes uniform deformation in the roll-bite. The Roughing Mill Model has been incorporated into the process model and released on May 13, 1996 with HSMM Version 3.2 for A36 and DQSK steel grades and other six steel grades were added later.

Detailed thermal, deformation and microstructure evolution models, program structure and numerical scheme are presented in the "Roughing Mill Model - Theoretical Manual".

A typical schedule for rough rolling is shown in Figure 1.3 for a HSLA-Nb/Ti80 steel coil. As many as 20 points along the workpiece can be tracked at the same time. If there is a coilbox attached at the end of rougher, the information regarding the coilbox setup has to be entered as shown in Figure 1.3c. Prediction of the thermal history of the strip during rough rolling for a HSLA-Nb steel coil received from U. S. Steel is presented in Figure 1.4 (Coil #544726). Assuming that the initial oxide scale thickness on the slab from the reheating furnace is 2mm, the model calculates a scale thickness of 0.06mm at the exit of the roughing mill (pyrometer location) (Figure 1.6). The comparison of temperature predictions from the roughing mill model for various steel grades at two companies is presented in Figure 1.5. Measured roll forces have been employed for the thermal calculations for HSLA-Nb and V steels. Good agreement is evident between prediction and measurements.

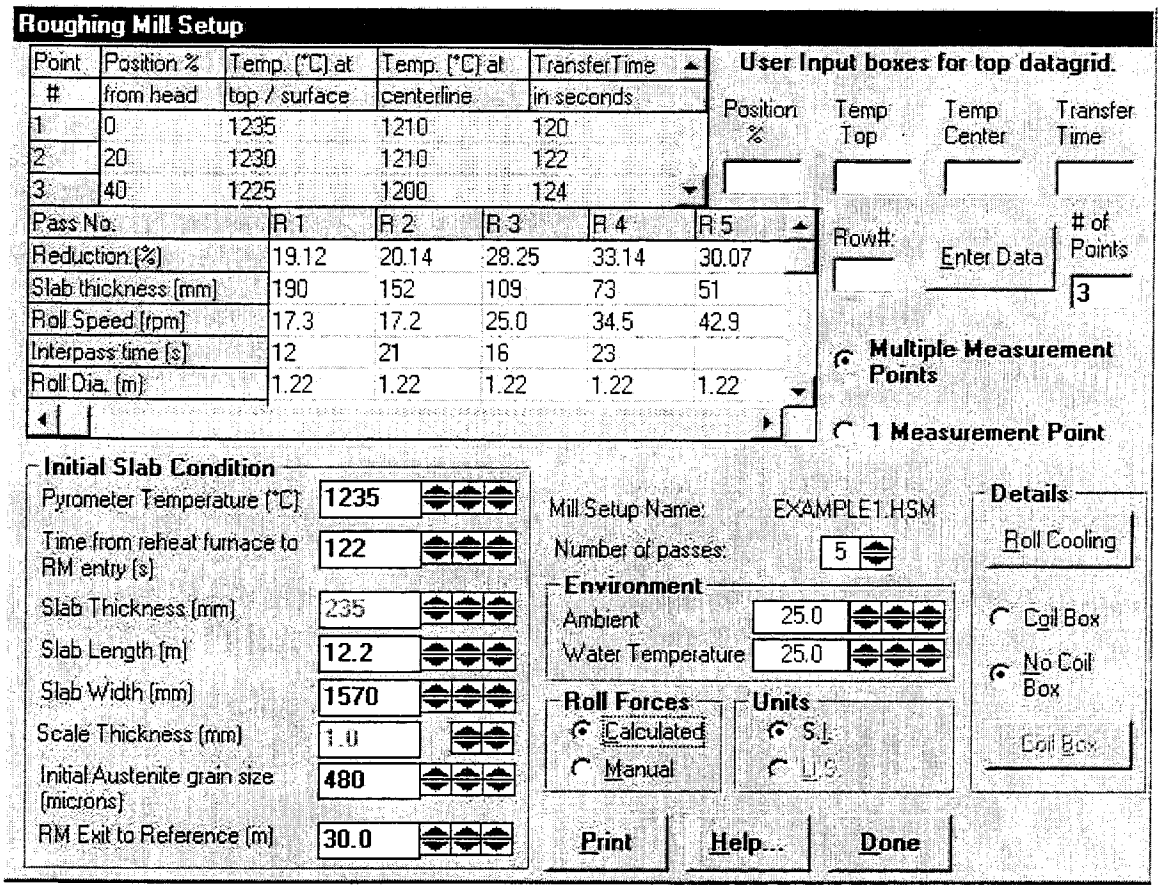

Figure 1.3a. A typical rolling schedule of roughing mill for a HSLA-Ti/Nb80 steel.

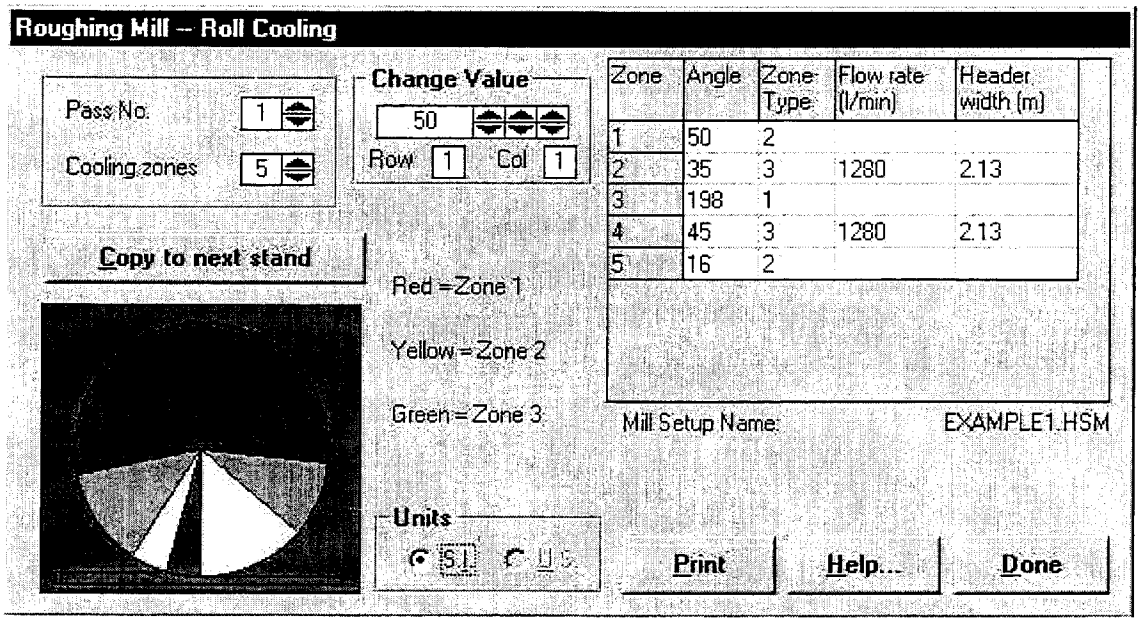

Figure 1.3b. Roughing mill setup - Roll cooling.

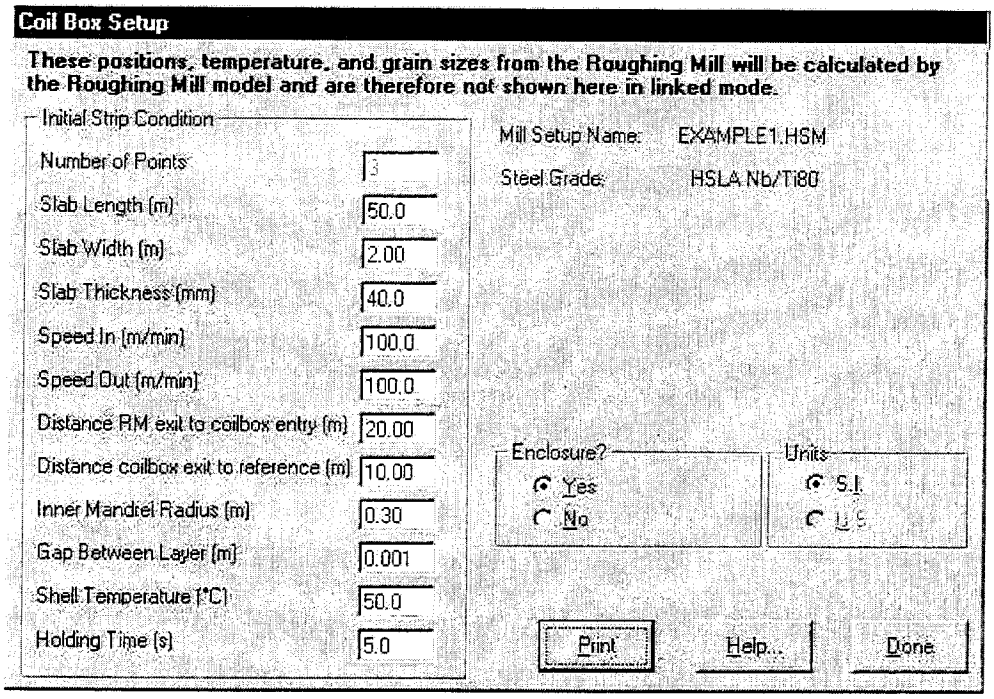

Figure 1.3b. Roughing mill setup - Coil box.

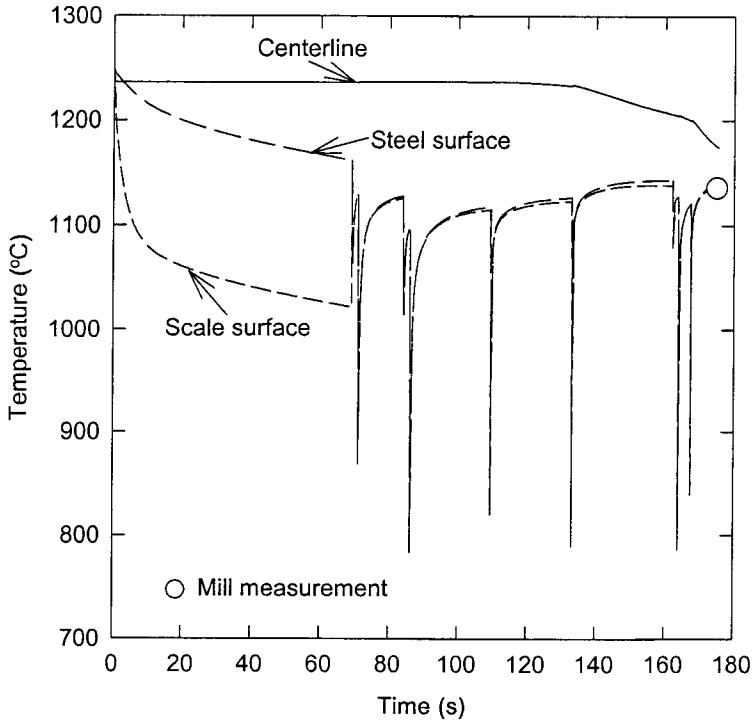

Figure 1.4 Thermal history during rough rolling for HSLA-Nb steel. (Coil #544726, USS)

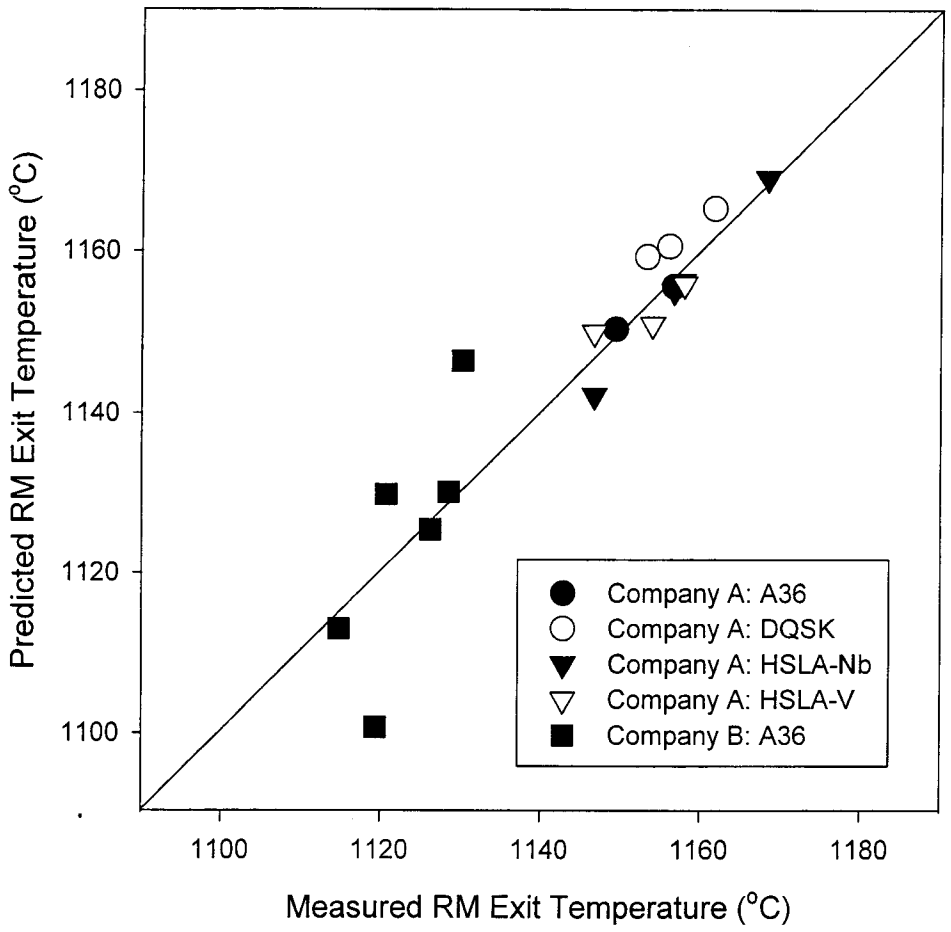

Figure 1.5. Comparison of predicted roughing mill exit temperature with mill measurements.

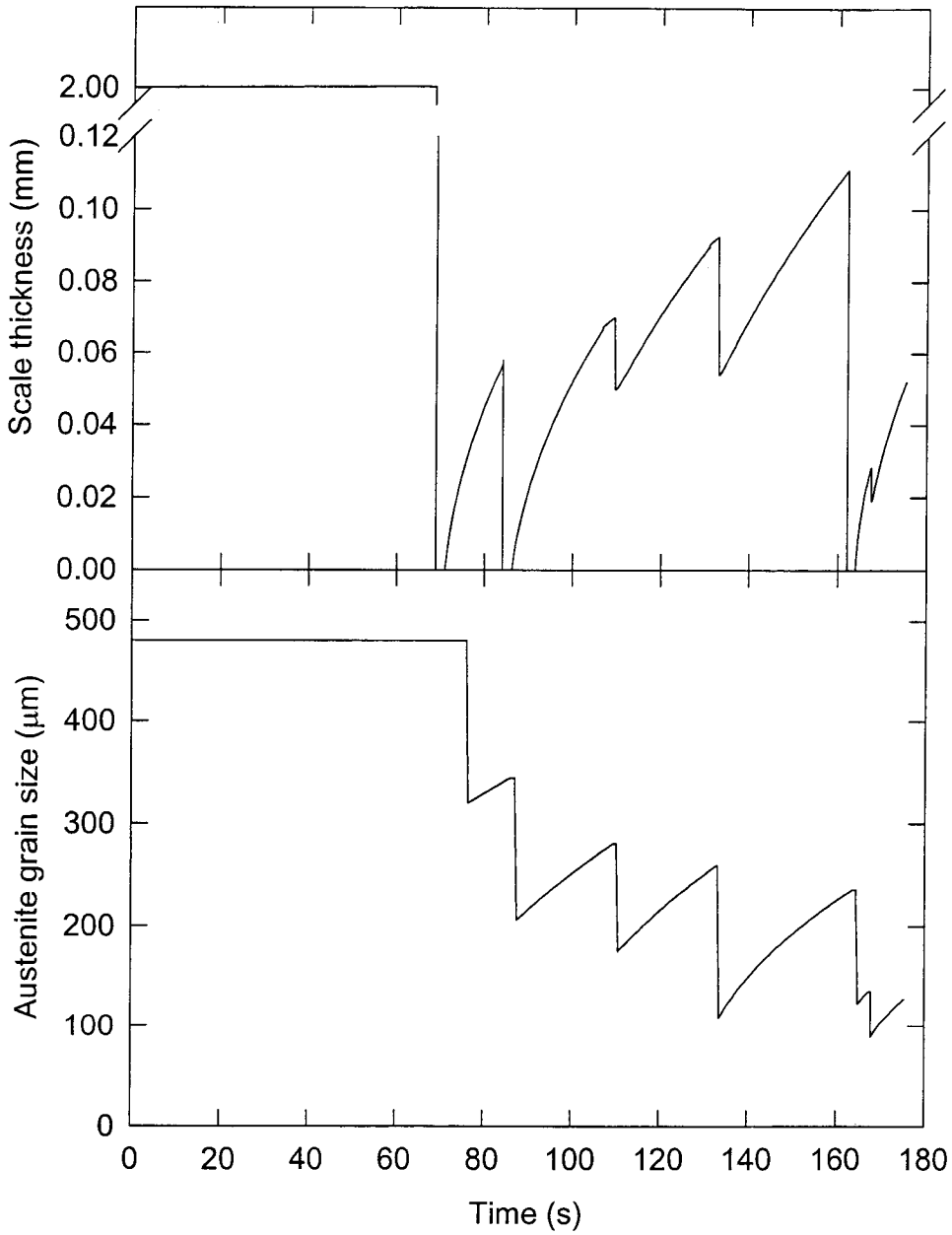

Figure 1.6. Time-oxide scale growth and time-austenite grain size profiles predicted by roughing mill model during 6-pass rough rolling for a HSLA-Nb steel.

Coilbox Model

Coilbox model was developed based on the program provided by Stelco Inc.. The detailed thermal model was described in the "Coilbox Model - Theoretical Manual". Microstructure evolution model which was employed in the coilbox model can be found in Roughing Mill Model - Theoretical Manual".

The setup screen is shown in Figure 1.7. As many as 20 points can be tracked at the same time along the strip length. In the coilbox operation, the head of the workpiece at the coilbox entry will become the tail at the coilbox exit. The top surface of the strip at the coilbox entry will become the bottom surface of the strip at the coilbox exit. Workpiece temperature through the thickness is given in the output file for six points from top surface to the bottom surface (Figure 1.8).

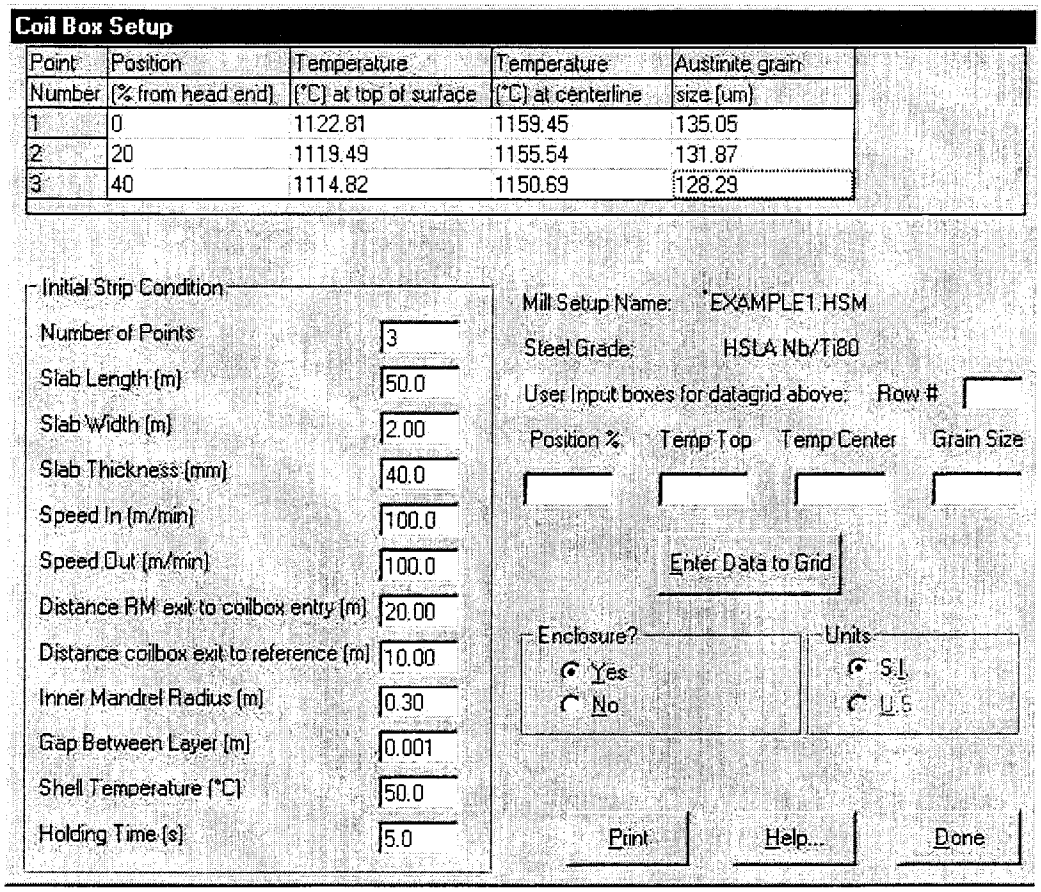

Figure 1.7. Coilbox Model Setup.

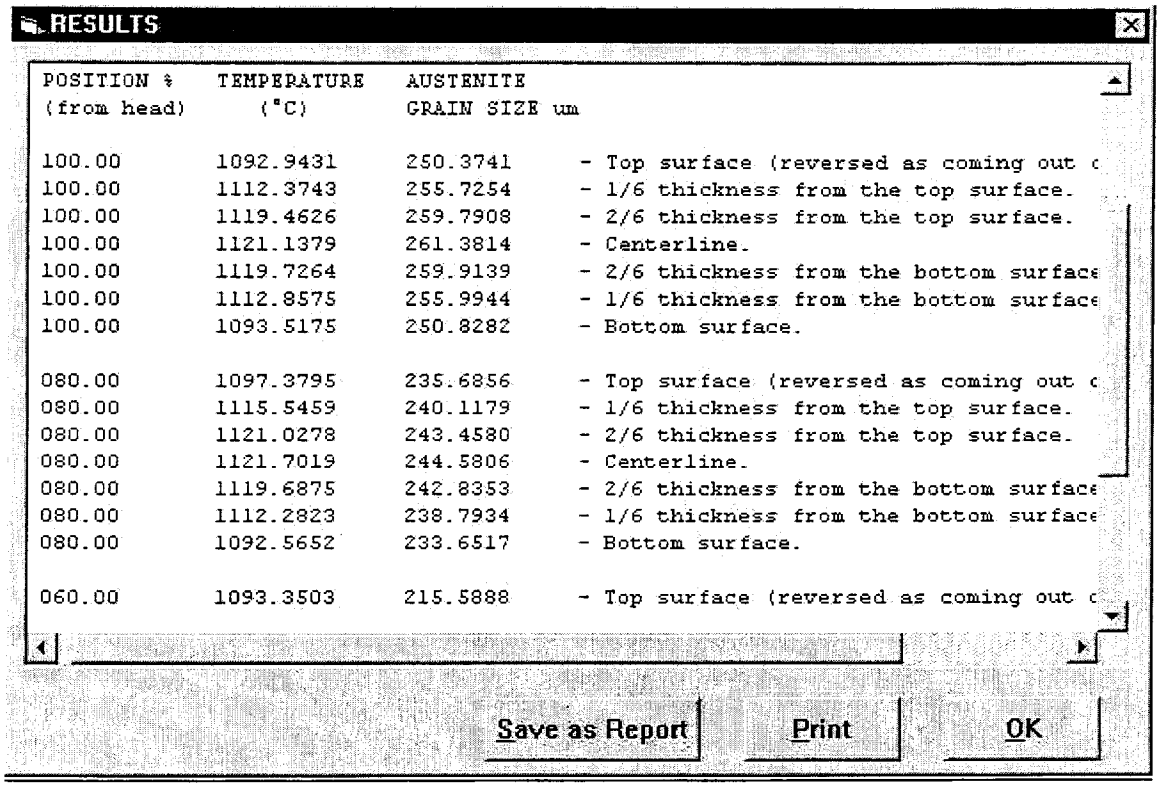

Figure 1.8. Temperature through the workpiece thickness at the coilbox exit.

Finishing Mill Temperature Model

The finishing mill model is based on the work of Devadas and Samarasekera. A finite-difference scheme has been applied to compute the thermal history of the strip and work roll during finish rolling. The model assumes uniform deformation in the roll-bite and predicts the microstructure evolution. Detailed thermal, deformation and microstructure evolution models, program structure and numerical scheme which were employed are presented in the "Finishing Mill Model - Theoretical Manual". User instructions were described in the "Hot Strip Mill Model - User Manual".

Typical input screens for the finishing mill model are shown in Figure 1.9 illustrating the level of detail needed to run the model. The model requires data on mill geometry and allows for a variable number of stands, interstand sprays and descale sprays. A flexible workrolling cooling model was developed to allow users to place the sprays and setup the spray cooling conditions for each individual workroll. The calculation of workroll heat transfer is coupled with thermal and deformation analysis of the workpiece. The calculated work roll surface and strip surface temperatures will be used to determine the heat flux between the workroll and workpiece. An iterative approach was employed for the numerical calculation and work roll surface and workpiece surface temperatures are defined until the steady state conditions are reached. There are five types of work roll materials available which give the different thermal-mechanical properties for the calculation of heat transfer (Figure 1.9b).

The strip thickness is reduced from 38 mm to 3.6 mm for this HSLA-Nb coil. The predictions of temperature and austenite grain size for this HSLA-Nb coil are shown in Figure 1.10. The influence of the descale sprays and rolls on strip surface temperature is clearly evident. Good agreement was obtained both with measured and predicted finish mill exit temperatures. A comparison of predicted and measured finishing mill exit temperature for various steel grades with different conditions from three steel companies is shown in Figure 1.11. For most coils, model predictions are within ±20 °C with the exception of the thin gauge coils (final strip thickness less than 2.5 mm). In these cases the assumption of uniform temperature through the workpiece thickness is less accurate than for thick coils and the temperature rise due to deformation heat at the strip surface is consequently underpredicted.

During finishmill rolling of HSLA-Nb steel, recrystallization is not completed for most interpasses and the strain is accumulated, especially for later passes (Figure 1.12). Predictions of austenite grain size are around 10μm. An example of the predictions of rolling load which was compared with industrial measurement is shown in Figure 1.13. There is good agreement for all eight steel grades except for some coils in which precipitation may play an important role under those rolling conditions.

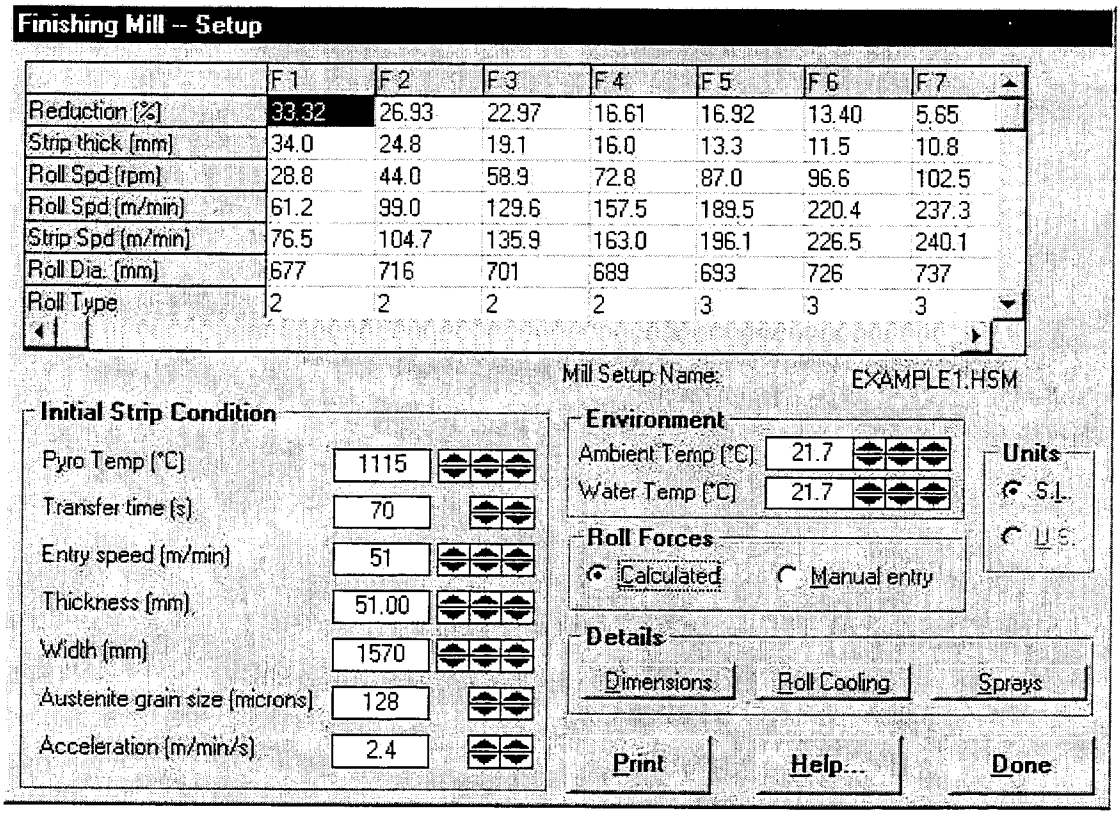

Figure 1.9a. Finishing mill setup - Rolling schedule of a HSLA-80Nb/Ti steel.

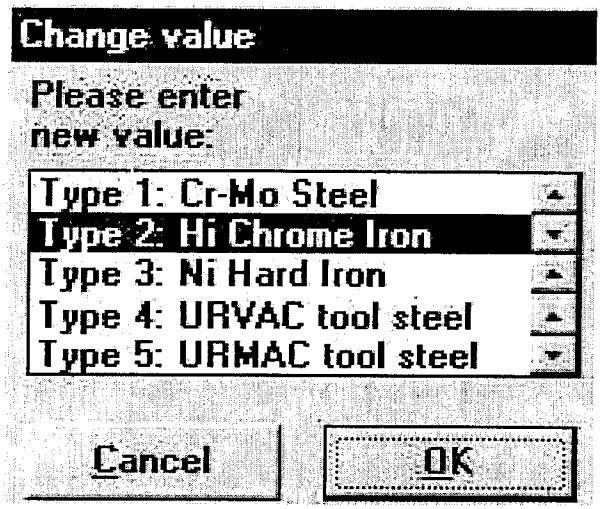

Figure 1.9b. Finishing mill setup - Work roll type.

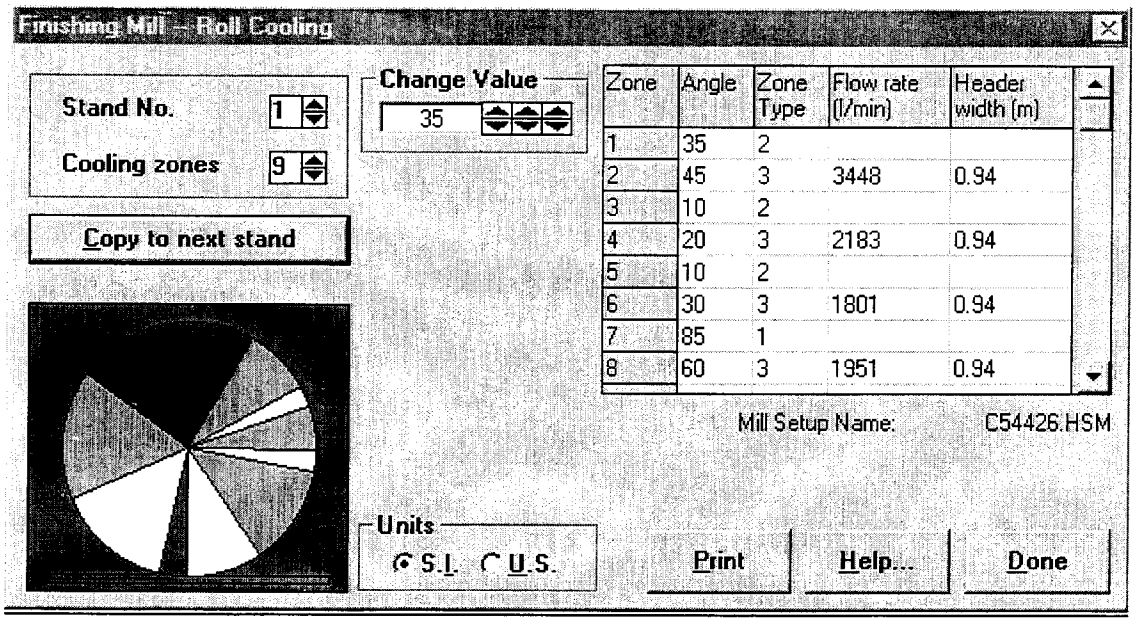

Figure 1.9c. Finishing mill setup - Work roll cooling.

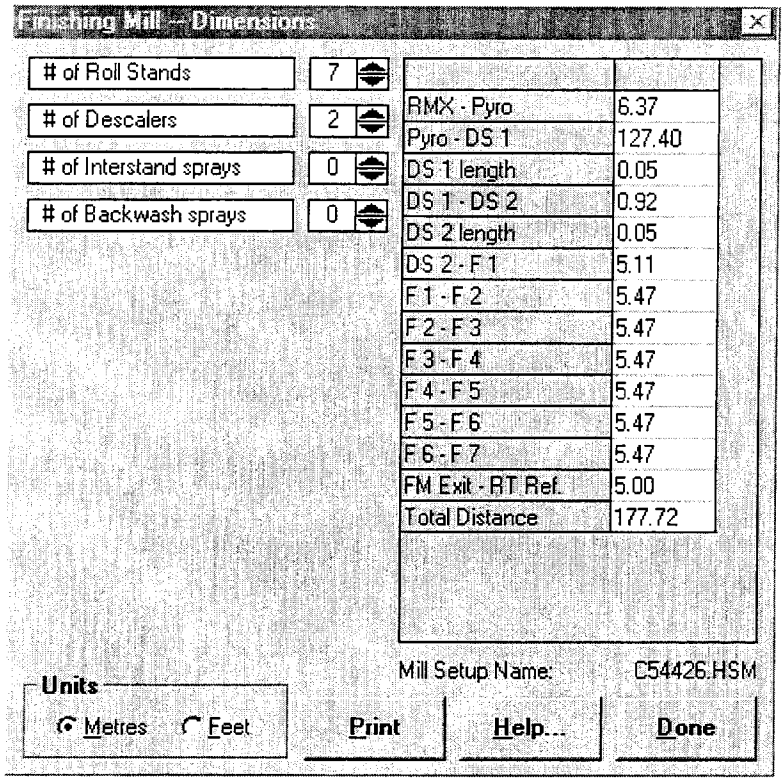

Figure 1.9d. Finishing mill setup - Dimensions.

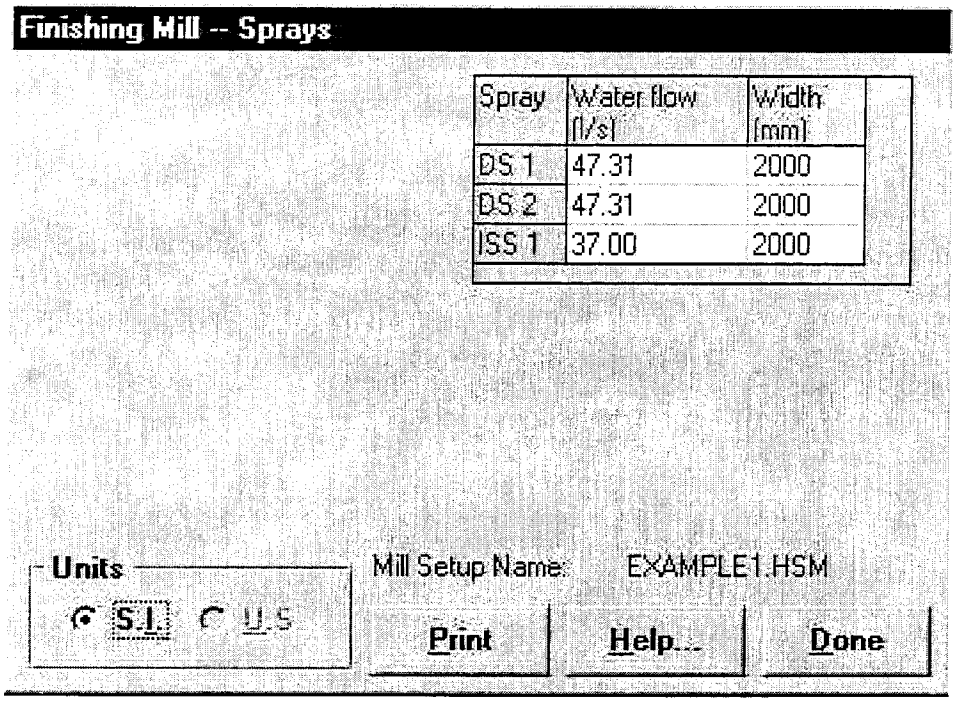

Figure 1.9e. Finish mill setup - Spray water flow.

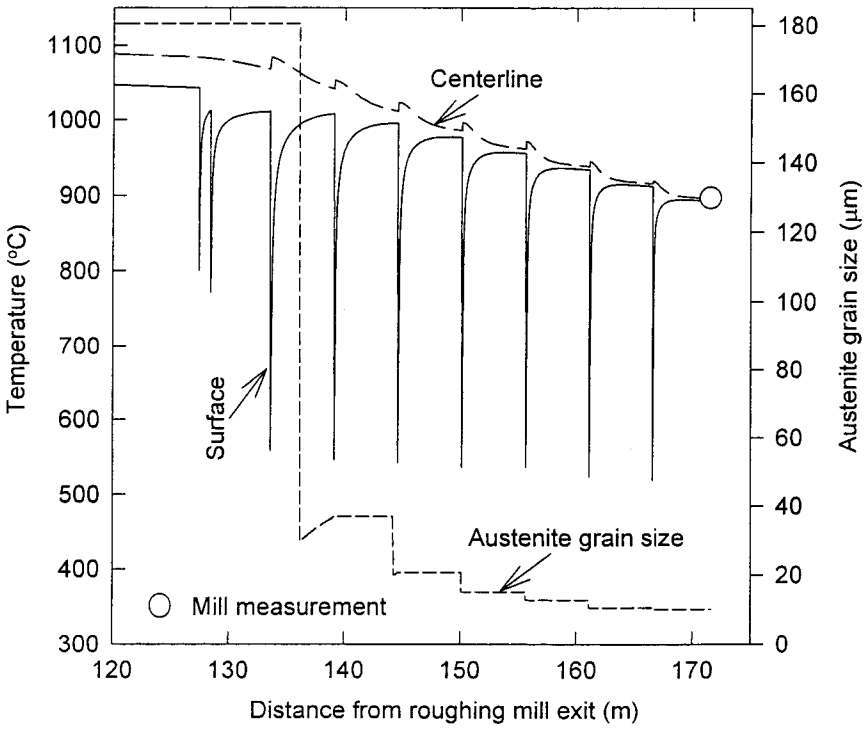

Figure 1.10 Predictions of thermal history and austenite grain size for a HSLA-Nb steel coil (Coil #565695).

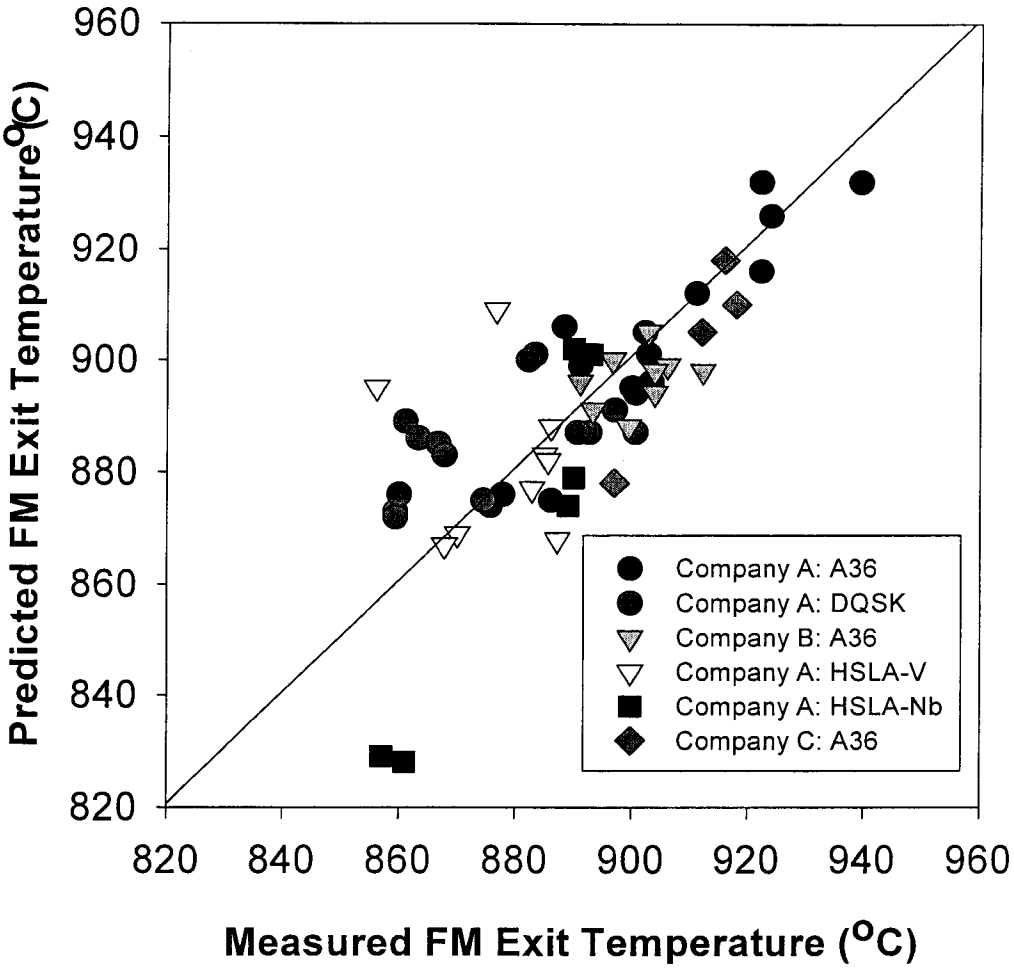

Figure 1.11 Comparison of predicted and measured finishmill exit temperature.

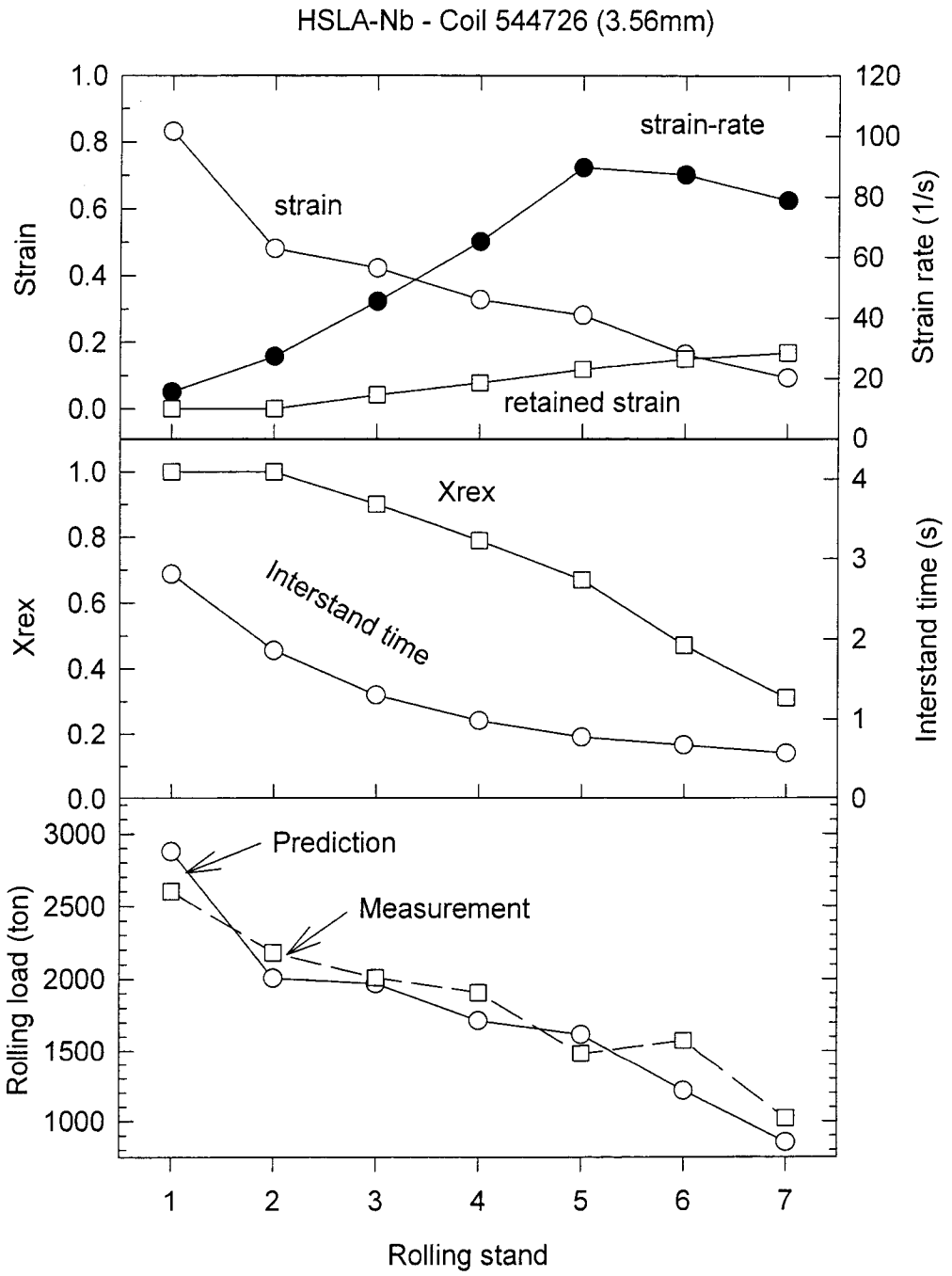

Figure 1.12 Predictions of strain, strain-rate, retained strain, fraction of recrystallization, and rolling loads during 7-pass finishmill rolling.

Runout Table Cooling Model

The runout table which follows the last finishing stand permits the strip to be conveyed to the coiler and utilizes water cooling to reduce the temperature from the finishing temperature of 800-950 °C to the coiling temperature of 510-750 °C. Runout tables are usually designed so that the strip cooling is carried out in three stages. Air cooling occurs between the last finishing stand and the first bank of sprays, followed by accelerated cooling under successive banks, and then air cooling prior to coiling. Usually, the sprays are grouped into sections, each section being controllable so that the desired coiling temperatures may be realized. Cooling is primarily from the boiling mode which is more stable than transition boiling. The surface temperature must be allowed to rebound before the strip comes under the next jet. Under each jet the heat transfer is largely transition boiling and high rates of heat extraction prevail which cause a significant reduction in surface temperature. The rate of thermal recovery is dependent on strip thickness, the degree or density of cooling and the time available for recovery before reaching the next jet or bank. The goal is to develop a fine-grained ferrite structure by rapid cooling through the austenite to ferrite transformation range and to avoid an acicular microstructure.

A more detailed description of this model has been given in the "Runout Table Cooling Model - Theoretical Manual", and only the general equations are presented here. The model solves the heat-conduction equation in the thickness direction:

$$\rho C_p \frac{\partial T}{\partial t} = \frac{\partial}{\partial x}\left(k \frac{\partial T}{\partial x} \right) + g \tag{1.10}$$

subject to the initial condition:

$$t = 0, 0 \le x \le L_s, T = T_0(x) \tag{1.11}$$

and boundary conditions:

$$x = 0; -k\frac{\partial T}{\partial x} + h_0 T = h_0 T_{\infty,0} \tag{1.12}$$

$$x = L_s;\ k\frac{\partial T}{\partial x} + h_{L_s} T = h_{L_s} T_{\infty,L_s} \tag{1.13}$$

The Crank-Nicholson finite-difference scheme was employed to solve the equations.

Transition boiling is assumed to be the dominant mode of the heat transfer in the jet impingement zone which is considered to be approximately 2.6 times the jet diameter; and outside this zone cooling is assumed to be due to film boiling. A heat generation term was computed from the phase transformation model. Transition boiling was

computed with the macrolayer dryout mechanism and the interfacial heat flux for transition boiling being written as follows:

$$q_{TB} = q_{l-s}F + q_{v-s}(1-F) \tag{1.14}$$

where $F = L / L_B$ is fractional area of liquid-solid contact, $q_{l\text{-}s}$ and $q_{v\text{-}s}$ are the heat fluxes during the liquid-solid and vapor-solid contacts respectively. The parameter F is calculated by the ratio of the area directly in contact with the liquid over the total area of the vapor. The model was run with 100 through-thickness nodes and a variable time step depending on the cooling zone to achieve the convergence.

The phase transformation kinetics for eight grades of steel have been developed by researchers at the University of British Columbia. The model also computes the yield and ultimate tensile strengths based on the IRSID equations which not only include the effects of chemistry and ferrite grain size but also takes into account the fraction of ferrite and pearlite in the final microstructure.

Figure 1.13 describes the run-out table configuration, water jet activity and initial parameters. A conventional runout table model and a flexible runout table model were developed to meet the needs of different types of runout table cooling devices. With the flexible runout table model, users can set up the runout table cooling sprays for each bank unit if there are any dimensional and operational differences on water sprays for the different water banks. Water heights from bottom sprays are optional for those runout tables in which water from the bottom sprays flows out with a high pressure.

A finite-difference scheme has been applied to the analysis of thermal history of strip during runout table cooling. Figure 1.14 shows the thermal history from finishmill rolling to runout table cooling for an A36 steel coil (Coil #934848, 9.8mm). Cooling rate at the strip centerline is predicted to be as high as 300°C/s for a 2.6 mm coil (Figure 1.15), 125 °C/s for a 6.2mm coil (Figure 1.16) and 78 °C/s for a 9.8mm coil (Figure 1.17). Cooling rate at the one-tenth strip thickness from the top surface and from the bottom surface are also given in Figure 1.15-1.17 for these three coils which shows that cooling rate ranges from 600 to 8000 °C/s for the top surface and 400 to 1750 °C/s for the bottom surface. The cooling effect from the top water jets is greater than that from the bottom because the water flow from the top jets is accelerated by gravity and an air cooling zone exists due to the water falling off the strip. Feedback from users has helped to eliminate coding errors and bugs from the program resulting in improved accuracy.

The model has been checked against the predictions for U.S. Steel, National Steel, Lukens, Stelco, Dofasco, Ipsco and ACME for eight steels. There is good agreement for a range of conditions from various steel companies for coiling temperature (Figure 1.18). In most cases model predictions are within ± 20°C with a relatively few points lying outside this band. Heat generation by phase transformation also plays an important role in runout table cooling. A slight difference in the steel's chemical composition may affect the phase transformation start temperature and the thermal history of the strip during run-out table

cooling. Model predictions have shown that the microstructure is sensitive to coiling temperature and cooling rate.

The model is being tested to examine its capability to predict final mechanical properties for the grades under study. A down coiler model has been developed and incorporated into the process model to predict the thermal profile, precipitation strengthening and phase transformation in the case of incomplete phase transformation on the run-out table cooling, especially for HSLA steel grades. The temperature profile during runout table cooling for a typical HSLA-V coil (Coil # 480733, 4.0mm) from USS is presented in Figure 1.19 which shows good agreement with measured coiling temperature. Examples of the microstructure and property variation through the strip thickness for this HSLA-V steel coil are shown in Figures 1.20 and are in an reasonable agreement with measured ferrite grain size, ductility, yield strength and tensile strength. The microstructure predictions close to the top surface, is not reliable in this case owing to the high cooling rate which is out of the range for which the equations were developed.

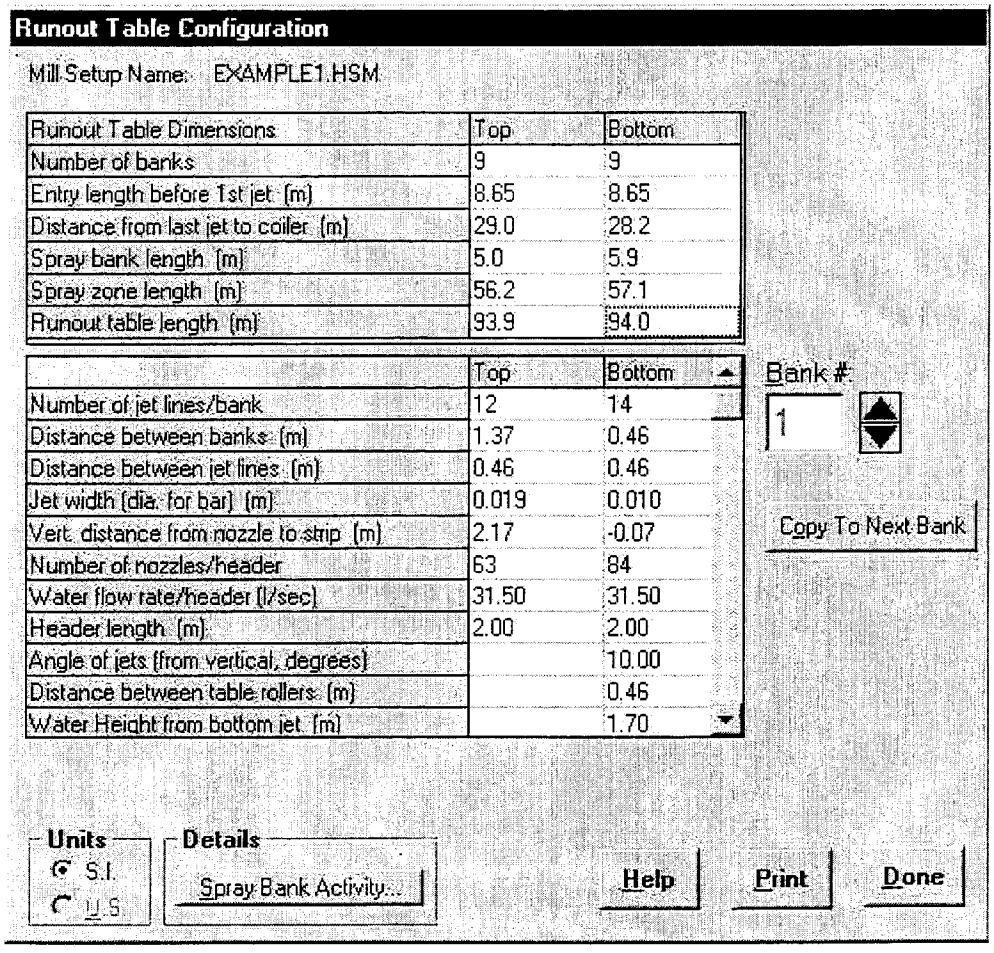

Figure 1.13a. Runout Table Setup - Configuration

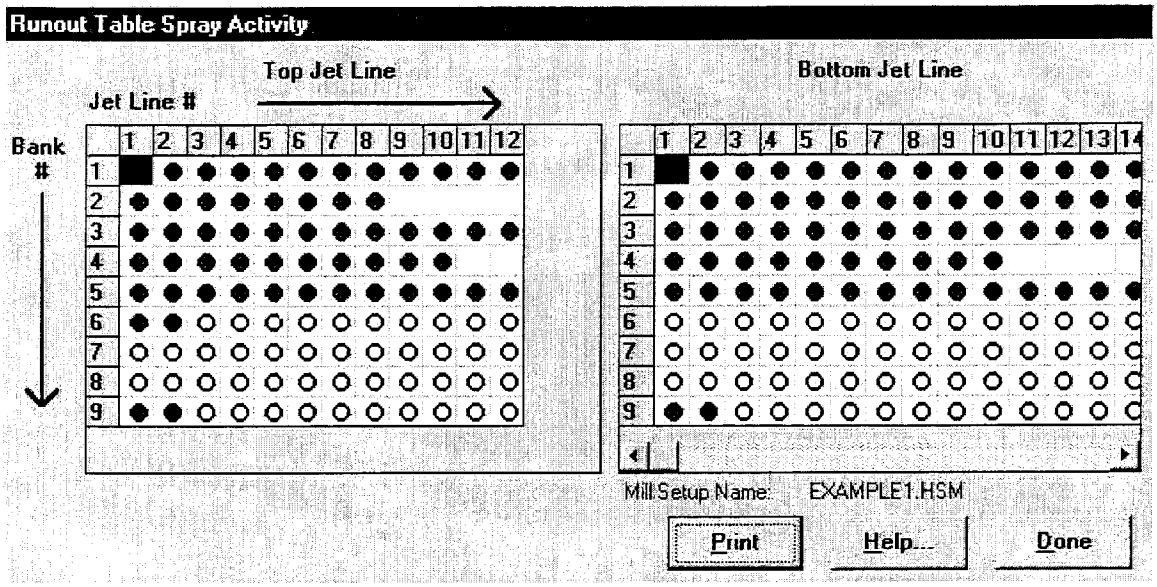

Figure 1.13b. Runout Table Setup - Water jet activity.

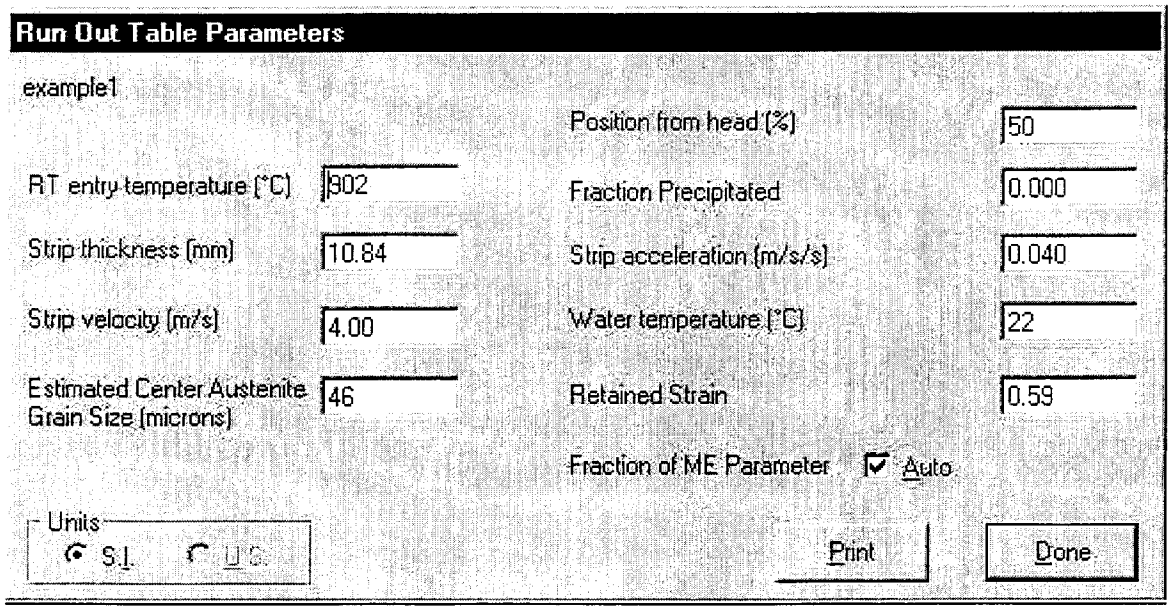

Figure 1.13c. Runout Table Setup - Initial parameters.

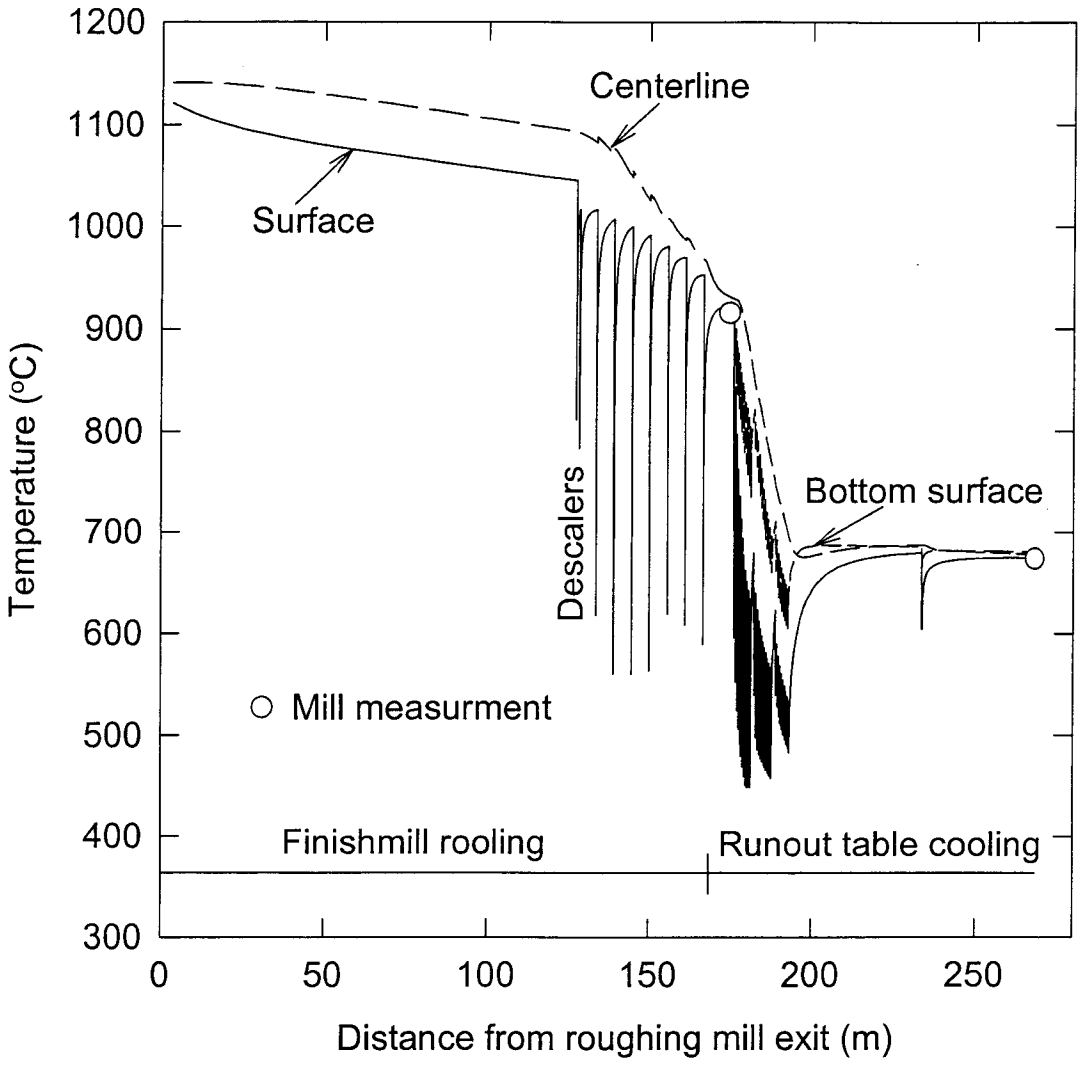

Figure 1.14 Thermal history from finishmill rolling to runout table cooling for 0.17% carbon steel with regular rolling schedule and temperature 1121°C at roughing exit.

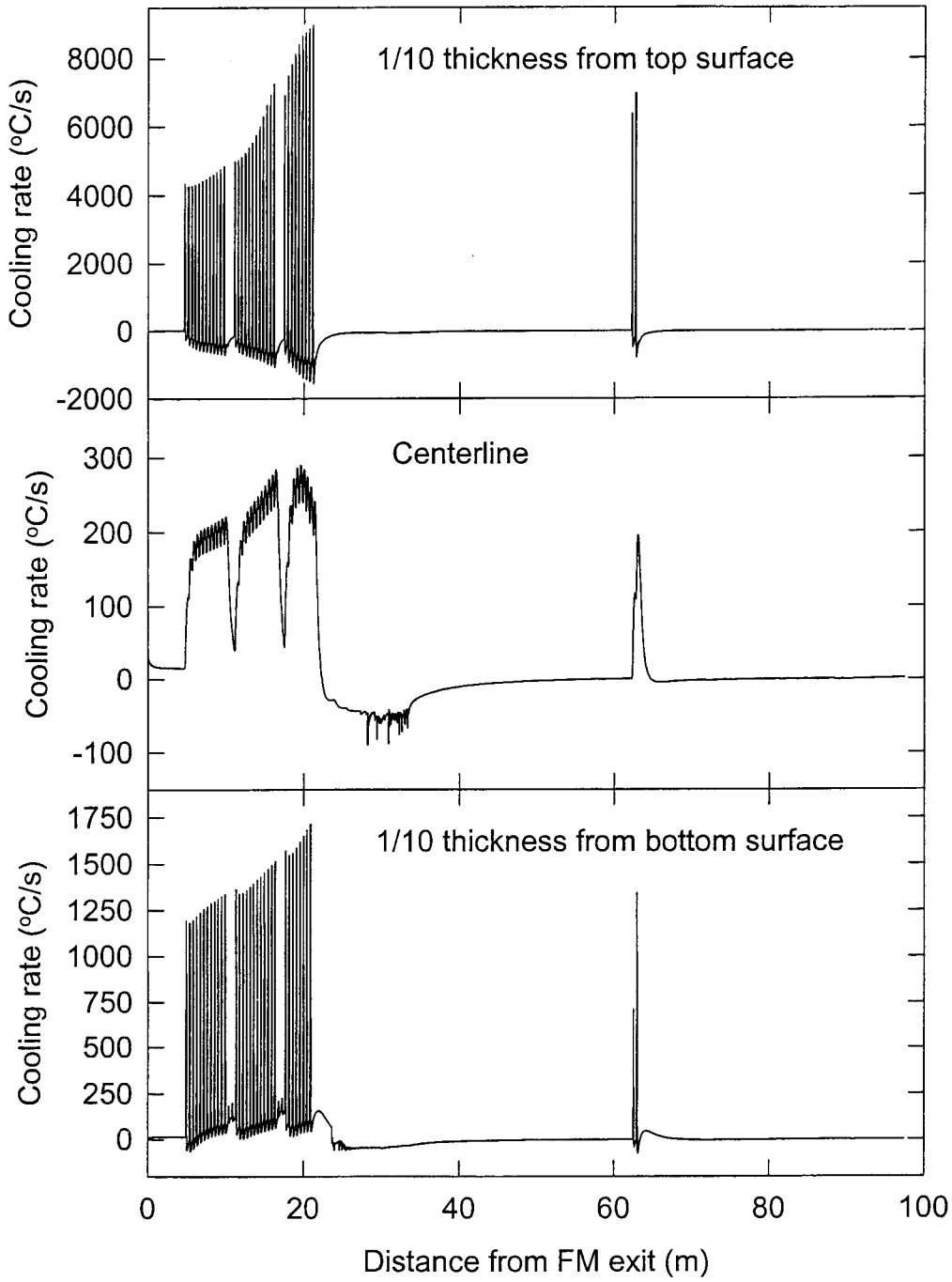

Figure 1.15 Cooling rate at different location through the thickness for 0.17 pct. carbon steel during ROT cooling (2.6mm).

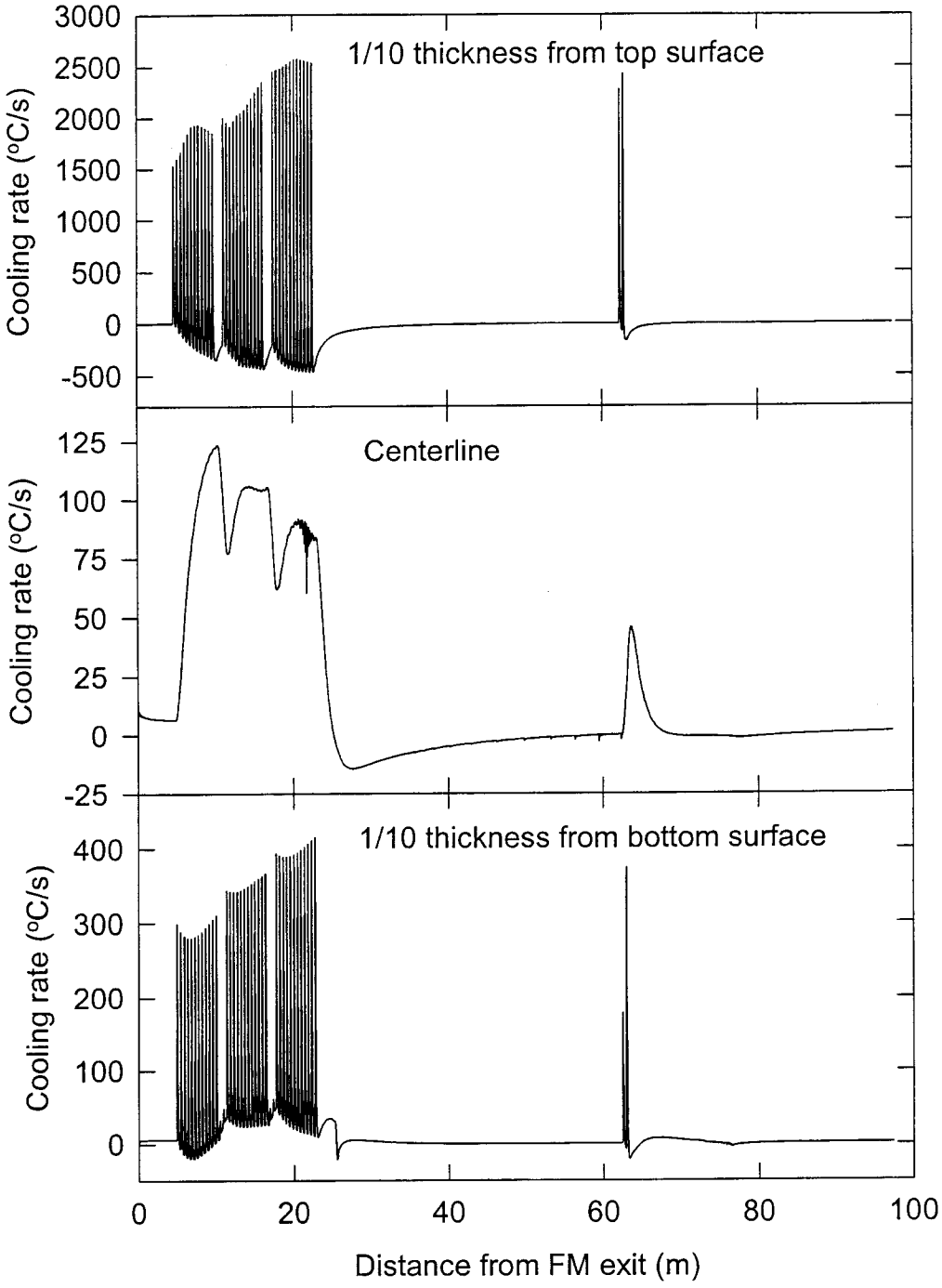

Figure 1.16 Cooling rate at different location through the thickness for 0.17 pct. carbon steel during ROT cooling (6.2mm).

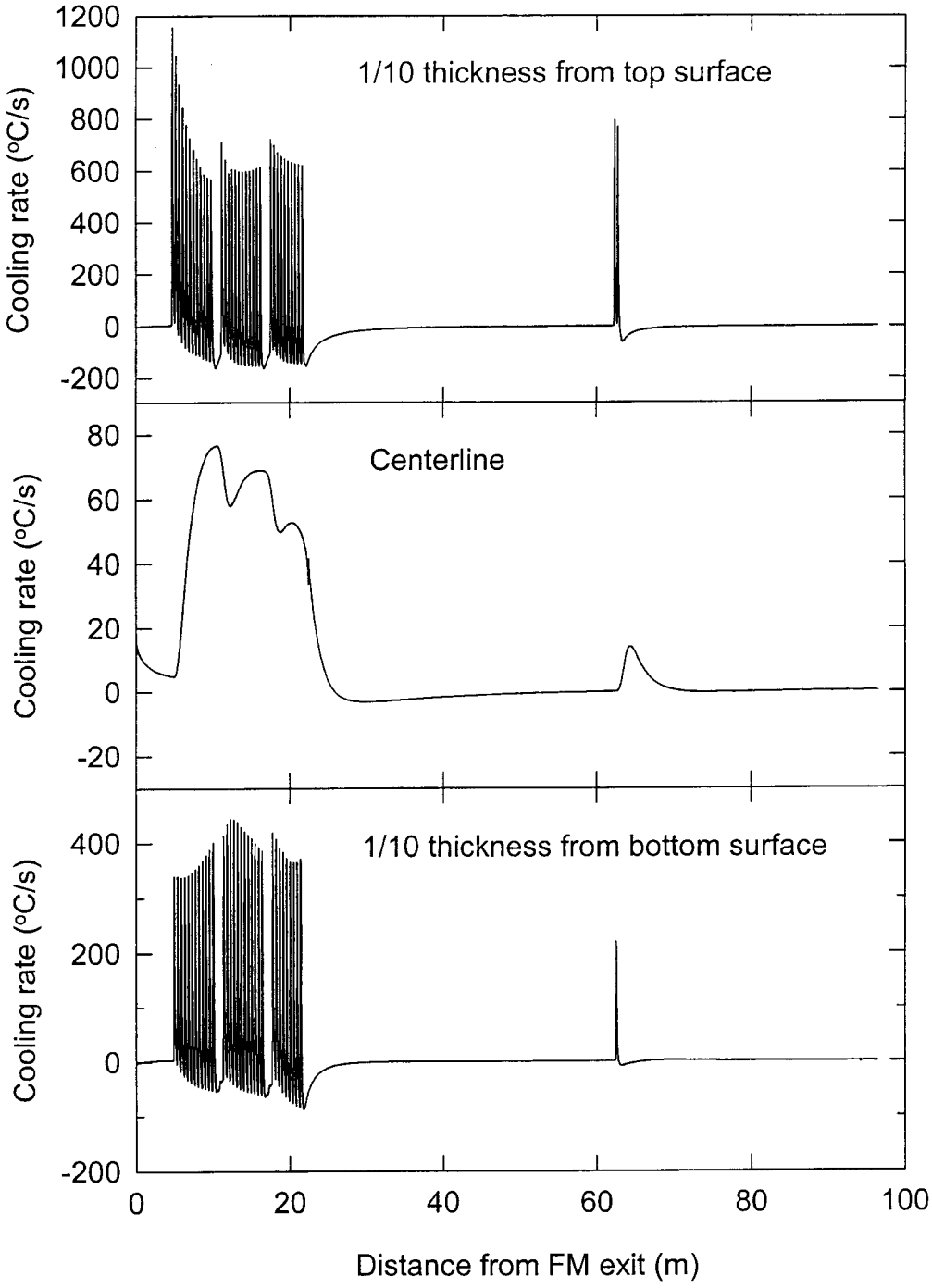

Figure 1.17 Cooling rate at the different position through the thickness for 0.17 pct. carbon steel during ROT cooling (9.8mm).

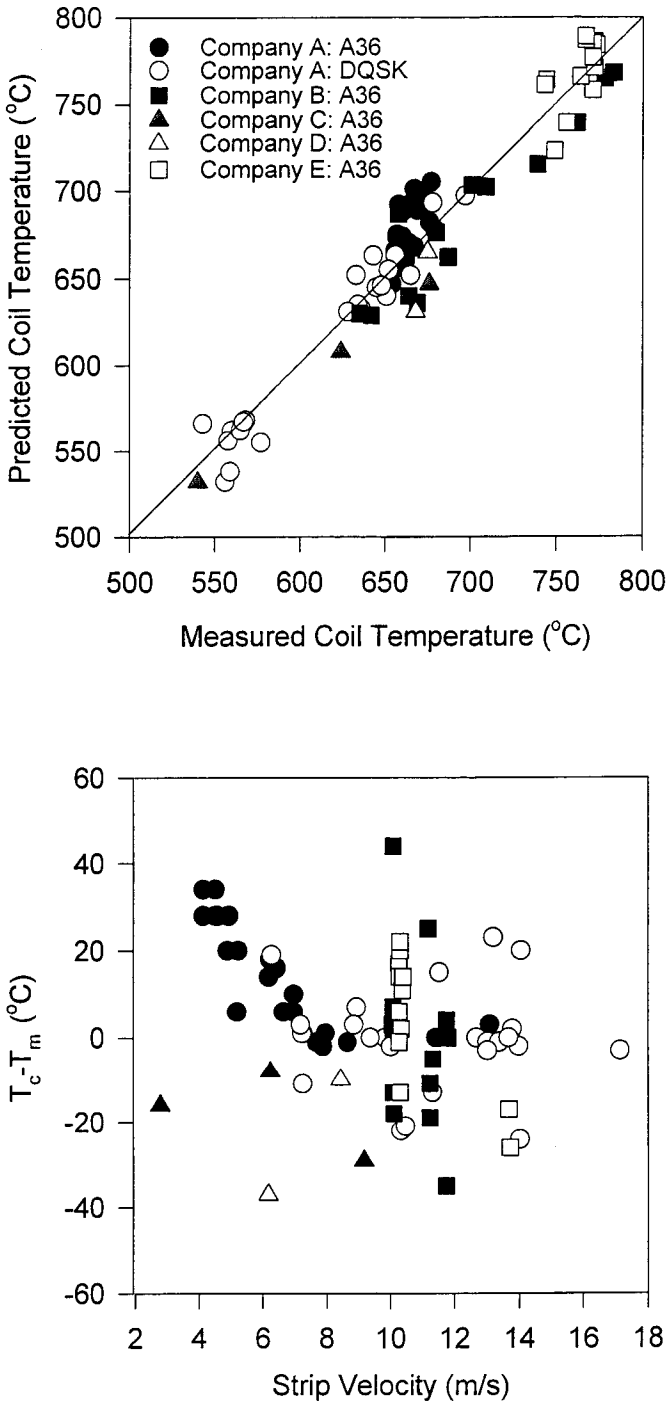

Figure 1.18. Comparison of predicted coiling temperature with mill measurement for A36 steel grades.

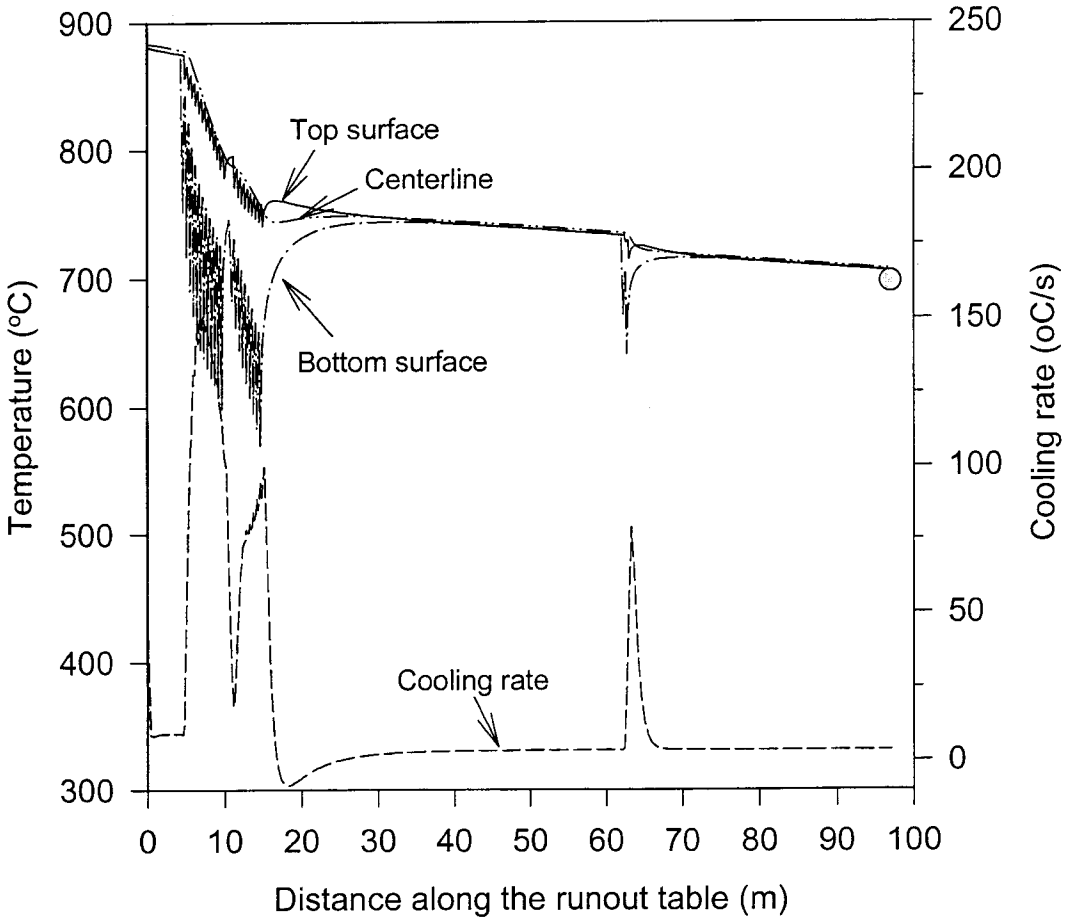

Figure 1.19 Predictions of thermal profile of strip during runout table cooling for a HSLA-V steel coil #480733 (4.0mm).

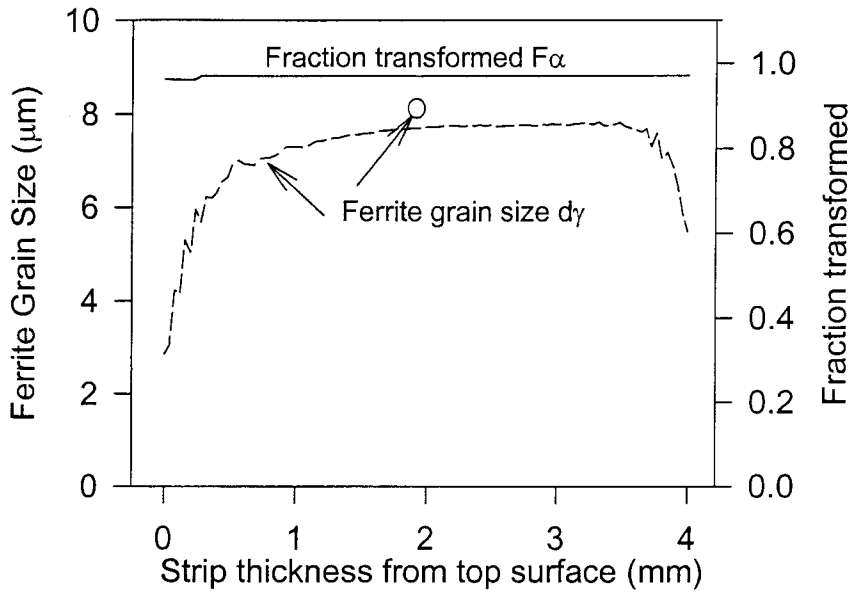

Figure 1.20a. Predictions of Ferrite grain size and fraction of ferrite transformed for acHSLA-V steel coil #480733 (4.0mm).

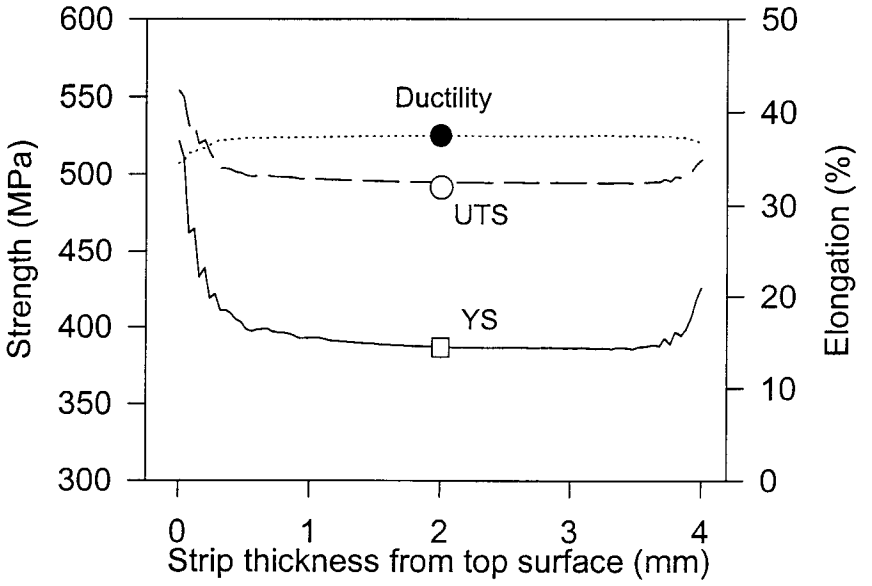

Figure 1.20b. Predictions of mechanical properties for a HSLA-V steel, coil #480733 (4.0mm).

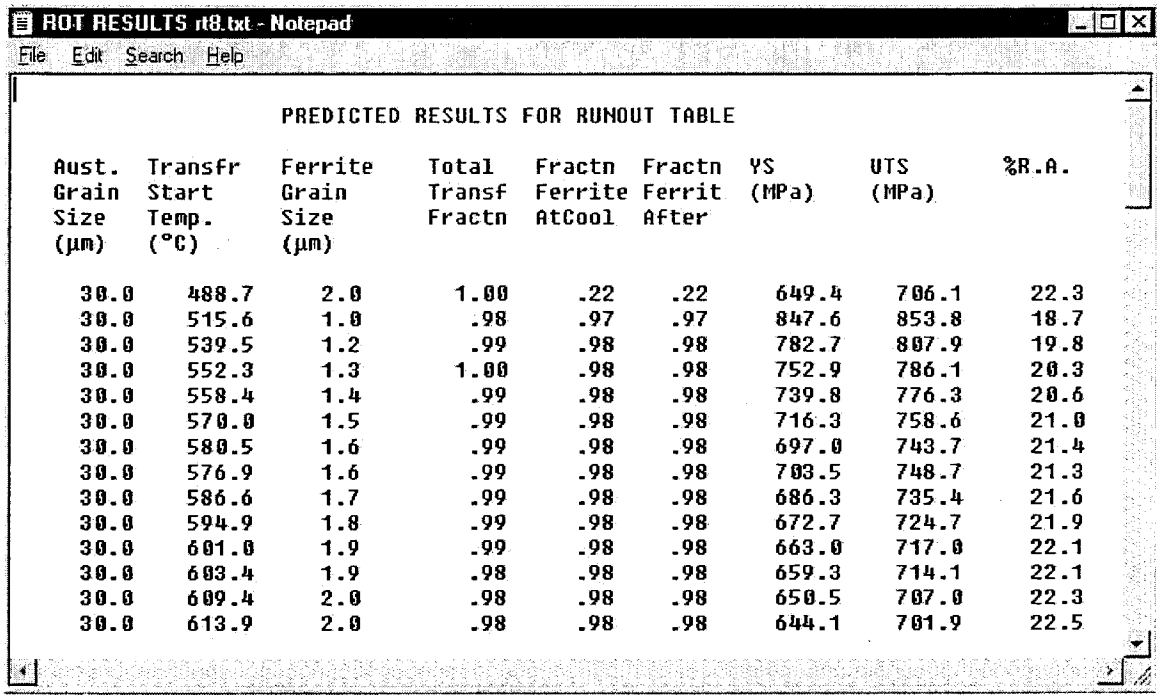

ROT RESULTS rt8.txt - Notepad

File Edit Search Help

PREDICTED RESULTS FOR RUNOUT TABLE

Aust. Grain Size (μm)	Transfr Start Temp. (°C)	Ferrite Grain Size (μm)	Total Transf Fractn	Fractn Ferrite AtCool	Fractn Ferrit After	YS (MPa)	UTS (MPa)	%R.A.
30.0	488.7	2.0	1.00	.22	.22	649.4	706.1	22.3
30.0	515.6	1.0	.98	.97	.97	847.6	853.8	18.7
30.0	539.5	1.2	.99	.98	.98	782.7	807.9	19.8
30.0	552.3	1.3	1.00	.98	.98	752.9	786.1	20.3
30.0	558.4	1.4	.99	.98	.98	739.8	776.3	20.6
30.0	570.0	1.5	.99	.98	.98	716.3	758.6	21.0
30.0	580.5	1.6	.99	.98	.98	697.0	743.7	21.4
30.0	576.9	1.6	.99	.98	.98	703.5	748.7	21.3
30.0	586.6	1.7	.99	.98	.98	686.3	735.4	21.6
30.0	594.9	1.8	.99	.98	.98	672.7	724.7	21.9
30.0	601.0	1.9	.99	.98	.98	663.0	717.0	22.1
30.0	603.4	1.9	.98	.98	.98	659.3	714.1	22.1
30.0	609.4	2.0	.98	.98	.98	650.5	707.0	22.3
30.0	613.9	2.0	.98	.98	.98	644.1	701.9	22.5

Figure 1.21. Structure and properties through strip thickness.

Steckel Mill Model

Reversing Roughing and Steckel Mill model

The reversing roughing mill model was developed based on the model which was developed by Chen and Samarasekera at UBC previously. A finite-difference scheme has been applied to compute the thermal history of the strip and work roll during rolling in a reversing roughing and reversing finishing mill. The model assumes uniform deformation in the roll-bite and includes the effect of the oxide layer on the temperature distribution. The detailed mathematical model which describes thermal, deformation and microstructure evolution during reversing rough rolling is given in the "Steckel Mill Model - Theoretical Manual".

Coil Box/Furnace Model

The coil box model had been developed previously by Stelco and transferred to UBC. The coil furnace model has been integrated into the Steckel mill model. The reversing roughing mill model and the Steckel Mill Model can be used to simulate a Steckel mill by combining these models with a coilbox or a coil furnace model. Figure 1.21 shows the Steckel mill setup for a typical Steckel mill. Output from the Steckel mill model includes temperature, austenite grain size and scale thickness profiles and roll forces, as shown in Figure 1.22. The uniform temperature and austenite grain size distribution through the strip thickness has been predicted due to the homogenizing characteristics of the coilbox.

Models which predict the precipitation in austenite for carbon steel grades and Nb bearing microalloy steel grades were also incorporated into the Steckel Mill model necessarily in consideration of long rolling and coiling time during the Steckel Mill rolling process. Fraction precipitated is given as the input of Runout Table Cooling Model.

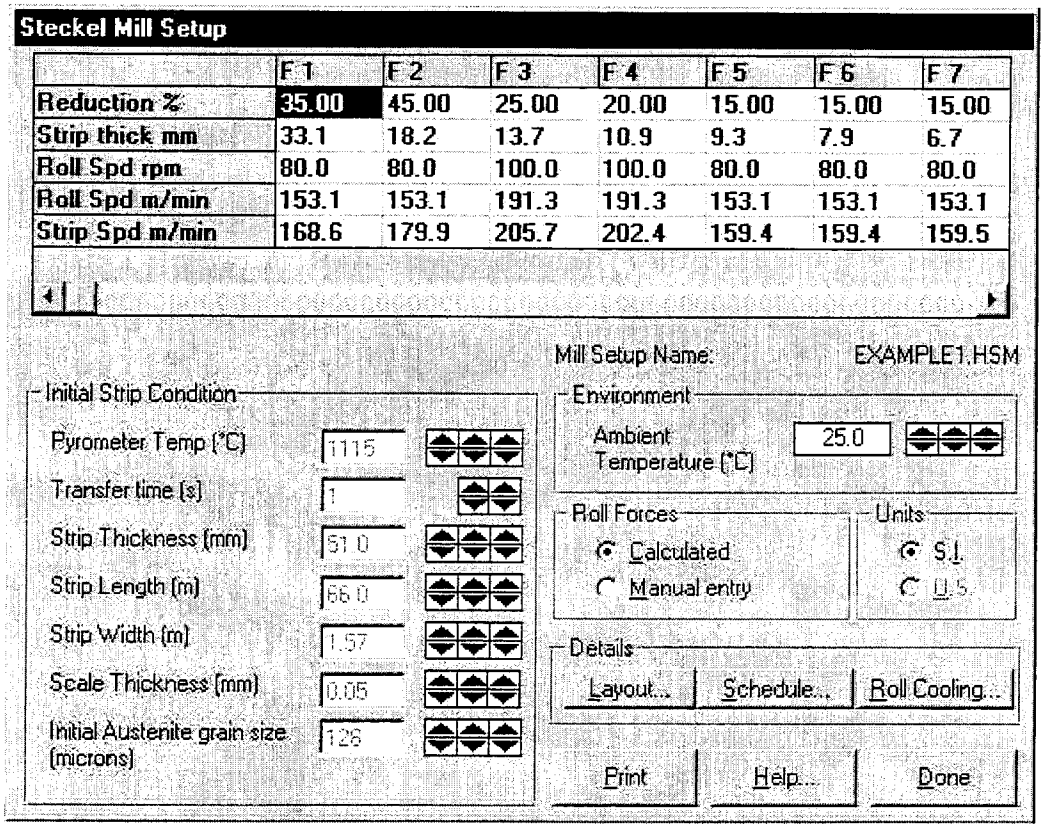

Figure 1.21a. Steckel Mill Setup - Rolling schedule

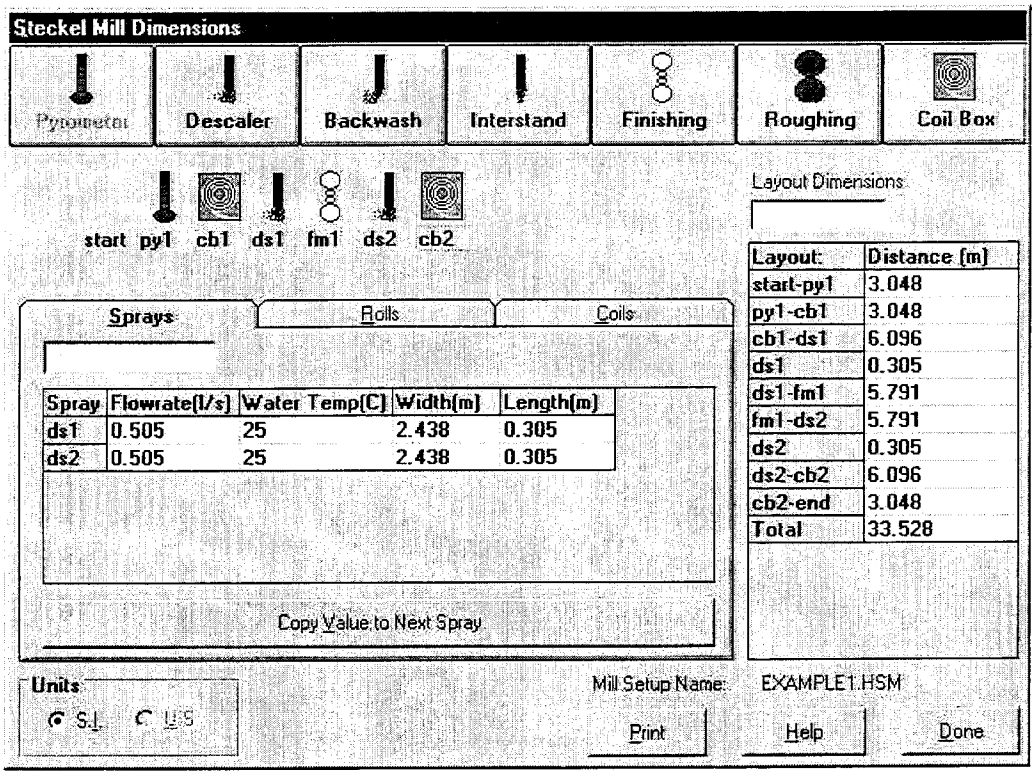

Figure 1.21b. Steckel Mill Setup - Dimensions.

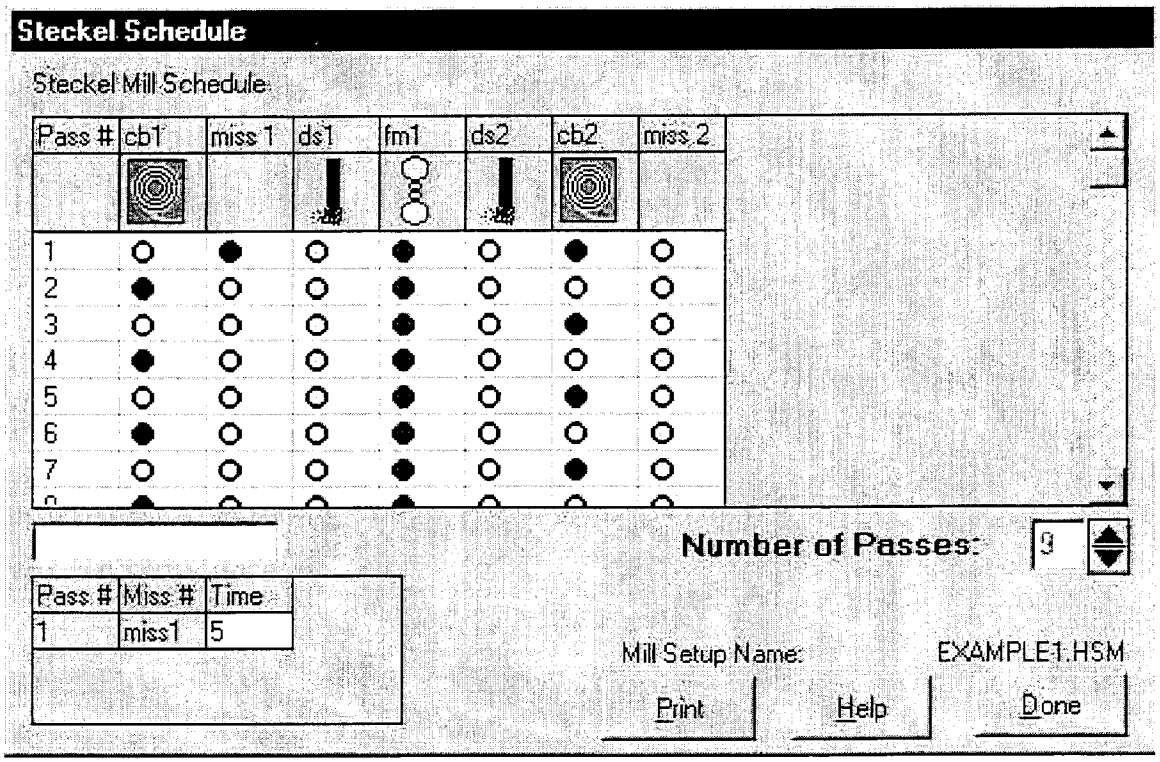

Figure 1.21c. Steckel Mill Setup - Rolling passes.

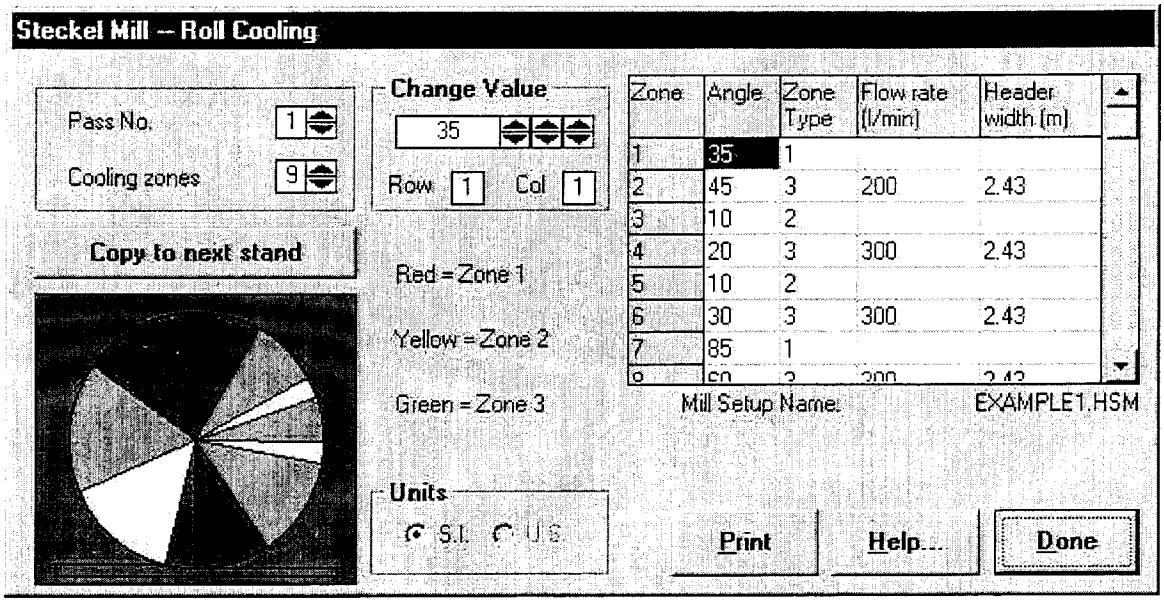

Figure 1.21d. Steckel Mill Setup - Work Roll Cooling

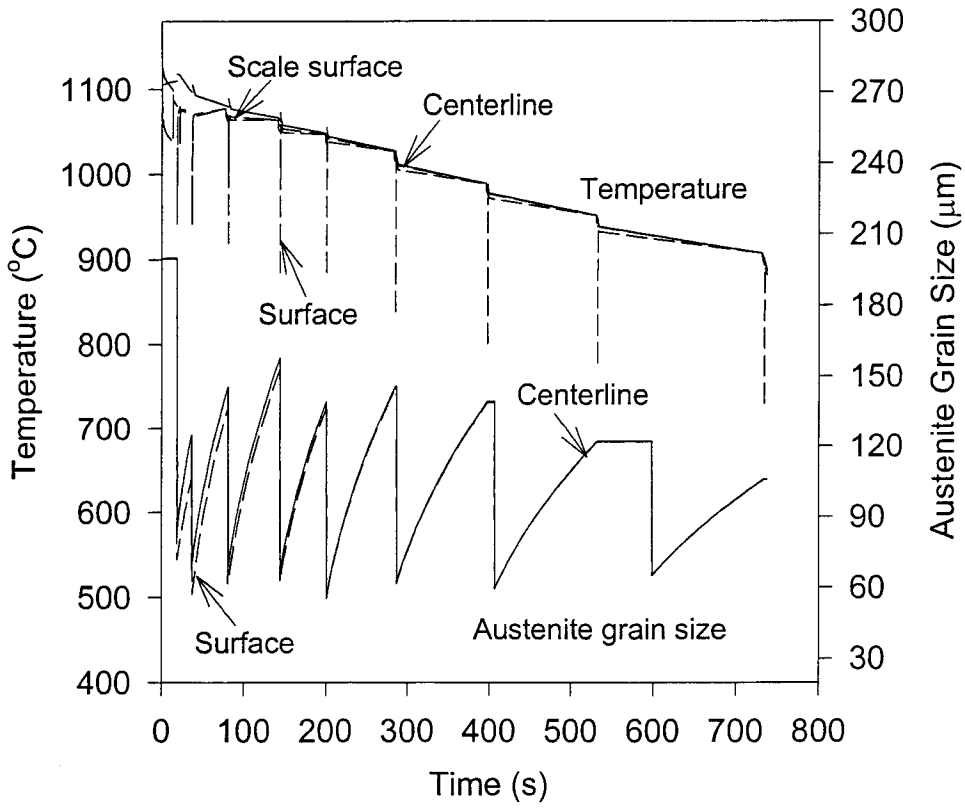

Figure 1.22. Time-temperature profile predicted by Steckel mill model for a Steckel mill rolling schedule.

1.2. Verification of Existing Deformation Model

A visco-plastic finite element model based on the flow formulation and Eulerian approach has been developed to simulate the deformation and temperature and predict the roll forces accurately. This code has been modified to run on a PC. Validation of the model for the prediction of strain, strain rate, temperature and roll force has been completed for both roughing and finishing rolling. The deformation model was released in October, 1996.

The model assumes visco-plastic material behaviour, flow formulation and the Eulerian approach. Thermal and mechanical equations are solved separately and the results are iterated between the two solutions. The principal potential energy is expressed as

$$\int_V \{\delta\dot{\varepsilon}\}^T \{\sigma\} dV - \int_V \{\delta v\}^T \{F\} dV - \int_{St} \{\delta v\}^T \{\tilde{t}\} dS = 0 \tag{1.15}$$

For von Mises-type visco-plastic materials, the material is assumed to an isotropic, incompressible, non-Newtonian fluid,

$$\dot{\varepsilon}_{ij} = \frac{1}{2\mu} \sigma_{ij}'; \quad \sigma_{ij}' = \sigma_{ij} - \delta_{ij} p \tag{1.16}$$

where the nonlinear viscosity is

$$\mu = \frac{\sigma_y + (\dot{\varepsilon} / \gamma\sqrt{3})^{1/n}}{\sqrt{3}\dot{\varepsilon}} \tag{1.17}$$

n is the work hardening coefficient and γ is the viscous coefficient which becomes infinite in the case of pure plastic flow; σ_y is the uniaxial yield stress of the material.

The friction is simulated through a set of narrow interface elements along the arc of contact. The interface element nodes are assigned a velocity equal to the roll velocity, which is essentially a no-slip condition. However, to determine the roll force, shear stress was calculated by applying the following equation within the interface elements,

$$\tau = \mu p \tag{1.18}$$

where p is the pressure at the interface. 200 eight-node isoparametric elements are used to divide the domain in the deformation model.

The accuracy of roll force predictions with a finite-element model depends on the form of the equations employed to describe the deformation resistance at high temperature and its range of validity. The constitutive equation has been developed by NIST to simulate the material behaviour at high temperature as a function of strain, strain rate, temperature and austenite grain size.

The finite-element deformation model gives accurate prediction of strain, strain rate, temperature distribution and resulting microstructure in the roll bite. The model can operate with initial parameters provided by manual entry or from a previous calculation using the roughing mill or finishing mill models, as shown in Figure 1.23. The finite-element analysis predicts the extent of inhomogeneous deformation, temperature rise due to the deformation heat and austenitic microstructure.

A detailed mathematical model which describe the numerical scheme of Visco-plastic finite element analysis, heat transfer and constitutive equations for eight steel grades is presented in the "Deformation Model - Theoretical Manual".

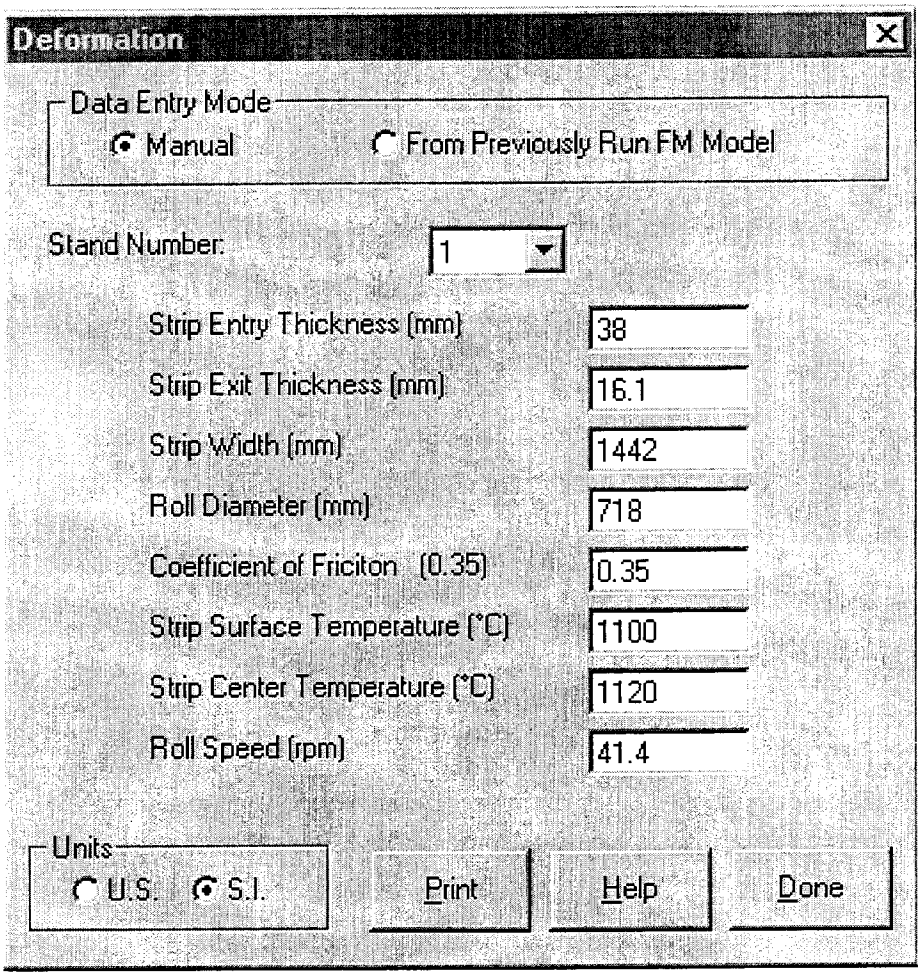

Figure 1.23. Deformation Model Setup - Manual entry.

1.3. Development of Down Coiler Model

The development of a down coiler thermal model is important for DQSK and HSLA steel grades. A down coiler model has been developed and incorporated into the runout table cooling model and released. The independent down coiler model was created for users to evaluate the impact of down coiler on the final structure and properties of steel. As many as 20 points along the strip length can be tracked at the same time so users can evaluate the mechanical properties from the head to the tail of the strip in the coil.

In agreement with the previous work reported in the literature, the present coil cooling model assumes that the coil can be considered as a continuous orthotropic hollow cylinder. Only air is considered as a cooling medium. The general heat conduction equation for an orthotropic cylinder is given

$$\rho_s C_{p_s} \frac{\partial T}{\partial t} = \frac{1}{r}\frac{\partial}{\partial r}\left(k_r r \frac{\partial T}{\partial r}\right) + \frac{1}{r^2}\frac{\partial}{\partial \phi}\left(k_\phi \frac{\partial T}{\partial \phi}\right) + \frac{\partial}{\partial z}\left(k_z \frac{\partial T}{\partial z}\right) + g \tag{1.19}$$

$$T = T(r,\phi,z,t);\ \rho_s = \rho_s(T);\ C_{p_s} = C_{p_s}(T);\ k_r = k_r(r,T);\ k_z = k_z(z,T);$$

$$k_\phi = k_\phi(\phi,T);\ g = g(r,z,T)$$

The coil cooling model was developed under the following assumptions:

(1) The angular component of the heat flux vector is negligible

$$q_\phi = -\frac{k_\phi}{r}\frac{\partial T}{\partial \phi} \approx 0 \tag{1.20}$$

(2) There is no phase transformation in the coil

$$g = 0 \tag{1.21}$$

(3) The thermal conductivity in the axial direction is that of the steel

$$k_z = k_s \tag{1.22}$$

(4) The thermal resistance due to the imperfect contact between wraps may be computed by assuming an equivalent thermal conductivity, k_r.

Under these assumptions the heat conduction differential equation becomes:

$$\rho_s C_{p_s} \frac{\partial T}{\partial t} = \frac{1}{r}\frac{\partial}{\partial r}\left(k_r r \frac{\partial T}{\partial r}\right) + \frac{\partial}{\partial z}\left(k_z \frac{\partial T}{\partial z}\right) \tag{1.23}$$

which is solved subject to the initial condition

$$t = 0;\ r_a \le r \le r_b;\ 0 \le z \le L_c;\ T = T_0(r,z) \tag{1.24}$$

and boundary conditions:

$$r = r_a;\ -k_r \frac{\partial T}{\partial r} + h_a T = h_a T_{\infty,a} \tag{1.25}$$

$$r = r_b;\ k_r \frac{\partial T}{\partial r} + h_b T = h_b T_{\infty,b} \tag{1.26}$$

$$z = 0;\ -k_z \frac{\partial T}{\partial z} + h_0 T = h_0 T_{\infty,0} \tag{1.27}$$

$$z = L_c;\ k_z \frac{\partial T}{\partial z} + h_{L_c} T = h_{L_c} T_{\infty,L_c} \tag{1.28}$$

Equation (5) with initial and boundary conditions was solved by an ADI finite differences scheme obtained by applying the conservation principle to a control volume. The model was run using 50-nodes in each direction and 1200-time steps during calculations. The thermophysical properties of the steel used in this work were obtained from regression analysis of data published elsewhere, and a summary of the equations obtained is presented as

Density:

$$\rho = 7846.31 - 0.10177T - 8.3576\times10^{-4}T^2 + 7.9739\times10^{-7}T^3 (kg/m^3) \tag{1.29}$$

The thermal conductivity for alloy steel grades:

$$k = 33.521 + 0.0261T - 9.2395\times10^{-5}T^2 + 2.3436\times10^{-7}T^3 - 4.2111\times10^{-10}T^4 + 2.5357\times10^{-13}T^5 \tag{1.30}$$

The thermal conductivity for carbon steel grades:

$$\begin{aligned} a &= 19.09314 - 17.7866 \times C_{arb} \\ b &= 0.008834 + 0.014706 \times C_{arb} \\ k_s &= a + bT_{sc} \end{aligned} \tag{1.31}$$

The specific heat for alloy steel grades:

$$C_p = 417.216 + 1.68332T - 0.012291T^2 + 4.73341\times10^{-5}T^3 - 8.1892\times10^{-8}T^4$$

$$+5.3968\times10^{-11}T^5 \tag{1.32}$$

The thermal conductivity for carbon steel grades:

$$\begin{aligned} a &= 657.4553 - 414.832\times C_{arb} \\ b &= 0.005852 + 0.35783\times C_{arb} \\ C_{ps} &= a + bT \end{aligned} \tag{1.33}$$

The model considers only horizontal-cross flow air cooling configurations, and the heat transfer surfaces are:

(1) Internal cylinder $(r = r_a, 0 \le z \le L)$

(2) External cylinder $(r = r_b, 0 \le z \le L)$

(3) Disk at $(r_a \le r \le r_b, z = 0)$

(4) Disk at $(r_a \le r \le r_b, z = L)$

Similarly to the case of air cooling in the runout table, radiation and convection boundary conditions are considered for all the heat transfer surfaces. The resulting set of equations for each cooling configuration and each heat transfer surface are presented as:

The *radiation heat transfer* obeys the Stefan-Boltzmann law as follows:

$$q_r = S\varepsilon A((T_s + 273.1)^4 - (T_\infty + 273.1)^4) \tag{1.34}$$

Radiation heat transfer coefficient

$$h_{rad} = S\varepsilon(T)\frac{((T_s + 273.1)^4 - (T_\infty + 273.1)^4)}{(T_s - T_\infty)} \tag{1.35}$$

where S is the Stefan-Boltzmann's constant $S = 5.6705\times10^{-8}$, the emissivity, ε, of the hot tube is expressed as a function of temperature, T_s:

$$\varepsilon(T_s) = \frac{T_s}{1000}\left(0.125\frac{T_s}{1000} - 0.38\right) + 1.1 \tag{1.36}$$

For the *convection*, the heat transfer is governed by the equation below:

$$q_{conv} = Ah_{conv}(T_s - T_\infty) \tag{1.37}$$

$$h_{conv} = 0.332\left(\frac{k_{air}}{L}\right)R_e^{0.5}P_r^{1/3} \quad R_e \le 5\times10^4 \tag{1.38}$$

$$h_{conv} = 0.0288\left(\frac{k_{air}}{L}\right) R_e^{0.8} P_r^{1/3} \qquad R_e > 5 \times 10^4 \tag{1.39}$$

here $$R_e = \frac{\rho_{air} V_s L}{\nu_{air}} \tag{1.40}$$

The radial thermal conductivity was adjusted according to the gap factor. Thermal histories for small electric steel coils were received from the USS Research Center and have been analyzed to examine the accuracy of the model predictions. The analysis is based on the assumption that the coil is in a quasi-steady state condition in each time step. In this way, it is possible to obtained an expression of the thermal resistance of a composite cylinder, which is defined by the ratio (density of the coil/density of the steel). This expression has been included in the coil cooling model.

A typical setup for a independent coiler is shown in Figure 1.24. Three points along the strip length at the positions of 20%, 50% and 80% from head are selected. In this case, initial temperatures, ferrite grain sizes and fraction transformed which were predicted by runout table cooling model are required to setup the model. An example of mechanical properties at the selected points predicted by down coiler model is shown in Figure 1.25. Variation of mechanical properties is small because the same initial temperature and grain size conditions were assumed. An example of thermal history for three selected points in the down coiler is presented in Figure 1.26.

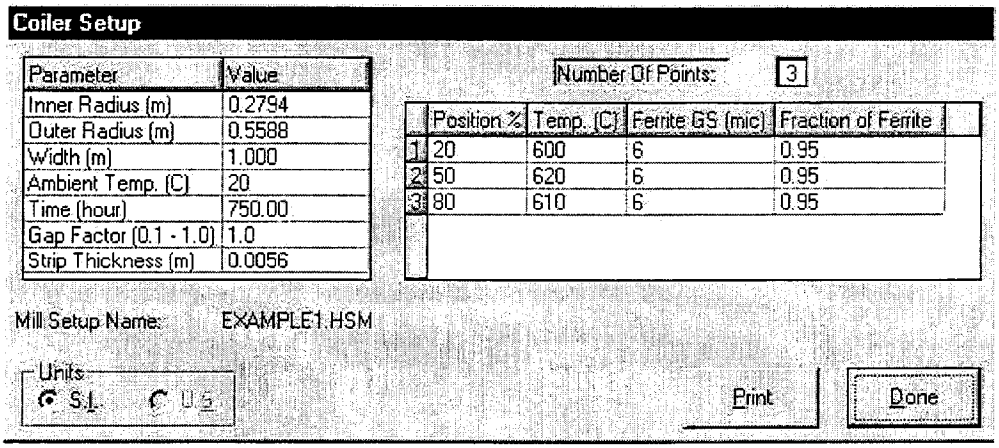

Figure 1.24. Setup of a down coiler.

PREDICTED RESULTS FOR DOWN COILER

PT #	YS (MPa)	UTS (MPa)	Elongation (%)
001	401.9	483.6	30.8
002	404.6	487.9	30.6
003	399.0	478.9	31.1

Figure 1.25. Mechanical properties of strip at selected points predicted by down coiler model.

Time hr.	Pt. 1(°C)	Pt. 2(°C)	Pt. 3(°C)
00.0000	600.00	620.00	610.00
00.0167	608.58	615.69	609.56
00.0333	609.15	615.05	608.76
00.0500	608.94	614.61	607.79
00.0667	608.50	614.15	606.75
00.0833	607.94	613.64	605.68
00.1000	607.33	613.09	604.60
00.1167	606.69	612.50	603.54
00.1333	606.04	611.87	602.48
00.1500	605.40	611.22	601.44
00.1667	604.75	610.54	600.42
00.1833	604.10	609.84	599.41
00.2000	603.46	609.13	598.41
00.2167	602.81	608.39	597.42
00.2333	602.16	607.64	596.44
00.2500	601.51	606.88	595.48

Figure 1.26. Thermal history of strip at selected points in the down coiler.

1.6. Process Model Integration

The Hot Strip Mill Model 4.0 has been released with user friendly interface.

MODELS INCORPORATED:

Roughing Mill Model
Reversing Roughing Mill Model
Coil Box Model
Finishing Mill Model
Runout Table Model
Deformation Model
Down Coiler Model
Steckel Mill model

STEELS GRADES INCORPORATED:

A36
DQSK
HSLA-V
HSLA-Nb
HSLA-Nb/Ti50
HSLA-Nb/Ti80
IF Nb-rich
IF Nb-lean

A list of typical chemical compositions for the above eight steel grades is given in Table I. A standard format for materials behaviors, microstructure evolution and structure-properties relation was developed as described in those Theoretical Manuals for each models. A database was created accordingly as

CHEM#..DAT - STEEL CHEMISTRY

SSPI#.DAT - CONSTITUTIVE EQUATION

PRECRY#.DAT - RECRYSTLLIOZATION, AUSTENITE GRAIN GROWTH

PARA#.DAT - AUSTENITE DECOMPOSITION, PRECIPITATION AND STRUCTURE-PROPERTIES RELATIONS

Table I. Supplier and Chemistry (wt%)

	A36	DQSK	HSLA-V	HSLA-Nb	HSLA-Nb/Ti 50	HSLA-Nb/Ti 80	IF Nb rich	IF Nb lean
	USS	USS	USS	USS	LTV	Stelco	USS	LTV
C	0.17	0.038	0.045	0.082	0.071	0.07	0.0028	0.002
Mn	0.74	0.30	0.45	0.48	0.758	1.35	0.17	0.106
P	0.009	0.010	0.012	0.012	0.014	0.009	0.011	0.010
S	0.008	0.008	0.005	0.005	0.013	0.003	0.006	0.008
Si	0.012	0.009	0.069	0.045	0.014	0.14	0.009	0.010
Cu	0.016	0.015	0.012	0.026	0.02			0.01
Ni	0.010	0.025	0.013	0.016	0.01		0.014	0.01
Cr	0.019	0.033	0.022	0.023	0.027		0.029	0.019
Mo	<0.005	<0.005	<0.005	<0.005	0.001		<0.005	0.002
V	<0.002	<0.002	0.080	<0.002	0.003		<0.005	
Ti	<0.002	<0.002	0.002	<0.002	0.013	0.047	0.035	0.059
Nb	<0.005	<0.005	<0.005	0.036	0.023	0.086	0.035	0.009
Al	0.040	0.040	0.078	0.024	0.053	0.044	0.027	0.033
N	0.0047	0.0052	0.0072	0.0054	0.0067	0.0070	0.0029	0.0041

2.0. PHYSICAL METALLURGY

2.1. Kinetics of Grain Growth

2.1.1. Objectives

The objective of the subtask on grain growth kinetics was to model the austenite grain growth kinetics during reheating and after roll passes when recrystallization has been completed. The effects of chemistry, temperature, heat treatment schedule and initial grain size on the kinetics were to be quantified. During rolling, austenite grain growth is the dominant process in reheating and during the delay between rough and finish rolling. The austenite grain size and shape results mainly from the conditions imposed by recrystallization and precipitation. The austenite microstructure after rolling and the cooling conditions on the run-out table determine finally the ferrite grain size.*

In addition to the above goal of modelling the austenite grain growth kinetics occurring in a hot strip mill, the following objectives of subtask 2.1 were essential to meet the overall goals of the program:

1. To provide pre-heat treatment schedules for variation of the initial austenite grain size for subsequent investigations of the recrystallization and transformation kinetics (subtasks 2.2 and 2.4).
2. To establish the methods of grain size measurements which are to be employed also in quantifying the recrystallized grain size (subtask 2.2) and the ferrite grain size (subtask 2.4).
3. To establish a method to determine the three-dimensional grain size distribution since a more generic approach of predicting the microstructural evolution requires physically based models where the three dimensional character of grains cannot be neglected.
4. To develop techniques for revealing the austenite microstructures in ultra low carbon steels.

2.1.2. Results

2.1.2.1 Plain carbon steels

Austenite grain growth kinetics has been studied in the A36 and the DQSK plain carbon steels in the temperature range 950 - 1150°C employing various pre-heat schedules. The grain size has been measured in terms of the linear intercept, l, and the equivalent area diameter (EQAD), d_A. The three-dimensional (3D) grain size distribution can be estimated with the method of Takayama et al.[1] or the Matsuura-Itoh method.[2]

---

* In the original outline of the program, the quantification of the γ-α relationship; i.e., the ferrite grain size, was part of subtask 2.1. Because the ferrite grain size results from the austenite decomposition (subtask 2.4), the quantification of the ferrite grain size is dealt with in subtask 2.4 Kinetics of Austenite Decomposition.

[1] Y. Takayama et al., *Mat. Trans. JIM* **32**, 214 (1991).

[2] K. Matsuura and Y. Itoh, *Mat. Trans. JIM* **32**, 1042 (1991).

Takayama's method assumes only one grain shape (tetrakaidecahedron) and a log normal grain size distribution (normal grain growth), but has the advantage that only the quantification of l and d_A is required. The Matsuura-Itoh method appears to be more realistic by assuming a variety of grain shapes and can be applied to an arbitrary grain size distribution. However, the estimation procedures for this method are more complex and require the two-dimensional (2D) grain size distribution to be measured. The Matsuura-Itoh method is to be preferred when the grain size distribution is of interest; both methods can be applied when only an average volumetric grain size is to be estimated and no abnormal growth occurs. The following relations between measured 2D and estimated 3D grain sizes have been approximated for austenite[+] and ferrite grain sizes in plain carbon steels

$$d_V = 1.1 d_m = 1.2 d_A = 1.5 l \qquad (2.1.1)$$

where d_V is the equivalent volume diameter (i.e. the diameter of the grain with the average volume) and d_m is the mean volumetric diameter (i.e. the average diameter of the 3D grain diameter distribution).

Austenite grain growth depends on the pre-heat schedule, as illustrated in Figure 2.1.1, where the results for the A36 steel are shown for two different heating rates, ϕ, to the 1100°C measurement temperature. In both cases, a limiting grain size is achieved which depends on the heating rate. This is indicative of pinned grain growth, presumably because of the presence of AlN precipitates. The pinning force associated with the AlN depends on the temperature *and* pre-heat treatment. Therefore, the literature proposed empirical relationships, which describe austenite grain growth as a definite function of temperature, could not be used in this process model.

The experimental results can be verified with the statistical grain growth model proposed by Abbruzzese and Lücke[3] in which a pinning parameter, P, is employed as an adjustment parameter. The solid lines in Figures 2.1.1 and 2.1.2, represent the statistical model for the austenite grain growth kinetics in the A36 and DQSK steel, respectively. The good fit with the experimental data demonstrates that this approach yields a realistic description of the observed grain growth. Figure 2.1.3 summarizes the values of the pinning parameter, P, obtained for both grades. For the A36 steel, the heating rate dependence of P is clearly indicated. For the DQSK steel, the variation of the pre-heat schedule was limited because the low hardenability of this steel required that the grain growth tests be performed in a vertical tube furnace which permitted a rapid downward quench into an iced brine bath. The stepped grain growth behavior observed at 1100°C for the DQSK grade (cf. Figure 2.1.2) illustrates a case of abnormal growth, which occurs when P decreases with holding time, because of dissolution or coarsening of existing AlN particles. Consequently, two values of P had to be employed to reflect this condition, where initially strong pinning is followed by significantly weaker pinning at later times (cf. Figure 2.1.3).

[+] normal grain growth

[3] G. Abbruzzese and K. Lücke, *Mat. Sci. Forum* **94-96**, 597 (1992).

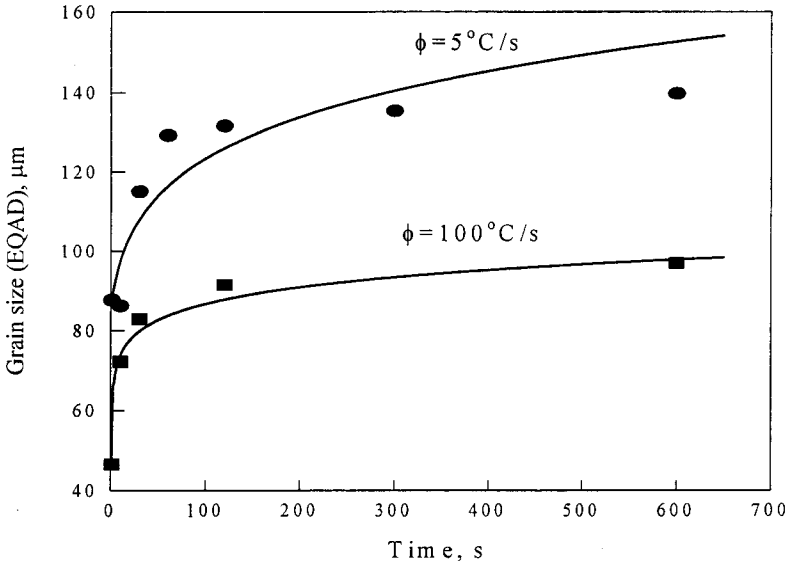

Figure 2.1.1 Austenite grain growth for the as-received A36 steel after heating to 1100 °C at different rates, ϕ.

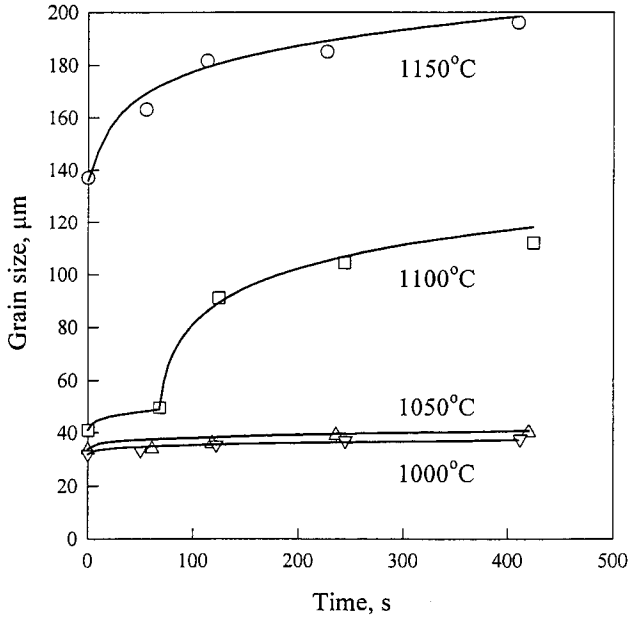

Figure 2.1.2: Comparison of the isothermal grain growth kinetics in the DQSK steel with the predictions from the statistical grain growth model.

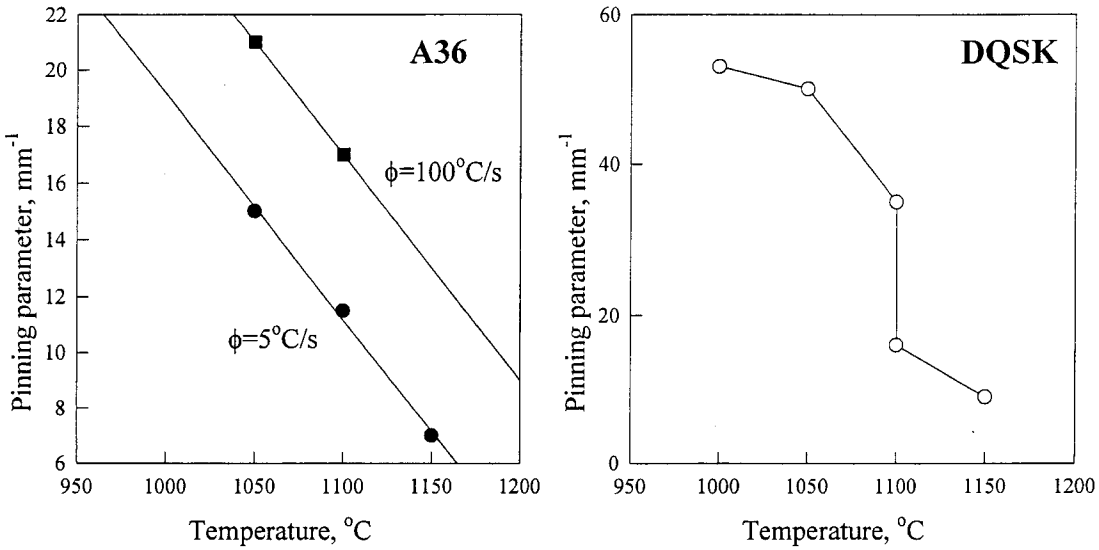

Figure 2.1.3: Pinning parameter as calculated from the laboratory tests for the A36 and DQSK steels.

Unlike the measured grain growth obtained under experimental conditions, austenite grain growth in a hot strip mill occurs essentially unpinned since AlN particles are dissolved in the reheat furnace. Re-precipitation is a slow process and does not occur before the last stands in the finish mill where strain-induced AlN precipitation cannot be excluded. Thus, to predict austenite grain growth in a hot strip mill, P=0 shall be assumed, resulting in the classical parabolic grain growth behavior. Consistent with the Abbruzzese-Lücke model, the grain growth equation is given by

$$d_\gamma = \left(d_\gamma^2(t_0) + 3\gamma_{gb} b^2 \int_{t_0}^{t} \frac{D_{gb}(T(t'))}{kT(t')} dt' \right)^{1/2} \qquad (2.1.2)$$

Here d_γ is the mean volumetric austenite grain size, b is the magnitude of the Burgers vector, γ_{gb} is the grain boundary energy which, according to Gjostein et al.[4], decreases with carbon content by

$$\gamma_{gb} = (0.8 - 0.35C^{0.68}) \times Jm^{-2} \qquad (2.1.3)$$

where C is the carbon content in wt% with $C \leq 0.8$, and the grain boundary diffusivity is given by

[4] N.A. Gjostein et al., *Acta Metall.* **14**, 1637 (1966).

$$D_{gb} = 0.9cm^2s^{-1}\exp(-1.66eV/kT) \qquad (2.1.4)$$

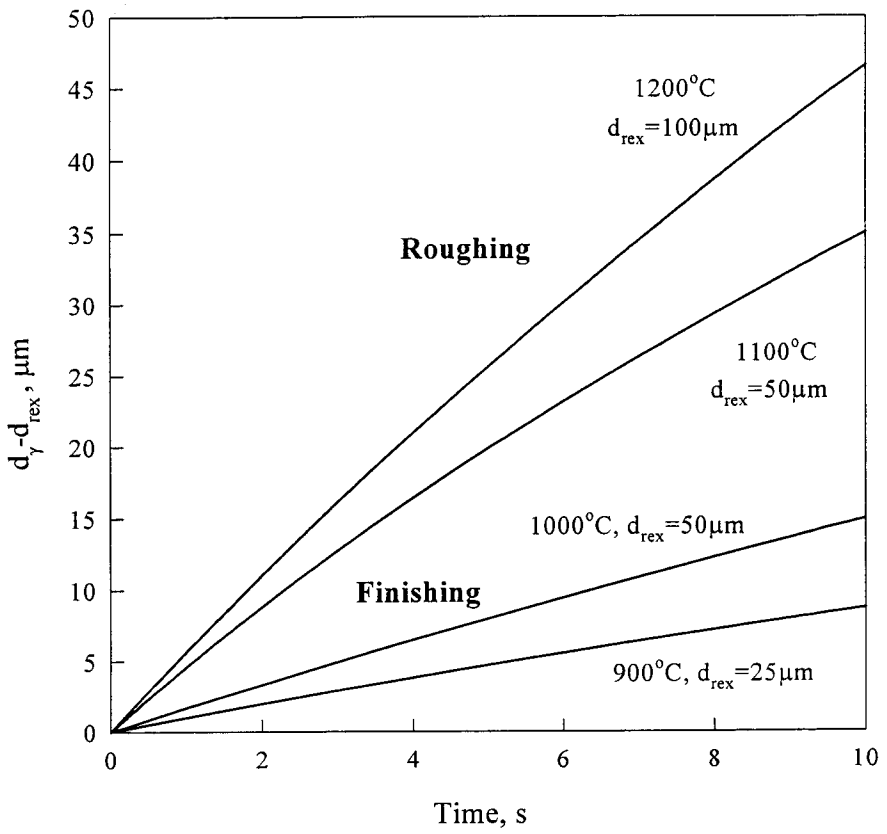

Figure 2.1.4: Estimation of grain growth after completion of recrystallization for rough and finish mill conditions for the DQSK steel.

Figure2.1.4 illustrates the calculated grain growth in the interstand times of the roughing mill and the finishing mill after completion of recrystallization. There is substantial grain growth taking place during rough rolling and on the delay table between the rougher and finisher. Relatively independent of the grain size after rough rolling (assumed to be in the range of 50 - 100 μm), an austenite grain size in the order of 160 - 200 μm is predicted at the entry to the finish mill. The prediction is in good agreement with measurements made on the A36 transfer bar obtained from the crop shear prior to entrance to the finish mill at USS Gary Works. It should be noted that the assumption of unpinned growth indicates the maximum grain growth for the final interstands where strain-induced AlN precipitation may occur. These final interstand times are usually approximately 1s or less; maximum grain growth which can take place under these

conditions is less than 5μm. Therefore, the assumption of unpinned austenite grain growth in Al-killed plain carbon steels is justified for the entire process of rough *and* finish rolling. Further, the proposed grain growth model appears to be applicable to a wide variety of plain carbon steels with the chemistry effect altering the grain boundary energy term (cf. Equation 2.1.3).

2.1.2.2 Microalloyed steels

Austenite grain growth in the HSLA-V steel is similar to that in the plain carbon steels. Consequently, the above described model remains applicable for this steel grade. More complex, albeit similar, grain growth is observed in those grades microalloyed with Nb and/or Ti due to solute drag by Nb and particle pinning of TiN, as described below.

Austenite grain growth in Nb containing HSLA and IF steels does show similar patterns to those observed in plain carbon steels. The results of an isochronal test series shown in Figure 2.1.5 confirms the three grain growth stages of strongly inhibited growth at the lower temperatures, abnormal grain growth at the grain growth temperature, which increases with microalloying content from 1050 to 1150 °C, and finally, normal grain growth at the higher temperatures. This grain growth pattern can be attributed to the dissolution of Nb and Ti carbides and nitrides. The transition from grain growth inhibition to grain coarsening is usually characterized by a period of abnormal grain growth in which non-homogeneous microstructures consisting of areas of small grains embedded in networks of larger grains develop.

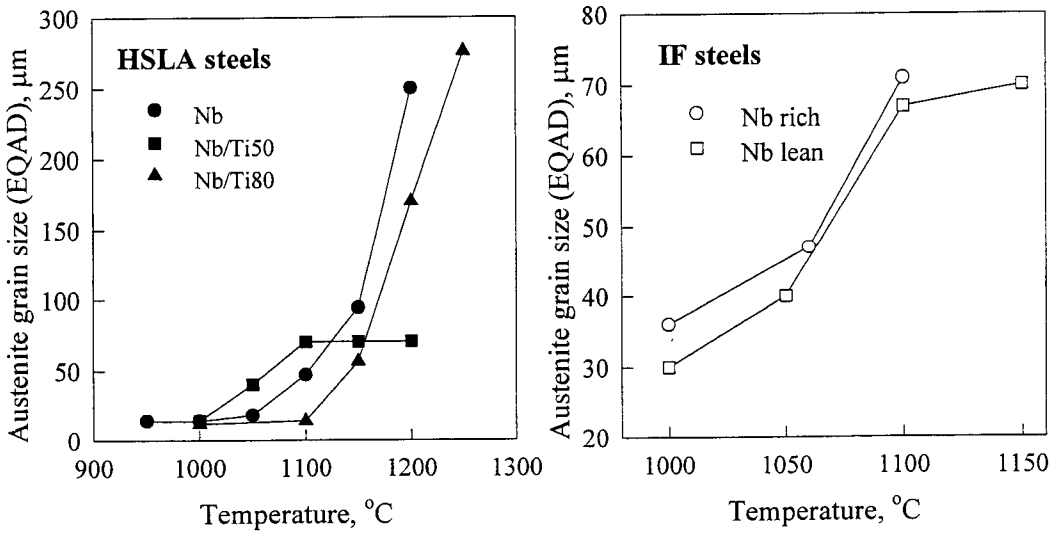

Figure 2.1.5: Austenite grain size as a function of temperature for holding times of 600 s for HSLA steels and IF steels.

It is important to note that the austenite grain structure in IF steels could not be revealed by traditional quenching techniques. Thus, high temperature glass etching

techniques were employed for assessing the austenite grain sizes in IF steels for temperatures from 1000 to 1150 °C and soaking times of 2 to 20 minutes. Interestingly, the observed surface grain growth tendencies in the IF steels appear to be similar to those of the bulk grains in HSLA steels. This observation supports the otherwise somewhat dubious assumption of taking surface grains as representing the actual internal grain size. However, additional work is in progress to test this assumption using laser ultrasonic measurements in collaboration with the IMI (AISI/DOE Project D).

Figure 2.1.5 also shows that a limiting grain size is observed at higher temperatures for the HSLA-Nb/Ti50 grade but not for the 80 grade. This is indicative of a rather stable population of fine TiN in the 50 grade which effectively prevents austenite grain growth beyond a threshold of approximately 70 μm, whereas in the 80 grade a widely spaced population of rather coarse TiN particles develops with particle sizes of approximately 1 μm being observed; these are not effective in grain boundary pinning.

A pilot mill trial was conducted at the USS Technical Center in Monroeville to investigate the austenite grain size evolution in the HSLA-Nb steel during multi-pass rolling. Austenite grain growth after completion of recrystallization indicated limited grain growth up to approximately 100 μm in the temperature range of 1100 - 1200 °C. These reduced grain growth rates as compared to those observed for the plain low-carbon steels can presumably be attributed to solute drag by Nb.

Grain growth after completion of recrystallization was also studied in the HSLA-Nb/Ti80 grade employing Gleeble tests. For this purpose, the samples were reheated for 10 minutes at 1250 °C, then air cooled to the measurement temperatures of 1100 and 1200 °C, respectively, where they were deformed in axisymmetric compression to an effective strain of 0.5 and held for various times up to one minute after complete recrystallization. The observed grain growth kinetics were described using the Abbruzzese-Lücke model in a similar way as previously proposed for the Al-killed plain carbon steels.

The comparison of predicted and experimental results is shown for grain growth at 1250 °C in Figure 2.1.6a and for grain growth after recrystallization in Figure 2.1.6b. As can be seen by the dotted line in Figure 2.1.6a, the initial growth rates at 1250 °C are slightly overpredicted when a constant P of 6.5 mm^{-1} is assumed. This indicates that dissolution of NbC and TiC has not been completed during heating. Adopting a time dependent pinning parameter which decreases linearly from 10 to 6.5 mm^{-1} within the first 175 s gives a more accurate prediction, as shown by the solid line. A decrease of the pinning force due to dissolution or coarsening of particles promotes the tendency for abnormal growth. Interestingly, the model reflects this tendency even for this rather modest decrease in the pinning parameter. Increased intermediate grain growth rates are calculated resulting in a slightly larger final grain size than that predicted for the small, but constant pinning force; a constant pinning force eliminates the potential for abnormal growth.

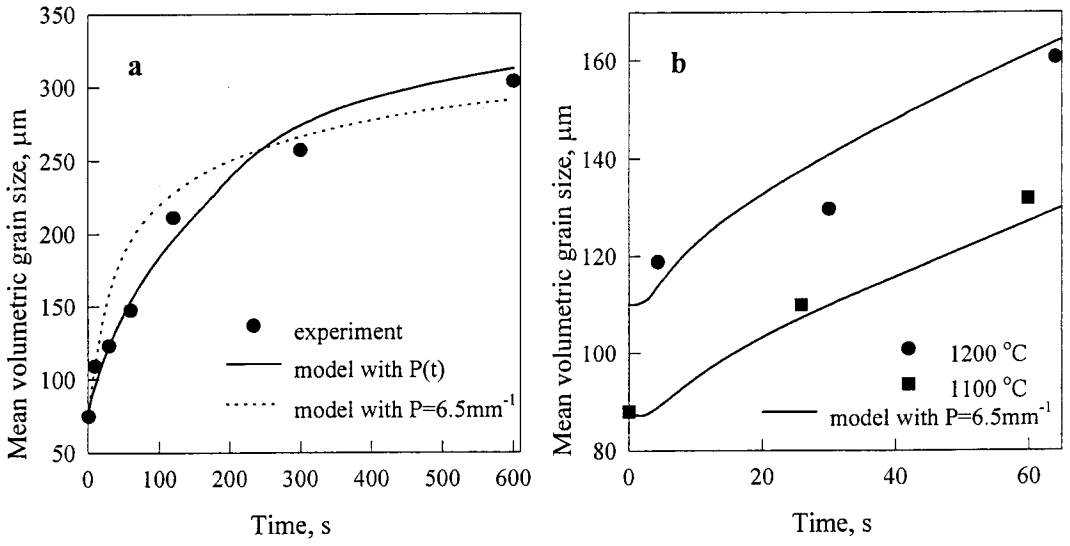

Figure 2.1.6: Comparison of predicted and measured grain growth in the HSLA-Nb/Ti 80 steel for reheating at 1250 °C (a) and after recrystallization (b).

Adopting the pinning parameter of 6.5 mm^{-1}, which develops during the 1250 °C reheating, grain growth after recrystallization at 1200 and 1100 °C can adequately be described, as illustrated in Figure 2.1.6b. This finding suggests that no re-precipitation takes place at these temperatures thereby leaving the pinning parameter unchanged from that developed during reheating. This is consistent with the solubility temperature for NbC and TiC of approximately 1050 °C in the HSLA-Nb/Ti80 steel, as calculated by employing THERMOCALC.

In summary, the Abbruzzese-Lücke grain growth model gives an adequate description of the complex austenite grain growth behavior in the HSLA-Nb/Ti80 steel, as observed during reheating and after recrystallization in laboratory tests. The predicted pinning forces are consistent with thermodynamic data for the dissolution of precipitates. Based on the laboratory results, substantial grain growth would be expected during industrial rolling of this steel above its NbC/TiC solubility temperature of approximately 1050 °C. In contrast, an austenite grain size of 30 μm has been estimated from the as-received transfer bar, indicating that the laboratory simulations do not accurately account for grain growth detail during industrial multi-pass high strain rate deformation conditions. It is believed that this discrepancy may be attributable to the phenomena of strain-induced Nb segregation and associated pinning of grain boundaries. Therefore, simple assumptions are currently being made for the grain growth model by adopting a transition from unpinned to totally pinned grain growth as the temperature decreases from 1150 to 1100 °C.

2.2. Kinetics of Recrystallization

2.2.1. Objectives

The evolution of austenite microstructure and flow strength during hot rolling is closely related to recrystallization. The objective of this subtask has been to investigate the effect of thermo-mechanical processing parameters on the kinetics of recrystallization and the resulting recrystallized grain size. In detail, the effect of temperature, strain, strain rate and initial austenite grain size on the austenite microstructure and its flow behavior were quantified to develop predictive models describing the recrystallization behavior under industrial rolling conditions.

2.2.2. Results

2.2.2.1 Recrystallization kinetics

The softening and recrystallization taking place between each rolling stand in the hot mill were simulated by double hit compression tests. Cylindrical specimens 10 mm in diameter and 15 mm in length were employed. Each specimen was first reheated to obtain a desired initial austenite grain size. Considering that a different microstructure enters each stand during industrial rolling, a variety of different reheating schedules was employed to vary the initial austenite grain size from 10 to 250 μm (EQAD). Each test sample was then cooled to the test temperature and held 60 s to achieve a uniform temperature distribution along the specimen. Subsequently, the specimen was deformed to a prescribed strain, unloaded for a desired time interval, and finally re-deformed again at the same strain rate. The deformation temperature employed for these tests ranged from 900 to 1200 °C with strains varying from 0.1 to 0.7 at strain rates from 0.01 to 100 s^{-1}. The low strain rate tests (up to 10 s^{-1}) were conducted using the Gleeble 1500 thermo-mechanical simulator, while higher strain rate experiments were performed using a cam plastometer. In analyzing the softening curves it was assumed that the initial 20% softening is attributable to recovery and the remainder is due to recrystallization. The test matrix was designed to study both static and metadynamic recrystallization.

Whether static or metadynamic recrystallization takes place was evaluated based on the flow stress curves of the first hit. The potential for metadynamic recrystallization can be indicated with a limiting Zener-Hollomon parameter which separates those flow curves which exhibit a peak from those without a peak. Only the former deformation conditions would lead to metadynamic recrystallization, as long as the hit strain is larger than 5/6 of the peak strain. The Zener-Hollomon parameter is a temperature corrected strain rate, i.e.,

$$Z = \dot{\varepsilon} \exp(\frac{Q_{def}}{RT}) \qquad (2.2.1)$$

where Q_{def} is an effective deformation activation energy. The limiting Zener-Hollomon parameter has the form

$$Z_{\lim} = \eta \exp(-\upsilon d_0) + Z_0 \qquad (2.2.2)$$

where d_0 is the initial austenite grain size. Table 2.2.1 summarizes the magnitude of the parameters Q_{def}, Z_0, η and υ used for the steel grades examined in this study. For $Z<Z_{lim}$, metadynamic recrystallization may occur since the effective deformation times are sufficiently long because of the low strain rates and/or the high temperatures. In general, these conditions can only be fulfilled in the initial stands in the roughing mill where temperatures are comparatively high, strain rates are relatively low and reductions per pass are high. For the later stands, and in particular during finish rolling, static recrystallization dominates.

Table 2.2.1: Parameters describing the boundary separating static and metadynamic recrystallization.

Steel	$\eta(s^{-1})$	$Z_0(s^{-1})$	$\upsilon(\mu m^{-1})$	Q_{def}(kJ/mol)
A36	5×10^{15}	0	0.0155	334
DQSK	5×10^{15}	0	0.0155	334
HSLA-V	5×10^{15}	0	0.0155	334
HSLA-Nb	3.76×10^{19}	0	0.0139	421
HSLA-Nb/Ti50	3.76×10^{19}	0	0.0139	421
HSLA-Nb/Ti80	8.52×10^{18}	2.3×10^{16}	0.139	442
IF(Nb-rich)	3.76×10^{19}	0	0.0139	421
IF(Nb-lean)	3.76×10^{19}	0	0.0139	421

The effects of processing parameters on the kinetics of recrystallization can be summarized as follows. Increasing the applied strain increases the recrystallization rate, which can be attributed to the higher dislocation density generated by the increased deformation, which leads to the higher driving force for static recrystallization. It is worth noting that the rate of metadynamic recrystallization is independent of strain. The effect of strain rate on recrystallization is similar to that of strain. Increasing the strain rate increases the rate of both static and metadynamic recrystallization. This is due to the reduced time for dynamic recovery of the deformation at a higher strain rate, which in turn leaves a higher dislocation density leading to an increased driving force for recrystallization. Increasing the deformation temperature also increases the rates of static as well as metadynamic recrystallization. This effect can be explained by the higher mobility of the grain boundaries at the higher temperatures. The role of initial microstructure can be represented by the initial austenite grain size. Increasing the grain size leads to a delay of static recrystallization. This is because larger deformed austenite grains have a smaller boundary area per unit volume, thereby decreasing the density of potential nucleation sites for static recrsytallization and the associated nucleation rates. It

is of interest to note that the kinetics of metadynamic recrystallization is not markedly affected by the initial austenite grain size.

After analysis of the experimental data, the following recrystallization equations were included in the model based on the Avrami equation for the fraction recrystallized,

$$F_X = 1 - \exp\left[-0.693\left(t / t_{0.5}\right)^k\right] \qquad (2.2.3)$$

where k is the Avrami exponent and the time for 50% static recrystallization, $t_{0.5}$, is defined as

$$t_{0.5} = A d_0 \varepsilon^{-\beta} \dot{\varepsilon}^{-1/3} \exp\left(\frac{Q_{rex}}{RT}\right) \qquad (2.2.4)$$

where d_0 is the initial austenite grain size, ε is the strain, $\dot{\varepsilon}$ the strain rate, T is the temperature in K, Q_{rex} is an apparent activation energy and A a constant. The specific parameters used for all eight grades are summarized in Table 2.2.2.

Table 2.2.2: Parameters to predict the extent of static recrystallization.

Steel	k	A (s)	β	Q_{rex} (kJ/mol)
A36	2	8.31×10^{-15}	1.5	263
DQSK	2	5.22×10^{-13}	0.68	248
HSLA-V	0.5	5.15×10^{-15}	2.0	262
HSLA-Nb	0.5	4.92×10^{-17}	2.0	338
HSLA-Nb/Ti50	0.77	1.83×10^{-14}	1.5	275
HSLA-Nb/Ti80	1.32	8.7×10^{-18} ($T<1120$ °C) 1.2×10^{-12} ($T>1120$ °C)	2.8	349 ($T<1120$ °C) 216 ($T>1120$ °C)
IF(Nb-rich)	2.4	5.12×10^{-12}	2.1	214
IF(Nb-lean)	1.8	3.66×10^{-13}	2.1	236

Static recrystallization is the dominant recrystallization mode during finish rolling. The A36, DQSK and HSLA-V steels show complete recrystallization under industrial rolling conditions. The recrystallization rates depend primarily on the Nb content and decrease with increasing Nb levels. Under industrial mill processing conditions this can be attributed primarily to solute drag by Nb. As a result, strain may be retained in the Nb microalloyed grades at the exit of finish rolling due to incomplete recrystallization. Figure 2.2.1 illustrates this behavior by showing the model predicted recrystallization kinetics for conditions typical of the final passes in the finishing mill. Further, this leads also to an increase of the no-recrystallization temperature, T_{nr}, with

increasing Nb content; i.e. from 910 °C for the HSLA-Nb/Ti50 to 930 °C for the HSLA-Nb and 970 °C for the HSLA-Nb/Ti80 steel grade.

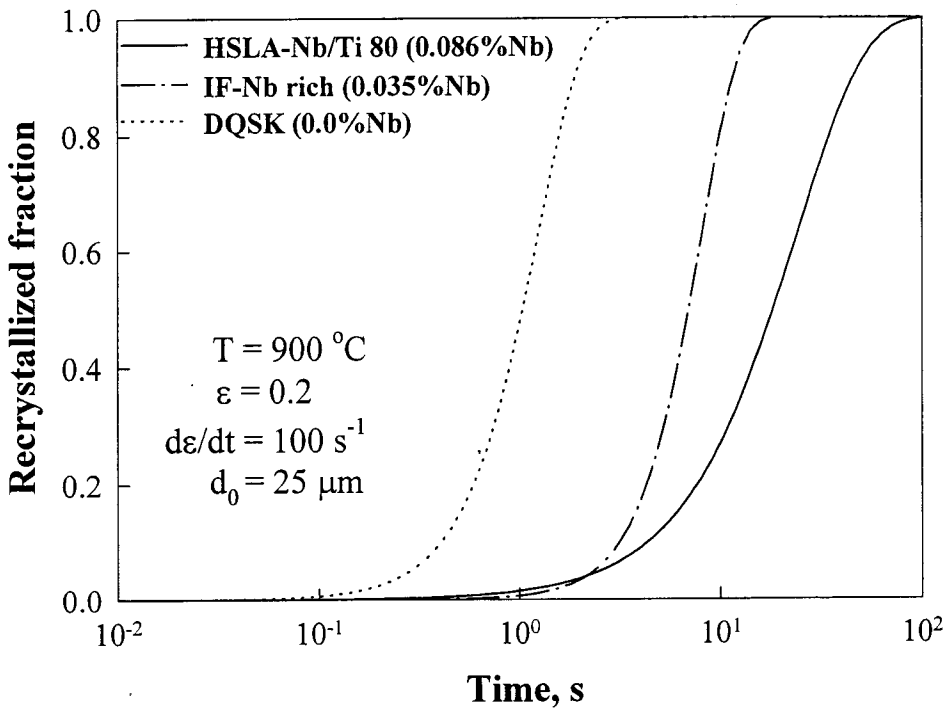

Figure 2.2.1: Comparison of the predicted recrystallization kinetics for steels with different Nb content.

In general, the recrystallization curves in Figure 2.2.1 show a sigmoidal shape. However, for Nb containing grades, the occurrence of a plateau or an abrupt change in the slope of the recrystallized fraction curve has been recorded under laboratory conditions for sufficiently low temperatures and low strain rates. The development of a plateau under laboratory conditions can be attributed to the strain-induced precipitation of Nb carbides or carbonitrides. However, as discussed in more detail in Section 2.3, the no-recrystallization condition due to strain-induced precipitation is only relevant in Steckel mills where longer interstand times are realized. The model reflects this situation by adopting a zero recrystallization rate between precipitation start and finish times.

Metadynamic recrystallization may occur during rough rolling, but is of minor importance for the overall microstructure evolution during hot rolling. An Avrami exponent of $k = 1$ has been adopted for all eight steel grades with $t_{0.5}$ being a function of stain rate and temperature

$$t_{0.5}(s) = A_{md}\dot{\varepsilon}^{-2/3}\exp\left(\frac{Q_{md}}{RT}\right) \qquad (2.2.5)$$

The steel specific parameters A_{md} and Q_{md} are summarized in Table 2.2.3 where, for simplicity, the values for Nb containing steels are based on a detailed study on the HSLA-Nb grade; this approach was justified by the minor chemistry dependencies of these two parameters and the similarity of the flow stress behavior for all of Nb containing steels investigated.

Table 2.2.3: Parameters used for metadynamic recrystallization.

Steel	A_{md} (s)	Q_{md} (kJ/mol)
A36	2.13×10^{-6}	133
DQSK	1.54×10^{-6}	127
HSLA-V	1.54×10^{-6}	127
HSLA-Nb	2.97×10^{-6}	136
HSLA-Nb/Ti50	2.97×10^{-6}	136
HSLA-Nb/Ti80	2.97×10^{-6}	136
IF(Nb-rich)	2.97×10^{-6}	136
IF(Nb-lean)	2.97×10^{-6}	136

2.2.2. Recrystallized grain size

The study of recrystallized grain sizes emphasized static recrystallization since it is the dominant mode to obtain grain refinement due to recrystallization. The recrystallized grain size (EQAD in μm) after static recrystallization has been described as

$$d_{rex} = \Lambda d_o^z \varepsilon^{-p}\exp(-Q_{gx}/RT) \qquad (2.2.6)$$

with the parameters Λ, z, p and Q_{gx} being summarized in Table 2.2.4. The statically recrystallized grain size decreases with increasing strain, decreasing initial austenite grain size and decreasing temperature; strain rate does not markedly affect the grain size produced by static recrystallization. The more extensive grain refinement obtained at lower temperature can be attributed to the reduced recovery and the associated increased dislocation density, which enhances the driving force for nucleation. It also reflects the lower mobility of recrystallizing grain boundaries resulting in lower growth rates, thereby allowing for a comparatively longer period for additional nucleation. Larger deformation (strain) generates a higher dislocation density and introduces smaller subgrains, thus increasing the density of nucleation sites for static recrystallization, which results in finer new grains. The effect of initial austenite grain size can be rationalized assuming that the predominant nucleation occurs at grain boundaries and that the nucleation rate per

boundary area is independent of grain size. These assumptions suggest z=1/3, in good agreement with the empirical values shown in Table 2.2.4. Consequently, larger initial grains are better grain refiners than smaller grains. A grain refinement limit is attained when $d_{rex} = d_0$. Under industrial rolling conditions, this limit falls usually in the range 20 to 40 μm. Figure 2.2.2 shows the recrystallized grain size in plain low-carbon steels as a function of initial grain size for a variety of temperatures and strains, thereby illustrating the effect of the processing parameters in attaining the grain size limit. The significance of rolling temperature and strain for the HSLA-Nb steel was confirmed in a pilot mill trial at the USS Technical Center.

Table 2.2.4: Parameters used for recrystallized grain size.

Steel	$A(\mu m^{2/3})$	z	p	$Q_{gr}(kJmol^{-1})$
A36	89	0.37	0.37	28
DQSK	89	0.37	0.37	28
HSLA-V	89	0.37	0.37	28
HSLA-Nb	12000	0.33	0.79	88
HSLA-Nb/Ti50	12000	0.33	0.79	88
HSLA-Nb/Ti80	416	0.33	0.65	46
IF(Nb-rich)	12000	0.33	0.79	88
IF(Nb-lean)	12000	0.33	0.79	88

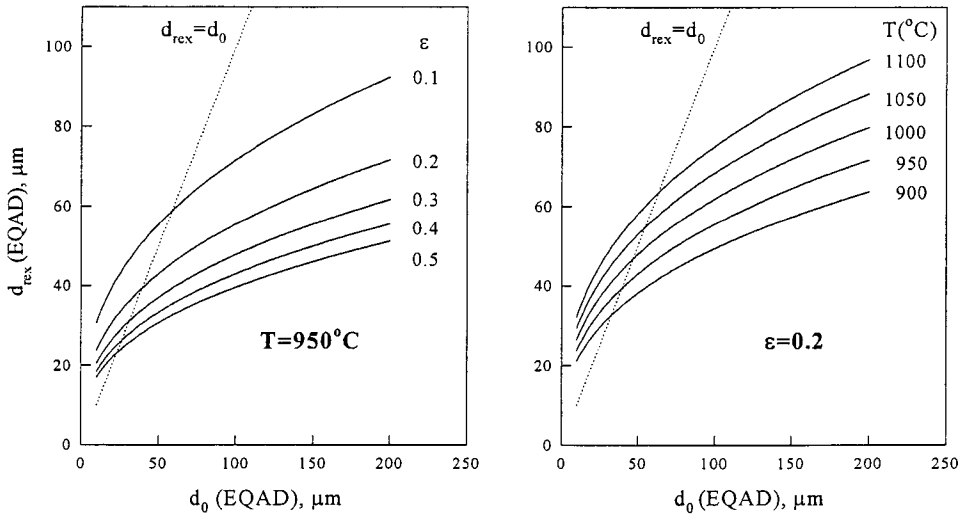

Figure 2.2.2: Effect of initial grain size, temperature and strain on the statically recrystallized grain size in plain low-carbon steels.

2.3. Kinetics of Precipitation

2.3.1. Objectives

The addition of microalloying elements (V, Nb, Ti) to low-carbon steels led to the development of HSLA steels which experience precipitation strengthening due to the formation of microalloy carbides and nitrides during processing. Precipitation may occur in austenite during hot rolling as strain-induced precipitation or in ferrite during run-out table cooling and coiling. The latter precipitation process provides the anticipated strengthening of the hot-rolled steel. Thus, the objectives of this subtask were twofold. Firstly, the precipitation kinetics in austenite were to be investigated along with their potential interaction with the recrystallization and grain growth processes. Secondly, the precipitation strengthening kinetics in ferrite during coiling were to be studied. The determination of the nature and the size distribution of precipitates in laboratory samples was to be supplemented with similar investigations on transfer bar and coil material in order to develop precipitation models applicable to mill conditions.

2.3.2. Results

2.3.2.1 Precipitation in austenite

The study of strain-induced precipitation in austenite emphasized the Nb containing steels, in particular the HSLA-Nb and the HSLA-Nb/Ti 80 steels. Based on the T_{nr} investigations (cf. Subtask 2.2) only these two grades show a marked tendency for strain-induced precipitation at hot rolling temperatures.

The precipitation kinetics in austenite were investigated with a stress relaxation technique carried out on the Gleeble 1500 thermo-mechanical simulator. After a solution treatment at 1200 °C for the HSLA-Nb steel and 1250 °C for the HSLA-Nb/Ti 80 steel, the specimens were cooled to the test temperature at a rate of approximately 5 °C/s; the test temperatures ranged from 850 to 1050 °C. After attaining a uniform temperature along the working zone of the specimen, a 10% prestrain was applied at a strain rate of 0.1 s^{-1}. Following the prestrain, the length of the specimen was held constant and the load relaxation was recorded continuously for one hour. The stress relaxation of the specimen was then calculated from the measurements.

The stress relaxation curves show two characteristic inflection points indicating a change in the relaxation rate. These two points can be identified as the precipitation start time, P_s, and the precipitation finish time, P_f. The P_s and P_f values measured at different test temperatures were used to construct the precipitation-time-temperature diagram shown in Figure 2.3.1.

In order to determine the nature and size distribution of precipitates in the tested specimens as well as in the industrial transfer bar and coil samples, extraction replicas were prepared. These replicas were examined in a Hitachi H-800 scanning transmission electron microscope (STEM). Chemical analysis of individual particles was performed using an Ortec EEDS-II energy dispersive X-ray (EDX) spectrometer. Both the scanning

and transmission modes were employed in analyzing the particle composition, while only the transmission mode was used in studying the particle size and morphology. The STEM analysis confirmed the presence of Nb particles, as well as TiN, and more complex Nb and Ti precipitates in the Ti containing HSLA grades. TiN are stable precipitates which do not dissolve during reheating. Interestingly, coarse TiN with sizes in the order of 1 μm were observed in the HSLA-Nb/Ti80 steel whereas a rather fine distribution of TiN was found in the HSLA-Nb/Ti50 grade; this information was used to explain their different grain growth behavior at higher temperatures (cf. Subtask 2.1). Based on these observations, it was concluded that strain-induced precipitation can be associated with Nb(CN) in the HSLA-Nb steel and NbC as well as TiC in the HSLA-Nb/Ti 80 steel.

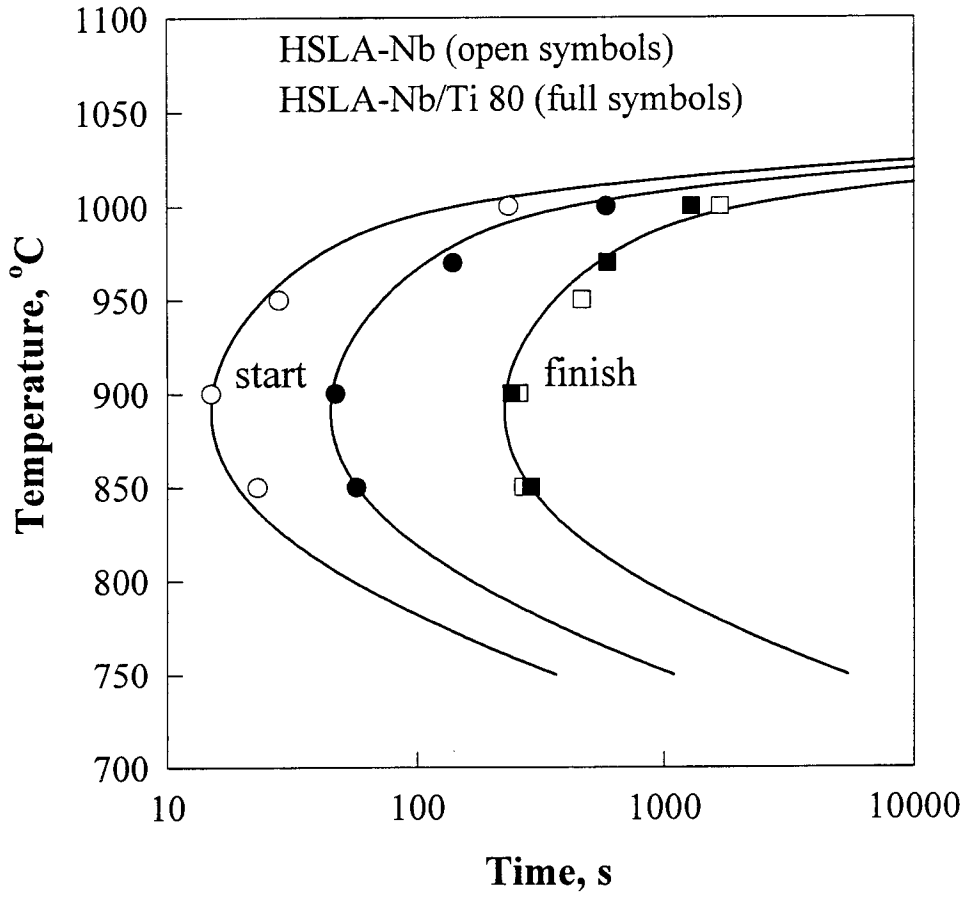

Figure 2.3.1: Precipitation-time-temperature diagram for the HSLA-Nb and HSLA-Nb/Ti 80 grades.

The experimental data were used to develop a kinetic model describing the start and progress of Nb(C,N) precipitation in austenite during hot rolling. As shown in Figure

2.3.1, an earlier precipitation start is observed for HSLA-Nb, the lower Nb grade. This is attributed to the presence of Nb(CN) in the HSLA-Nb grade, whereas in the higher Nb grade, the HSLA-Nb/Ti80, all N is tied up in TiN and only NbC and TiC can form; the carbides show lower nucleation rates. Apart from these details, the measured precipitation start times exceed in both grades the finish mill residence times. Thus, to a first approximation, it is assumed that all Nb (and excess Ti) remains in solution for the hot strip mill. However, Nb(C,N) precipitation is predicted for the extended processing times experienced in the Steckel mill. Significant precipitation may occur in the Steckel mill, with the degree of precipitation strengthening being a function of rolling temperature and mill residence time. This is illustrated in Figure 2.3.2 with results from torsion Steckel mill simulations.

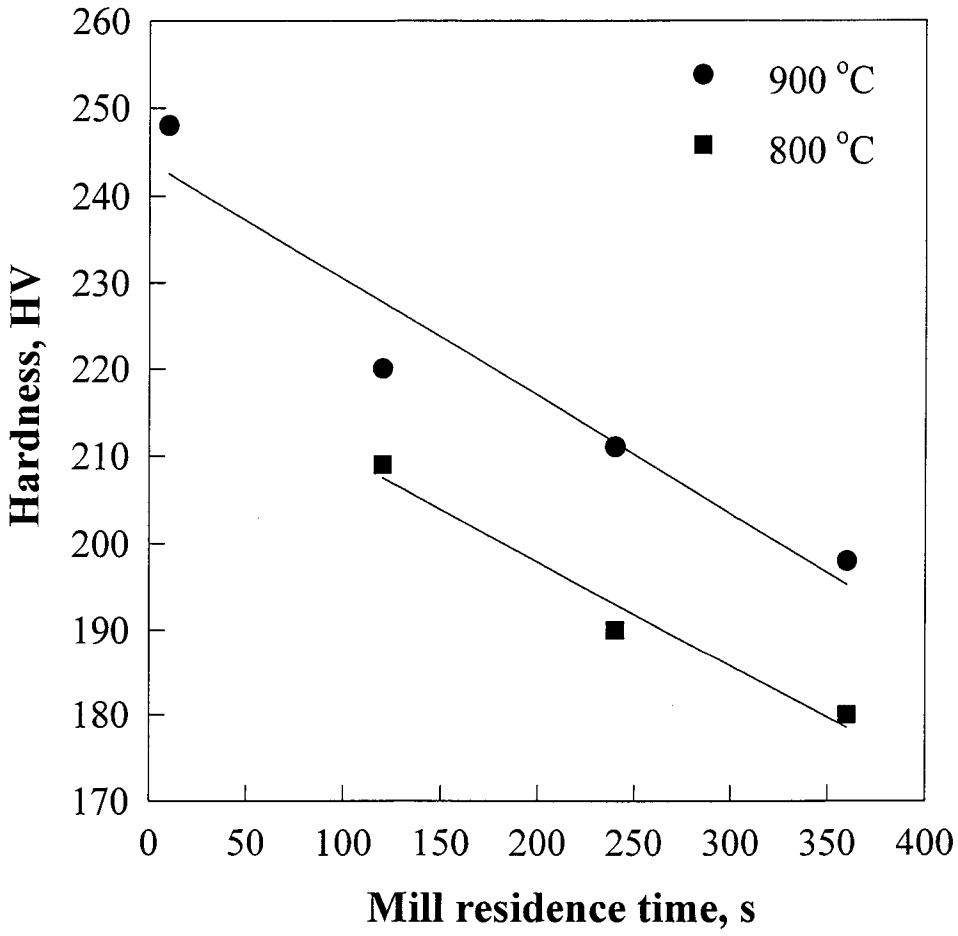

Figure 2.3.2: Strength of HSLA-Nb/Ti80 as a function of rolling temperature and mill residence time, as observed in torsion simulations.

The precipitation model[5] for the Steckel mill consists of two parts. Precipitation start is predicted based on classical nucleation theory, where the nucleation rate of Nb precipitates is given by

$$J = \frac{Dc}{a^2} N \exp\left(- \frac{16\pi(\xi\gamma)^3}{3\Delta G_{chem}^2 kT} \right) \qquad (2.3.1)$$

Here, $D = 1.49\text{cm}^2\text{s}^{-1}\exp(-28360/T)$ is the bulk diffusion coefficient of Nb in austenite,[6] c the Nb concentration in mole fraction, a=3.6 Å the lattice constant of austenite, γ the energy of the particle-matrix interface and ξ a constant describing the beneficial effect of heterogeneous nucleation. The chemical driving force, ΔG_{chem}, for precipitation is given by

$$\Delta G_{chem} = \frac{8kT}{a'^3}\left[\ln\left(\frac{c_1^e}{c_1}\right) + \ln\left(\frac{c_2^e}{c_2}\right) \right] \qquad (2.3.2)$$

where k is the Boltzmann constant, a' is the lattice constant of the precipitate, c_i (i=1,2) are the concentrations of the precipitate forming elements (mole fraction), and the equilibrium concentrations can be written as

$$c_1^e = \frac{c_1 - c_2}{2} + \sqrt{\left(\frac{c_1 - c_2}{2}\right)^2 + L} \qquad c_2^e = \frac{c_2 - c_1}{2} + \sqrt{\left(\frac{c_1 - c_2}{2}\right)^2 + L} \qquad (2.3.3)$$

with the solubility product, L. Assuming preferential nucleation at dislocations, the potential nucleation site density is expressed as

$$N = \frac{\rho_o + \rho(1 - F_X)}{a} \qquad (2.3.4)$$

with the recrystallized fraction, F_X, and the dislocation densities, $\rho_o = 10^8\text{cm}^{-2}$ and

$$\rho = \left(\frac{2\pi\sigma}{Mb\mu}\right)^2 \qquad (2.3.5)$$

where σ is the flow stress, M = 3.06 is the Taylor factor, b = 2.58 Å is the Burgers vector, and $\mu = 8.1\ [1 - 0.91(T-300)/1810]\ 10^{10}\ \text{J/m}^3$ is the shear modulus.

The nuclei density is given by

$$\Theta = \int_{T_o}^{T} \frac{JdT}{\Psi} \qquad (2.3.6)$$

[5] W.P. Sun, M. Militzer, D.Q. Bai and J.J. Jonas, *Acta Metall. Mater.* **41**, 3595 (1993).
[6] S.H. Park, S. Yue and J.J. Jonas, *Metall. Trans.* **23A**, 1641 (1992).

where Ψ is the instantaneous cooling rate. Precipitation start is realized if $\Theta = \Theta^* = 10^{19} m^3$. Table 2.3.1 summarizes the steel specific parameters of this precipitation start model.

Table 2.3.1: Parameters used for the precipitation start model.

	HSLA-Nb	HSLA-Nb/Ti50	HSLA-Nb/Ti80
1	Nb	Nb	Nb+Ti(excess)*
2	C+N	C	C
a'(Å)	4.445	4.47	4.44
L	$2.81\times10^{-4}10^{(2.26-6770/T)}$	$2.81\times10^{-4}10^{(2.81-7020/T)}$	$10^{(2.26-10869/T)}$
$\gamma(J/m^2)$	0.65	0.6	0.6
ξ	0.49	0.42	3.231-0.0020863T

$^* c_1 = c + \frac{56}{4800}(Ti - \frac{48}{14}N)$ with Ti, N in wt%

Growth of the precipitates after nucleation is controlled by long range diffusion of Nb in austenite. The fraction precipitated, Y ($0<Y<1$), can be expressed as

$$\int_0^{Y(t)} Y^{-1/3}(1-Y)^{-1}dY = 3R_f^{-2}(2c)^{1/3}\int_{t_s}^{t} D(T(t'))dt' \qquad (2.3.7)$$

which is equivalent to

$$dY = Y^{1/3}(1-Y)\frac{3D}{R_f^2}(2c)^{1/3}dt \qquad (2.3.8)$$

where

$$\log R_f = 13.245 - 0.02962(T-273) + 0.00001948(T-273)^2 \qquad (2.3.9)$$

has been obtained from the precipitation-time-temperature diagram for both investigated steels. The amount, X, of Nb remaining in solution after exiting the mill can then simply be obtained from

$$X = (1-Y)Nb \qquad (2.3.10)$$

where Nb is the total Nb concentration; a similar expression gives the amount of excess Ti remaining in solution for the HSLA-Nb/Ti 80 steel.

2.3.2 Precipitation strengthening kinetics

The strengthening effects of VC, VN, Nb(C,N) and TiC precipitates have been evaluated with aging tests on coil samples and torsion samples of the HSLA-V and HSLA-Nb/Ti 80 grades, respectively. Underaged coil samples of the HSLA-V steel were

aged in the temperature range 650 to 750 °C and showed the development of an aging peak with peak times increasing as temperature decreases. TEM studies confirmed that coarsening of V precipitates is responsible for the observed aging response. Similar aging studies were then performed on torsion samples of the HSLA-Nb/Ti 80 steel because no sufficiently underaged Nb containing HSLA steel coil samples were available. The torsion test rolling simulations were followed by aging studies in the 550-650 °C temperature range. The torsion samples were initially heated to 1250 °C and held for 10 minutes, then subjected to a multipass rolling simulation incorporating strains of 0.1 to 1 with interstand times of 10 to 1.3 seconds over the temperature range 1100 to 900 °C at a strain rate of 1/s. The aging response is qualitatively similar to that of the HSLA-V steel with TEM observations confirming the presence of fine Nb particles at the aging peak and significantly coarser precipitates in the overaged material.

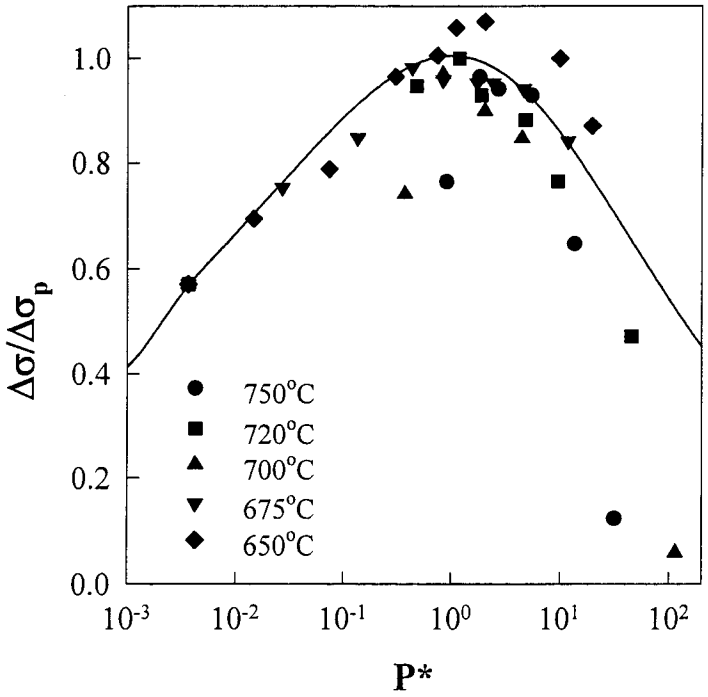

Figure 2.3.3: Precipitation hardening in the HSLA-V steel.

The strengthening kinetics is shown in Figure 2.3.3 for the HSLA-V steel. Figure 2.3.4 compares the results obtained from the HSLA-Nb/Ti 80 steel with literature data for a 0.046%Nb steel.[7] A temperature-corrected time scale is adopted in both figures. The temperature correction is based on the Shercliff-Ashby model[8] which assumes particle

[7] L.G.E. Vollrath et al., *Microalloying'88*, ASM, Metals Park, Ohio, 353 (1988).
[8] H.R. Shercliff and M.F. Ashby, *Acta Metall. Mater.* **38**, 1789 (1990).

coarsening as the rate controlling step; the model predictions are shown by the solid lines. The normalized temperature-corrected time is given by

$$P^* = \frac{\exp(-Q/kT)}{P_p T} \tag{2.3.11}$$

where Q is the effective activation energy of V and Nb diffusion in ferrite, respectively and P_p is a constant; the values are summarized in Table 2.3.2. The model, which was originally developed to describe aging of Al alloys, is valid, at least in a first approximation also for HSLA-steels. Interestingly, the kinetic parameters obtained for the HSLA-Nb steel remain applicable also for the HSLA-Nb/Ti 80 steel; this suggests that Nb diffusion is also the rate controlling parameter in the Nb/Ti grade. To describe precipitation during cooling of a coil, a more general form of equation (2.3.11) can be written; i.e.,

$$P = \frac{1}{P_p} \int_{t_o}^{t} \frac{\exp(-Q/kT(t'))}{T(t')} dt' \tag{2.3.12}$$

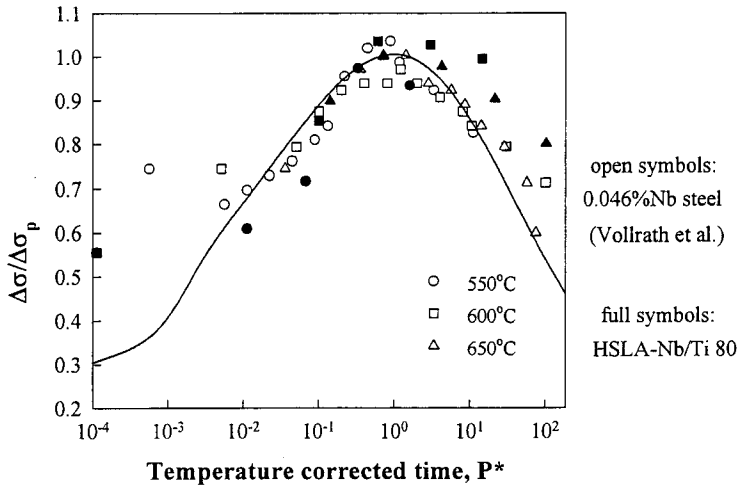

Figure 2.3.4: Precipitation hardening in Nb containing HSLA steels.

Table 2.3.2: Parameters used to describe precipitation strengthening

Steel	Q, eV	P_p, s/K
HSLA-V	4.0	1.3×10^{-21}
HSLA-Nb	2.8	4.7×10^{-16}
HSLA-Nb/Ti 50	2.8	4.7×10^{-16}
HSLA-Nb/Ti 80	2.8	4.7×10^{-16}

The maximum precipitation strength increment, $\Delta\sigma_p$, is chemistry dependent. Based on UTS predictions, 145 MPa has been determined for the HSLA-V steel. For the Nb and Ti microalloyed steels, the following relation has been applied

$$\Delta\sigma_p = 180(1-\exp(-52c_{Nb})) + 2000Ti_{excess} \qquad \text{(in MPa)} \qquad (2.3.13)$$

where the amount of excess Ti

$$Ti_{excess} = Ti - 48N/14 \qquad \text{(in wt\%)} \qquad (2.3.14)$$

is only of relevance for the HSLA-Nb/Ti 80 steel. To facilitate the strength prediction after Steckel mill rolling, the concentrations in equation (2.3.13) are given by the microalloying amount remaining in solution.

STEM analyses have also been performed on the as-received and aged HSLA-Nb/Ti 80 coil samples. Large, cubic shaped TiN particles of approximately 1 μm were observed in all samples. In addition, a dense population of 20-30 Å fine needle-like precipitates forming predominantly at dislocations characterized the strength peak condition, similar to the observation made in the torsion samples. EDX analysis indicates these fine precipitates to be a mixture of (Nb,Ti)C, which are believed to be responsible for the observed precipitation strengthening. In overaged samples, the needle-like precipitates do show coarsening and attain sizes of approximately 50 Å. Further, there is a tendency for changing their shape from needles to rounder particles.

In order to predict AlN precipitation in the DQSK steel, the precipitation model proposed by Duit et al.[9] has been incorporated. The amount of nitrogen in solution is then given by

$$N_{free} = N_{total} - 5190Al_{as}\left(1-\exp\left\{-\left[\int_{t_o}^{t}\frac{\exp(-260kJmol^{-1}/RT}{4.3\times10^{-10}s}\right]^{0.44}\right\}\right) \qquad (2.3.15)$$

where N_{total} is the total amount of nitrogen (ppm), Al_{as} is the amount of acid soluble aluminium (wt%). Equation (2.3.15) covers the following chemistry range: 15ppm< N_{total} <75ppm and 0.028%< Al_{as} <0.0052%.

[9] Duit et al.,*Thermec'88*, ISIJ, Tokyo, 114 (1988).

2.4. Kinetics of Austenite Decomposition

2.4.1. Objectives

The objective of the subtask on austenite decomposition kinetics is to model the transformation kinetics on the run-out table and to develop the associated $\gamma \rightarrow \alpha$ grain size relationship.* In low carbon steels, mechanical properties such as strength and toughness can be directly related to the ferrite grain size produced on the run-out table. In general, the austenite-to-ferrite transformation kinetics depend on the austenite microstructure obtained after rolling and the cooling conditions on the run-out table. The effects of cooling rate, chemistry, initial austenite grain size, retained strain (under no-recrystallization condition) and precipitation on the phase transformation and resulting ferrite grain size distribution are to be quantified.

2.4.2. Results

2.4.2.1 Transformation kinetics

Continuous cooling tests were performed using a dilatometer and a Gleeble 1500 thermo-mechanical simulator to quantify the austenite-to-ferrite transformation kinetics. Pre-treatment, i.e. reheating conditions and deformation conditions (for studies with retained strain) were varied to incorporate the effect of initial austenite microstructure on the transformation behavior. The investigations were designed to quantify the effect of cooling rate (1-150 °C/s), austenite grain size (10 - 100 μm) and retained strain (0 - 0.6) on the austenite-to-ferrite transformation kinetics and the resulting ferrite grain size. The transformation behavior is for all steels similar to that of the plain low-carbon steels (A36, DQSK). The major effects are exerted by cooling rate and initial austenite grain size. As illustrated in Figures 2.4.1 and 2.4.2 for the undeformed HSLA-Nb steel, increasing the cooling rate and/or the initial austenite grain size decreases the transformation temperature. The effect of retained strain on the austenite decomposition kinetics in the Nb containing steels is comparatively minor for accelerated cooling on the run-out table, as illustrated in Figure 2.4.3 for the transformation start temperature in the HSLA-Nb steel. The main effect of retained strain is to enhance the production of a ferritic microstructure. This is essential for the HSLA-Nb/Ti80 steel where retained strain is needed to produce a predominantly ferrite microstructure. Further, retained strain may lead to additional ferrite grain refinement, which is particularly pronounced for the IF steels.

* In the original outline of the program, the quantification of the γ-α relationship; i.e., the ferrite grain size, was part of the grain growth subtask 2.1. Because the ferrite grain size results from the austenite decomposition, the quantification of the ferrite grain size is dealt with in this subtask.

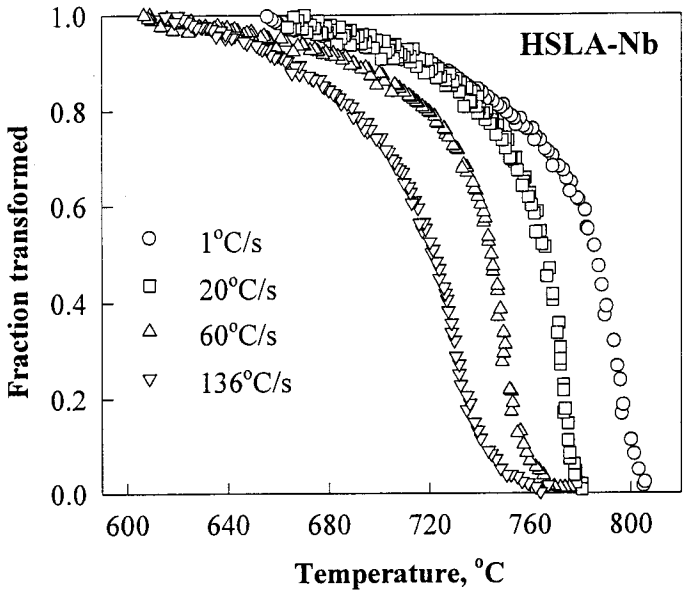

Figure 2.4.1: Austenite decomposition kinetics for different cooling rates in HSLA-Nb steel without retained strain and d_γ = 18 μm.

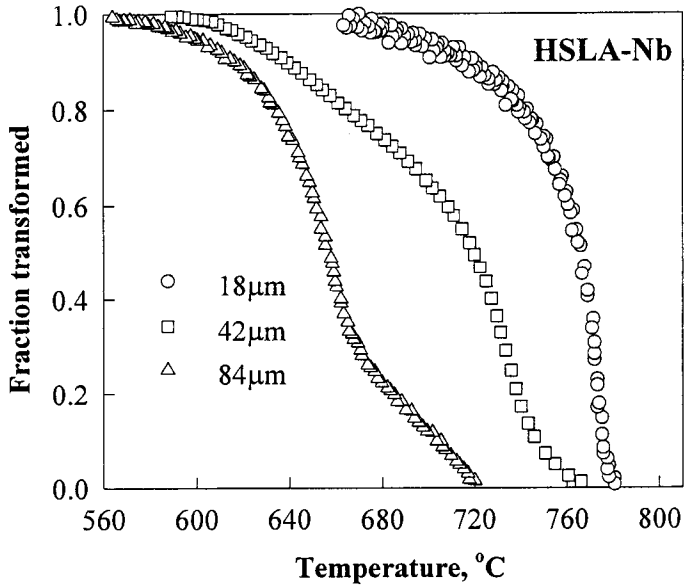

Figure 2.4.2: Austenite decomposition kinetics for initial austenite grain sizes in HSLA-Nb steel without retained strain at a cooling rate of 20 °C/s.

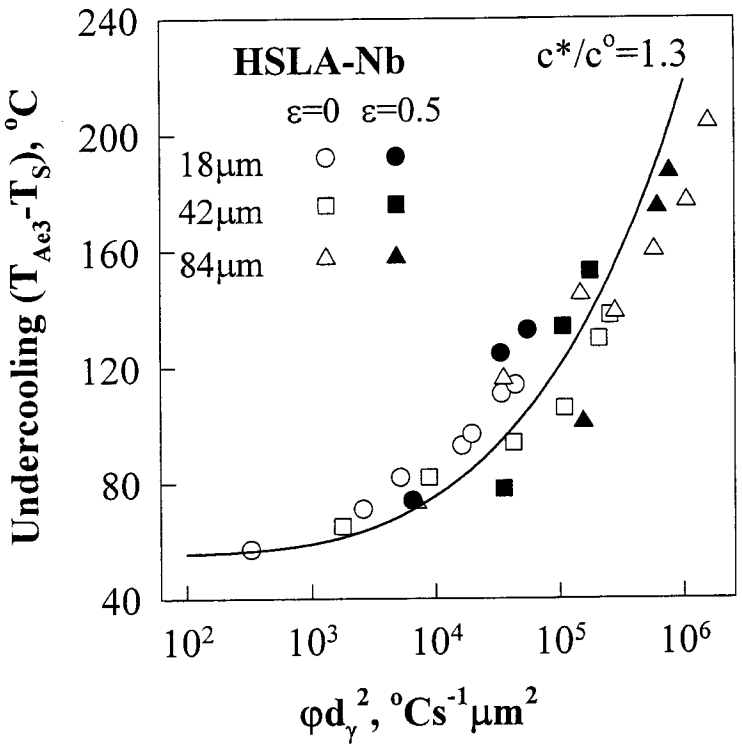

Figure 2.4.3: Effect of retained strain on the transformation start temperature, T_S, in HSLA-Nb steel as a function of the cooling rate, φ, and the austenite grain size, d_γ.

With the aid of the experimental results, a transformation model was developed for the plain low-carbon steels which could be extended to the microalloyed steels by adopting some minor modifications. In detail, the proposed transformation model is as follows. The start of the austenite decomposition can be predicted, based on nucleation and early growth of corner nucleated ferrite, by

$$\frac{dR}{dT}\frac{dT}{dt} = D_C \frac{c_\gamma - c^o}{c_\gamma - c_\alpha}\frac{1}{R} \qquad R(T_N)=0 \qquad (2.4.1)$$

where R is the radius of corner ferrite nucleated at T_N, D_C is the carbon diffusion coefficient,[10] c_o the carbon content, c_γ and c_α are the equilibrium carbon concentrations in austenite and ferrite, respectively. The transformation starts when

[10] J. Ågren, *Scripta Metall.* **20**, 1507 (1986).

$$\frac{R(c_\gamma - c^o)}{(c^* - c^o)} = \frac{d_\gamma}{\sqrt{2}} \qquad (2.4.2)$$

is attained, where d_γ is the volumetric austenite grain size (i.e., 1.2 x EQAD) and c^* is a limiting carbon concentration; the latter can be expressed as

$$c^* = (x^* + x_\gamma / d_\gamma + \Delta x \exp(-\tau(T_N - T)^\omega)c^o \qquad (2.4.3)$$

The parameter values are given in Table 2.4.1 for all steels except the HSLA-Nb/Ti 80 grade.

Table 2.4.1: Parameters used for the transformation start prediction.

Steel	T_N, K	x^*	x_γ	Δx	τ	ω
A36	1037	1.08	1.7	0.20	0.02	1
DQSK	1116	1.15	9.1	0.15	0.0003	2.2
HSLA-V	1116	1.18	4.2	0.15	0.0003	2.2
HSLA-Nb	1078	1.14	4.6	0.15	0.0003	2.2
HSLA-Nb/Ti50	1073	1.23	8.5	0.15	0.0003	2.2
IF(Nb-rich)*	1162	4.15	0	-0.15	0	0
IF(Nb-lean)*	1162	4.15	0	-0.15	0	0

* assumes a nominal austenite grain size = 40 μm

For the HSLA-Nb/Ti80 steel (T_N = 1058 K), the effect of retained strain, ε_r, has to be included such that

$$c^* = (2.2 - \varepsilon_r / 3)c^o \qquad \varepsilon_r < 0.6 \qquad (2.4.4a)$$

$$c^* = 2c^o \qquad \varepsilon_r > 0.6 \qquad (2.4.4b)$$

The latter indicates a minor acceleration of the transformation in the HSLA-Nb/Ti80 steel as a consequence of the retained strain. This effect is apparent in this grade since the comparatively high levels of Mn and Nb alloying tend to delay the transformation to lower transformation temperatures, as shown in Figure 2.4.4.

Subsequent ferrite growth can be described using an Avrami equation with the time exponent n = 0.9 and assuming additivity, where the normalized ferrite fraction, X, is given by

$$X = \frac{c_\gamma - c^o}{c_\gamma - c_\alpha}\left[1 - \exp\left\{\frac{1}{d_\gamma^m}\left(\int_{T_S}^{T}\frac{\exp[\{b_1(T_{Ae3} - T') + b_2\}/n]}{\varphi(T')}dT'\right)^n\right\}\right] \qquad (2.4.5)$$

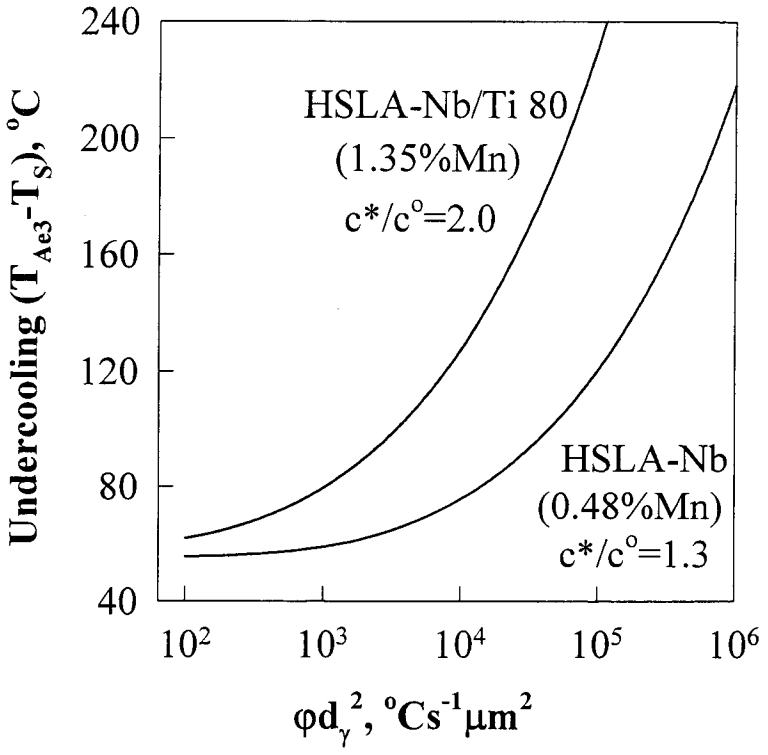

Figure 2.4.4: Effect of Mn on the transformation start temperature.

where $\varphi(T) = -dT/dt$ is the instantaneous cooling rate; values for b_1, b_2 and m are summarized in Table 2.4.2.

Table 2.4.2: Parameters used for the transformation model.

Steel	m	b_1	b_2
A36	1.7	0.043	-1.6
DQSK	2.2	0.033	4.8
HSLA-V	1.8	0.022	4.2
HSLA-Nb	1.8	0.030	1.1
HSLA-Nb/Ti50	1.3	0.026	-0.44
HSLA-Nb/Ti80	1.3	0.035	-3.6
IF(Nb-rich)*	0	0.057	-4.9
IF(Nb-lean)*	0	0.086	-5.5

* assumes a nominal austenite grain size = 40 µm

In general, a ferrite fraction of 95% or more is formed under industrial hot rolling, controlled cooling and coiling conditions for the low and ultra low carbon steels investigated in this study. However, the potential of non-ferritic transformation products has to be considered for the A36 and the HSLA-Nb/Ti 80 grades. For these two steels a more detailed assessment of the ferrite stop condition is required. In the A36 steel, this can be associated with the initiation of pearlite formation. Pearlite starts to form when the velocity of the α-γ interface, $v_{\alpha\gamma}$, is below a critical velocity for cementite nucleation; i.e.,

$$v_{\alpha\gamma} < v_{crit} = 0.164 T c_I D_C \{\ln(c_I / c_P)\}^2 \text{ (in } \mu\text{m/s)} \qquad (2.4.6)$$

where the velocity can be expressed as a function of the overall transformation rate and austenite grain size

$$v_{\alpha\gamma} = \frac{dY}{dt}\frac{d_\gamma}{6}(1-Y)^{-2/3} \qquad (2.4.7)$$

It should be noted that sufficiently low temperatures are required to form pearlite so that $c_I > c_P$ is fulfilled where c_I is the interfacial concentration of C and c_P is the solubility of C in austenite. Pearlite growth in the A36 steel can be described with an Avrami equation adopting additivity for the pearlite portion of the transformation, $(1-F)$, where F is the final ferrite fraction. The Avrami equation for pearlite growth is given by

$$X_P = 1 - \exp(-b_p t^{0.9}) \qquad (2.4.8)$$

with $b_P = 14.5 - 0.02 d_\gamma - 0.015 T$.

For the HSLA-Nb/Ti 80 steel, retained strain extends the cooling rate range for which polygonal (or quasi-polygonal) ferrite is being formed. However, detailed quantification of partly non-polygonal microstructures is difficult and only very rough estimates can currently be made to characterize the transition condition for the formation of non-polygonal structures. As a first approximation,

$$T_{transition} = 620 - 600\varepsilon_r^3 \quad \text{(in °C)} \quad \text{and} \quad T_{transition} > 490\ °C \qquad (2.4.9)$$

can be adopted as the temperature below which non-polygonal transformation products start to form. Alternatively, ferrite formation stops when a fraction of approximately 0.9 is reached. Transformation kinetics for non-polygonal products are then calculated using the A36 pearlite model as a first approximation.

2.4.2. Ferrite grain size

The ferrite grain size, d_α (EQAD in μm), is determined by the nucleation processes active at the transformation start. Consequently, the grain size can be expressed as a function of the transformation start temperature, T_S. In detail, the following relationships have been obtained, where F denotes the ferrite fraction.

A36: $$d_\alpha = \left\{F \exp(52.3 d_\gamma^{0.029} - 51{,}000 / T_S)\right\}^{1/3} \quad (2.4.10)$$

DQSK: $$d_\alpha = \left\{F \exp(50.7 d_\gamma^{0.024} - 51{,}000 / T_S)\right\}^{1/3} \quad (2.4.11)$$

HSLA-V: $$d_\alpha = 1.25\left\{F \exp(47.3 d_\gamma^{0.037} - 51{,}000 / T_S)\right\}^{1/3} \quad (2.4.12)$$

HSLA-Nb: $$d_\alpha = \left\{F \exp(49.6 d_\gamma^{0.036} - 51{,}000 / T_S)\right\}^{1/3} \quad \varepsilon_r = 0 \quad (2.4.13a)$$

$$d_\alpha = 12.5 \varphi^{-0.24} \quad \varepsilon_r \geq 0.5 \quad (2.4.13b)$$

where φ is the average cooling rate between T_N and T_S. For intermediate retained strain levels, a linear interpolation between equations 2.4.13a and 2.4.13b yields the ferrite grain size. This minor additional grain refinement due to retained strain in the HSLA-Nb steel is illustrated in Figure 2.4.5.

HSLA-Nb/Ti 50: $$d_\alpha = \left\{F \exp(50.7 d_\gamma^{0.037} - 51{,}000 / T_S)\right\}^{1/3} \quad (2.4.14)$$

HSLA-Nb/Ti80: $$d_\alpha = \left\{F \exp(19.5 + 1.7 \exp(-6\varepsilon_r) - 15{,}400 / T_S)\right\}^{1/3} \quad (2.4.15)$$

IF steel (Nb lean): $$d_\alpha = \left\{\exp(29.2 - 22{,}200 / T_S)\right\}^{1/3} \quad (2.4.16)$$

IF steel (Nb rich): $$d_\alpha = \left\{\exp(28.6 - 22{,}200 / T_S)\right\}^{1/3} \quad (2.4.17)$$

Figure 2.4.6 illustrates the validity of the model predictions for the HSLA-Nb/Ti 80 steel with a retained strain of 0.6 producing a pancaked austenite microstructure. Figure 2.4.7 shows the ferrite grain size predictions for typical austenite microstructures obtained at the exit of the finish mill for a number of the steels investigated. Clearly, the beneficial effect of accelerated cooling in terms of ferrite grain refinement is shown. Moreover, the predictions are in good agreement with observations made on coil samples, assuming that the typical cooling rates under the water sprays of a run-out table are in the order of 100 °C/s.

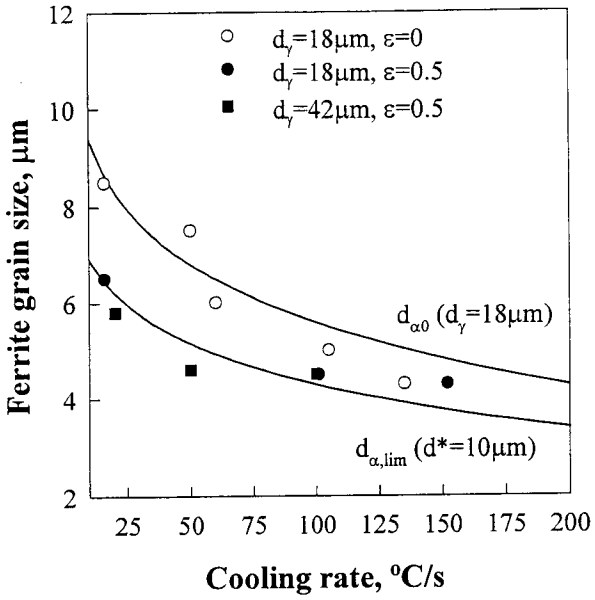

Figure 2.4.5: Comparison of predicted (lines) with measured (symbols) ferrite grain sizes obtained in the HSLA-Nb steel with and without retained strain as a function of cooling rate.

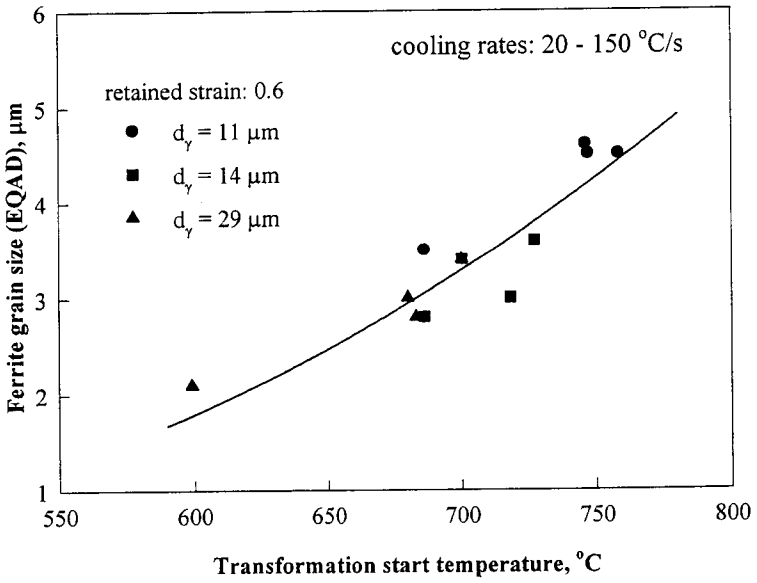

Figure 2.4.6: Ferrite grain size in the HSLA-Nb/Ti80 steel as a function of the transformation start temperature; solid line indicates the model prediction.

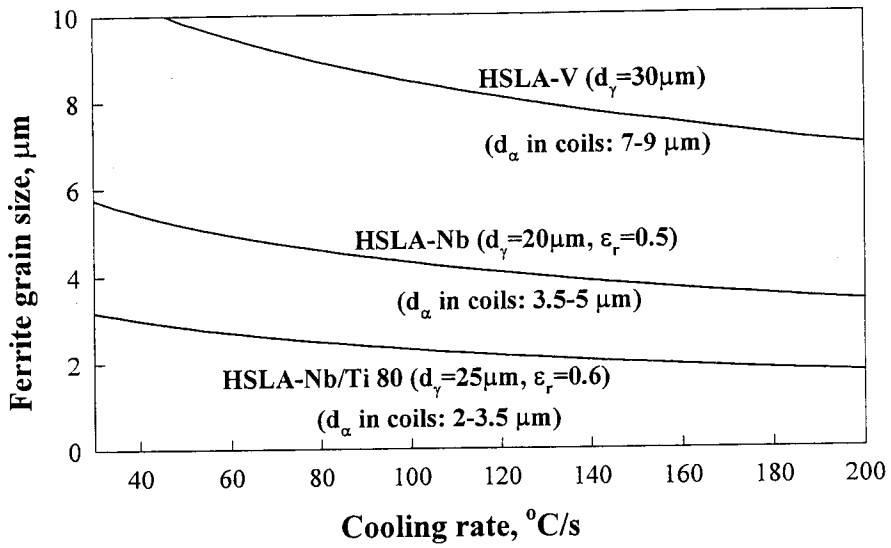

Figure 2.4.7: Ferrite grain size predictions for three classes of HSLA steels.

2.7. The Hot Torsion System

The development of the hot torsion testing facility was a collaboration between UBC and DSI Inc. Extensive discussions begun in late 1994 to develop the specific requirements that would be necessary for the creation of a state of the art facility. During 1995, the system was constructed and testing of its capabilities was initiated at DSI's manufacturing plant in Poestenkill, New York. As part of this process, UBC personnel visited DSI in July 1995 (W.J. Poole) and in December 1995 (W.J. Poole and X. Chen). Following the visit in December, the final modifications of the machine were completed which led to the subsequent visit by X. Chen in January, 1996. At this time, the system was deemed satisfactory and the preparations for shipping to UBC were made. The system arrived at UBC in February 1996 and the final installation was made by DSI personnel during the first week of March. After the installation, commissioning of the equipment was immediately initiated. During this period a number of shortcomings in the machine were identified and rectified (primarily related to temperature gradients in the sample and the sample gripping arrangement). Following this period, the efforts shifted towards i) gaining experience in operation of the equipment, ii) establishing the practical operational limits and iii) developing standard simulation procedures.

The basic operational capabilities, which are summarized in Table 2.7.1, were established by June, 1996, although constant minor improvements have been made since that time. After this time, the machine was heavily used to contribute to the development of microstructural models, as described in previous sections. The work started with the A36, DQSK and HSLA-V steels, however, by far the largest effort was expended on examinations of the HSLA-Nb, HSLA-Nb/Ti50 and particularly the HSLA-Nb/Ti80. Finally, the torsion machine was used to examine the high temperature properties of the two IF steels included in this project. It is useful, however, to describe some of the specific contributions of the torsion machine, particularly those which would not have been possible with any other experimental techniques.

Table 2.7.1: Processing range of the DSI torsion machine

Process Parameter	Range of Torsion capabilities
re-heat temperature	up to 1250 °C
level of strain per simulation pass	0- limit of material ductility
strain rate of test	0.1-10 s^{-1} (quality of stress-strain data deteriorates above 1 s^{-1})
interpass time	0.5 s - unlimited
cooling rate during rolling simulation	0-10 °C/s
cooling rate during runout table simulation	0-40 °C/s

One of the most important advantages of the hot torsion testing machine over other simulation equipment (e.g. the Gleeble 1500) is the ability to simulate the entire hot rolling schedule from roughing to finishing to the runout table. Figure 2.7.1 shows the results obtained for the HSLA-V, the HSLA-Nb and the HSLA-Nb/Ti 80 steels subjected to one of the standard simulation programs (the simulation has 1 roughing plus 7

finishing passes). The results from this simulation offers a very useful qualitative comparison of different steels grades and allows for initial estimates of i) the different flow stresses during rolling, ii) the pass number after which recrystallization is no longer possible during the interpass time and iii) in some cases, the critical temperature for entry into the interphase rolling zone. In addition to obtaining information regarding the high temperature flow characteristics, the resulting microstructures could be investigated using standard metallographic techniques (however, care is required to ensure that the area examined is near the surface of the torsion sample due to the strain gradient in the test specimen). In general, excellent agreement was observed between torsion simulation samples and the supplied coil microstructures, as illustrated in Figure 2.7.2 for the HSLA-Nb/Ti 80 grade.

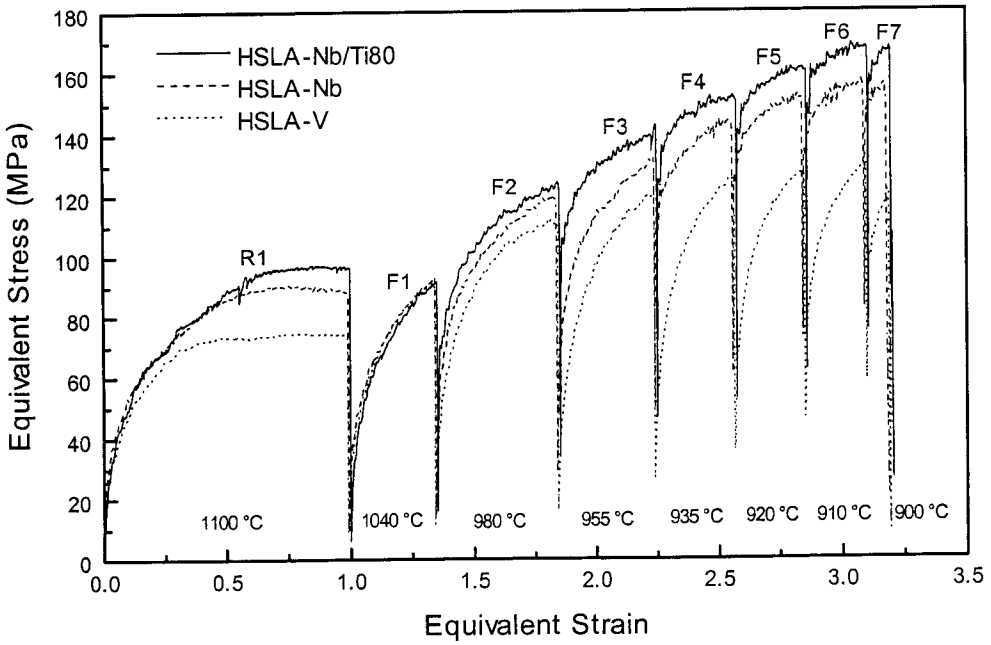

Figure 2.7.1: Comparison of the hot deformation behavior of the HSLA-V, HSLA-Nb and HSLA-Nb/Ti 80 steels.

Once the general behavior of a specific steel grade had been characterized, the torsion machine presented a unique opportunity to examine key process variables. For example, in the case of the HSLA-80 Nb/Ti, the reheat temperature, the finishing mill entry and the exit mill temperature could be varied. The resulting changes in the microstructure could be examined by metallography and also by making micro-hardness measurements. The latter measurements were particularly useful for examination of precipitation effects in all of the HSLA steels, as described in previous sections.

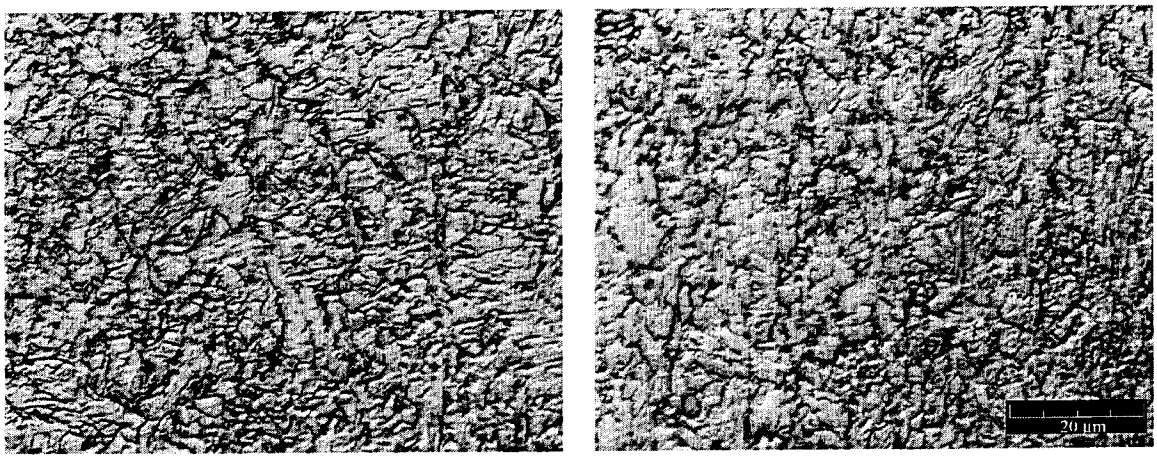

(a) (b)

Figure 2.7.2: Comparison of (a) the microstructure for the HSLA-Nb/Ti80 steel obtained in a torsion test rolling simulation with (b) that of an industrially hot-rolled coil.

In order to provide further information regarding room temperature mechanical properties, tensile samples were prepared from torsion samples after various hot rolling, runout table cooling and coiling simulations. Following the work of Hall and Worobec[11], the centre of the torsion samples were removed by drilling and the resulting cylindrical tube was tested in uniaxial tension. Using a wall thickness of approximately 1.5 mm, it was confirmed that the microstructure was essentially constant across the wall. The tensile test results from these samples were in excellent agreement with mechanical properties obtained from coil material supplied from the steel companies. For example, the HSLA 80-Nb/Ti coil samples (for a coiling temperature of 640 °C) had a yield stress and tensile stress of 650 and 730 MPa, respectively, which agrees favorably with the results from the torsion samples which were 660 and 740 MPa for the yield stress and tensile stress, respectively. Furthermore, this technique allowed for a detailed study of precipitation during coiling by supplementing the hardness data discussed in Sections 2.3 with yield strength (YS) and UTS, as shown in Figure 2.7.3. for aging of the HSLA-Nb/Ti80 torsion samples at 650 °C. This information has been critical for the development of the precipitation hardening models for the HSLA steels.

One of the last major efforts which involved extensive torsion testing was the development of Steckel mill simulations. The torsion machine was uniquely suited to these simulations since it is critical to capture the cumulative effects of longer interpass times during the hot rolling operation. A critical difference between hot strip rolling and Steckel mill rolling of HSLA 80-Nb/Ti steels is the amount of Nb and Ti precipitation which occurs in austenite relative to that in ferrite (i.e. during cooling). A series of torsion simulations were conducted to examine this effect and as a result it was possible to quantify the amount of precipitation in austenite vs. ferrite.

---

[11] D. Hall and J. Worobec, *Phase Transformations During the Thermal/Mechanical Processing of Steel*, ed. E.B. Hawbolt and S.Yue, CIM, Montreal, 305 (1995).

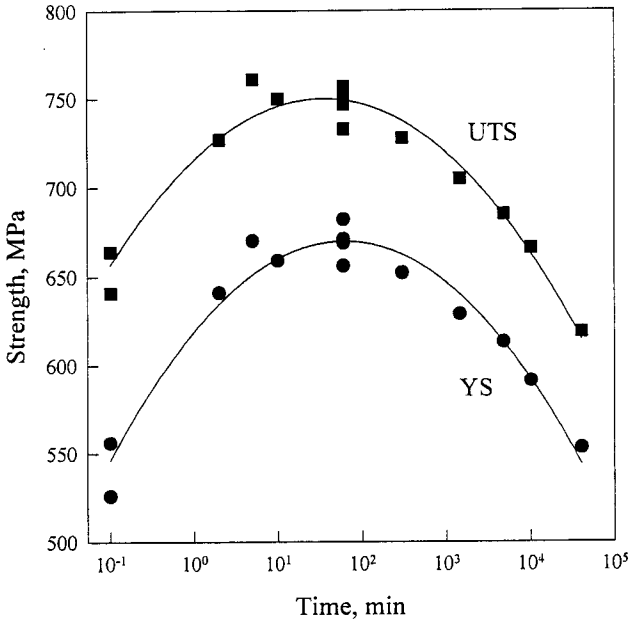

Figure 2.7.3: Mechanical properties of HSLA-Nb/Ti80 torsion samples during aging at 650°C.

In summary, the torsion machine provided a unique experimental tool to examine hot rolling processes. The torsion machine has been critical in completing the overall project. It was the only tool available which could duplicate hot mill conditions closely enough to allow for an evaluation of the effect of various processing parameters on structure and mechanical properties.

3.0. PUBLICATIONS

1. "Modelling the effect of pinning forces on recrystallization and grain growth", M. Militzer, W.P. Sun, E.B. Hawbolt and J.J. Jonas, *Advances in Hot Deformation Textures and Microstructures*, eds. J.J. Jonas, T.R. Bieler and K.J. Bowman , TMS, Warrendale, PA, 157-168 (1994).

2. "Influence of cooling rate on recrystallization and precipitation during hot rolling", W.P. Sun, M. Militzer, J.J. Jonas and E.B. Hawbolt, *35th Mechanical Working and Steel Processing Conference Proceedings*, ISS, Warrendale, PA, Vol. XXXI, 381-390 (1994).

3. "Austenite to ferrite transformation kinetics during continuous cooling", M. Militzer, R. Pandi and E.B. Hawbolt, *Solid → Solid Phase Transformations*, eds. W.C. Johnson, J.M. Howe, D.E. Laughlin and W.A. Soffa, TMS, Warrendale, PA, 177-182 (1994).

4. "Austenite and ferrite grain size evolution in plain carbon steel", M. Militzer, A. Giumelli, E.B. Hawbolt and T.R. Meadowcroft, *36th Mechanical Working and Steel Processing Conference Proceedings*, ISS, Warrendale, PA, Vol. XXXII, 375-384 (1995).

5. "Modelling recrystallization kinetics during strip rolling", W.P. Sun, E.B. Hawbolt and T.R. Meadowcroft, *36th Mechanical Working and Steel Processing Conference Proceedings*, ISS, Warrendale, PA, Vol. XXXII, 325-335 (1995).

6. "Mathematical modelling of deformation during hot rolling", D.Q. Jin, R.G. Stachowiak, I.V. Samarasekera and J.K. Brimacombe, *36th Mechanical Working and Steel Processing Conference Proceedings*, ISS, Warrendale, PA, Vol. XXXII, 401-407 (1995).

7. "Heat transfer model of runout table cooling: a fundamental approach", V.H. Hernandez, I.V. Samarasekera and J.K. Brimacombe, *36th Mechanical Working and Steel Processing Conference Proceedings*, ISS, Warrendale, PA, Vol. XXXII, 345-356 (1995).

8. "Ferrite nucleation during continuous cooling", M. Militzer, E.B. Hawbolt and T.R. Meadowcroft, *Phase Transformations During the Thermal/Mechanical Processing of Steel*, eds. E.B. Hawbolt and S. Yue, The Metallurgical Society of CIM, Montreal, PQ, 445-458 (1995).

9. "Modelling of austenite decomposition kinetics in steels during run-out table cooling", R. Pandi, M. Militzer, E.B. Hawbolt and T.R. Meadowcroft, *Transformations During the Thermal/Mechanical Processing of Steel*, eds. E.B. Hawbolt and S. Yue, The Metallurgical Society of CIM, Montreal, PQ, 459-471 (1995).

10. "Prediction of the onset of recrystallization after hot deformation", W.P. Sun and E.B. Hawbolt, *ISIJ International*, 35, 908-913 (1995).

11. "Interaction between precipitation and recrystallization during the hot rolling of Nb-containing HSLA steels", W.P. Sun, E.B. Hawbolt, T.R. Meadowcroft and J.J. Jonas, *HSLA Steels '95,* eds. G. Liu, H. Stuart, H. Zhang and C. Li, China Science & Technology Press, Beijing, 169-174 (1995).

12. "Modelling of austenite decomposition kinetics in Nb steel during run-out table cooling", R. Pandi, M. Militzer, E.B. Hawbolt and T.R. Meadowcroft, *HSLA Steels '95,* eds. G. Liu, H. Stuart, H. Zhang and C. Li, China Science & Technology Press, Beijing, 265-270 (1995).

13. "Prediction of the ferrite grain size in low carbon steels", M. Militzer, E.B. Hawbolt and T.R. Meadowcroft, *HSLA Steels '95,* eds. G. Liu, H. Stuart, H. Zhang and C. Li, China Science & Technology Press, Beijing, 271-276 (1995).

14. "Ferrite nucleation and growth during continuous cooling", M. Militzer, R. Pandi and E.B. Hawbolt, *Metallurgical and Materials Transactions*, 27A, 1547-1556 (1996).

15. "Thermomechanical history of hot steel strip during hot rolling - A comparison of conventional cold charge rolling and hot direct rolling of thin slabs", C. Muojekwu, D.Q. Jin, I.V. Samarasekera and J.K. Brimacombe, *37th Mechanical Working and Steel Processing Conference Proceedings*, ISS, Warrendale, PA, Vol. XXXIII, 617-633 (1996).

16. "Effect of cooling and deformation on the austenite decomposition kinetics", R. Pandi, M. Militzer, E.B. Hawbolt and T.R. Meadowcroft, *37th Mechanical Working and Steel Processing Conference Proceedings*, ISS, Warrendale, PA, Vol XXXIII, 635-643 (1996).

17. "On the nucleation kinetics of static recrystallization", W.P. Sun, E.B. Hawbolt and T.R. Meadowcroft, *37th Mechanical Working and Steel Processing Conference Proceedings*, ISS, Warrendale, PA, Vol. XXXIII, 679-688 (1996).

18. "Austenite grain growth kinetics in Al killed plain carbon steels", M. Militzer, A. Giumelli, E.B. Hawbolt and T.R. Meadowcroft, *Metallurgical and Materials Transactions*, 27A, 3399-3409 (1996).

19. "Modelling the phase transformation kinetics in low carbon steels", M. Militzer, R. Pandi, E.B. Hawbolt and T.R. Meadowcroft, *Hot Workability of Steels and Light Alloys-Composites*, eds. H.J. McQueen, E.V. Konopleva and N.D. Ryan, The Metallurgical Society of CIM, Montreal, PQ, 373-380 (1996).

20. "Austenite grain refinement and growth during the thermomechanical processing of steels", W.P. Sun, M. Militzer, E.B. Hawbolt and T.R. Meadowcroft, *Hot Workability of Steels and Light Alloys-Composites*, eds. H.J. McQueen, E.V. Konopleva and N.D. Ryan, The Metallurgical Society of CIM, Montreal, PQ, 285-292 (1996).

21. "An integrated process model for the hot rolling of plain carbon steel", D.Q. Jin, V.H. Hernandez-Avila, I.V. Samarasekera and J.K. Brimacombe, *Modelling of Metal Rolling Processes*, eds. J.H. Beynon, P. Ingham, H. Teichert and K. Waterson, The Institute of Materials, London, 36-58 (1996).

22. "The application of microstructure engineering to the hot rolling of steel", I.V. Samarasekera, D.Q. Jin and J.K. Brimacombe, *38th Mechanical Working and Steel Processing Conference Proceedings*, ISS, Warrendale, PA, Vol. XXXIV, 313-327 (1997).

23. "Modeling inhomogeneous deformation during hot rolling of plain carbon steels", D.Q. Jin, I.V. Samarasekera and J.K. Brimacombe, *38th Mechanical Working and Steel Processing Conference Proceedings*, ISS, Warrendale, PA, Vol. XXXIV, 329-337 (1997).

24. "Controlling mechanisms of austenite recrystallization under industrial mill processing conditions", W.P. Sun, E.B. Hawbolt and T.R. Meadowcroft, *Proceedings of ReX'96: Recrystallization and Related Phenomena*, ed. T.R. McNelley, Monterrey, CA, 429-436 (1997).

25. "The effect of controlled rolling on the austenite decomposition kinetics in an HSLA-Nb steel", M. Militzer, R. Pandi, E.B. Hawbolt and T.R. Meadowcroft, *Accelerated Cooling/ Direct Quenching of Steels*, ed. R. Asfahani, ASM, Materials Park, OH, 151-157 (1997).

26. "Effect of vanadium on recrystallization, phase transformation and precipitation during steel processing", W.P. Sun, M. Militzer, R. Pandi and E.B. Hawbolt, *Accelerated Cooling/ Direct Quenching of Steels*, ed. R. Asfahani, ASM, Materials Park, OH, 109-116 (1997).

27. "Critical challenges in the prediction of mechanical properties of hot-rolled steel strip", I.V. Samarasekera, D.Q. Jin and J.K. Brimacombe, *Thermec '97*, eds. T. Chandra and T. Sakai, TMS, Warrendale, PA, 57-66 (1997).

28. "Modelling of microstructure and properties in HSLA steels", M. Militzer, W.P. Sun, W.J. Poole and P. Purtscher, *Thermec '97*, eds. T. Chandra and T. Sakai, TMS, Warrendale, PA, 2093-2099 (1997).

29. "Microstructural evolution during the thermomechanical processing of Nb- and V-containing HSLA steels", W.P. Sun, M. Militzer, E.B. Hawbolt and T.R. Meadowcroft, *Thermec '97*, eds. T. Chandra and T. Sakai, TMS, Warrendale, PA, 685-691 (1997).

30. "Modelling the microstructure of microalloyed low-carbon steels", M. Militzer, W.P. Sun, E.B. Hawbolt and T.R. Meadowcroft, *IPMM '97: Australasia-Pacific Forum on Intelligent Processing & Manufacturing of Materials, Volume 2: Modelling, Processing and Manufacturing*, eds. T. Chandra, S.R. Leclair, J.A. Meech, B. Verna, M. Smith and B. Balachandran, Watson Ferguson & Co., Brisbane, Queensland, 1227-1233 (1997).

31. "The role of downcoiler in hot strip rolling of steel", Z.D. Liu, D.Q. Jin, J.K. Brimacombe and I.V. Samarasekera, presented at the *39th Mechanical Working and Steel Processing Conference Proceedings*, Indianapolis, IN (1997).

32. "Comparison between static and metadynamic recrystallization - An application to the hot rolling of steels", W.P. Sun and E.B. Hawbolt, *ISIJ International*, 37, 1000-1009 (1997).

33. "Analysis and modeling of austenite grain refinement and growth during hot rolling", W.P. Sun, M. Militzer, E.B. Hawbolt and T.R. Meadowcroft, *Transactions of the Iron and Steel Society*, Vol. 25, No. 5, 85-94 (1998).

34. "Numerical simulation of deformation during hot rolling of steel", D.Q. Jin, I.V. Samarasekera and R. Stachowiak, *Transactions of the Iron and Steel Society*, in press.

35. "Precipitation hardening of HSLA steels", M. Militzer, W.J. Poole and W.P. Sun, *Steel Research*, 69, 279-285 (1998).

36. "Microstructure engineering for hot strip rolling of HSLA-80 steel", M. Militzer, D.Q. Jin and I.V. Samarasekera, *Advances in Industrial Materials*, eds. D.S. Wilkinson, W.J. Poole and A. Alpas, The Metallurgical Society of CIM, Montreal, PQ, 63-77 (1998).

37. "Austenite grain growth in microalloyed low carbon steels", M. Militzer and E.B. Hawbolt, *Third International Conference on Grain Growth*, TMS, Warrendale, PA, in press.